1-1-2011

Analytical modeling of bond stress at steel-concrete interface due to corrosion

Luaay Hussein
Ryerson University

ANALYTICAL MODELING OF BOND STRESS AT STEEL-CONCRETE INTERFACE DUE TO CORROSION

By:
Luaay Hussein
B. Sc. in Civil Engineering, University of Baghdad, 1989
MASc. in Civil Engineering, Saddam University, 1993

A thesis presented to
Ryerson University
in partial fulfillment of the
requirements for the degree of
Master of Applied Science
in the program of Civil Engineering

Toronto, Canada, 2011

Author's Declaration

I hereby declare that I am the sole author of this thesis or dissertation.
I authorize Ryerson University to lend this thesis or dissertation to other institutions or individuals for the purpose of scholarly research.

Luaay Hussein ----------

I further authorize Ryerson University to reproduce this thesis or dissertation by photocopying or by other means, in total or in part, at the request of other institutions or individuals for the purpose of scholarly research.

Luaay Hussein ----------

Borrower's Page

No.	Borrower's Name	Address	Phone No.	Date	Signature
1					
2					
3					
4					
5					
6					
7					
8					
9					
10					
11					
12					
13					
14					
15					
16					
17					
18					
19					
20					
21					
22					
23					
24					
25					
26					
27					
28					
29					
30					

ANALYTICAL MODELING OF BOND STRESS AT STEEL-CONCRETE INTERFACE DUE TO CORROSION

Luaay Hussein
MASc., Department of Civil Engineering, Ryerson University, 2011

Abstract

An analytical model that describes the deterioration of bond strength, due to corrosion of steel reinforcement, at the steel-concrete interface in a reinforced concrete is developed. Concrete is assumed as a thick-walled cylinder subjected to internal pressure exerted from the growth of corrosion products on the concrete at the steel-concrete interface. The concrete in the inner cylinder is considered as an anisotropic material with stiffness degradation factor as an exponential function, while at the outer cylinder, the concrete is treated as isotropic material. A frictional model is used to combine the action of confining pressure resulted from radial pressure produced by principal bar ribs on surrounding concrete, and corrosion pressure resulted from the expansion of corrosion products.

The results of the proposed model are validated with experimental results by several researchers and a good agreement was noted; this shows that the derived analytical model was able to satisfactory predict the reduction of bond strength between steel and concrete.

Acknowledgment

The author would like to express his deepest appreciation to his supervisor Dr. Lamya Amleh, for her invaluable advice, guidance, suggestion, patient and encouragement throughout the execution of this research program. Her unfailing optimism and constant encouragement always prompted the author to overcome the difficulties in completing this research.

The author would like to express his sincerely thanks to the Civil Engineering Department in Ryerson University.

Finally, the author is grateful to his family, colleagues, and all friends for their support, and encouragement throughout this work.

To

My Family with all

Respect and Appreciation

Table of Content

List of Figures

List of Tables

List of Symbols

α	= Stiffness reduction factor
φ	= Friction angle between steel and concrete
φ_a	= Maximum size of aggregate
μ	= Coefficient of friction
μ_k	= Coefficient of kinetic friction
μ_s	= Coefficient of static friction
υ_{rs}	= Ratio between the volumes of the corroded and virgin steel
δ	= Angle between face of the rib and the bar axis
γ_{eq}	= Slip
σ_θ	= Tangential stress
σ_n	= Radial pressure produced by principal bar ribs on surrounding concrete
σ_{rc}	= Residual tensile stress in cracked concrete
σ	= Radial bond stress
σ_s	= Stress in steel
τ	= Bond stress
τ_c	= Bond strength when the concrete cracks
$t_b^o(x)$	= Cohesive bond strength contribution
τ_{crx}	= Splitting bond anchorage strength
τ_{bu}	= Ultimate bond strength for corroded reinforcing bar;
τ_{CP}	= Bond strength contribution of maximum confining pressure at anchorage
τ_{AD}	= Bond strength contribution due to adhesion between corroded steel and concrete
τ_{COR}	= Bond strength contribution due to expansion of corrosion products between corroded steel and concrete
ε_θ	=Tangential strain

ε_{ct} = Tensile strain capacity of concrete

υ_{rs} = Ratio between the volumes of the corroded and virgin steel

A_r = Rib area in the plane at right angles to the bar axis

A_s = Area of steel

A_{ct} = Concrete area subjected to tension

c = Concrete cover thickness

d_c = Effective rust layer

d_o = Thickness of the porous zone

D_r = Reduced diameter of the corroded reinforcing bar

D_i = Initial diameter of the reinforcing bar

d_b = Diameter of the steel reinforcing bar

E_0 = Young modulus of concrete

E_{ef} = Effective modulus of elasticity of concrete

E_s = Elastic modulus of steel

E_{st} = Modulus of elasticity of stirrups

f_{coh} = Adhesion strength

f_{ct} = Concrete tensile strength

f_{ct0} = Maximum residual strength of cracked concrete at onset of cracking

f'_c = Compressive strength of concrete

h_r = Rib height

k = Experimentally determined coefficient related to fracture energy

L = Percentage loss of contact pressure

l_b = Bar embedded length

l_r = Rib spacing

M = Percentage mass loss of steel bar

n = Number of transverse ribs at a section

n_s = Number of legs of the stirrups in the cross section

n_b = Number of reinforcing bars

P = Contact pressure

P_{crx} = The average radial force

$P_{corr}(x)$ = Pressure developed by corrosion product expansion

$P^{max}(x)$ = Maximum pressure at anchorage bond failure

P_{max} = Applied force at failure

P_{cor} = Corrosion pressure

P_{conf} = Confining pressure

r_b = Radius of the bar

R_o = Outer radius of thick wall cylinder

R_i = Inner radius of thick wall cylinder

R_c = Crack front

R_p = Radius of porous zone

R_s = Radius of initial bar after corrosion

R_r = Radius of initial bar included the expansion of corrosion products

r = Radius at any point of thick wall cylinder

S_r = Rib spacing

S_v = Spacing of the stirrups

t = Thickness of corrosion products

T_C = Tensile capacity at a section

T = Steel force

u = Displacement

V_a = Adhesion resistance

V_b = Bearing of the lug

V_f = Frictional resistance

w = Crack width

W_{cr} = Crack width at cover cracking

w_{icorr} = opening of each single radial crack

x = depth of the corrosion attack

x_{cr} = Corrosion depth at the onset of primary cracking

xp = Corrosion level

Chapter 1

INTRODUCTION

1.1. Introduction

One of the major degradation processes of reinforced concrete structures is the corrosion of the steel reinforcement. The corrosion problem of the build infrastructure has a significant impact on the economy, according to a study done by the Federal Highway Administration (FHWA) by Koch et al. (2001) on the total direct cost of corrosion in the U.S., which is estimated at $267 billion per year, which is equivalent to 3.1% of the U.S. gross national product (GNP). For instance, approximately 15 percent of the 586,000 bridges in the U.S. are recorded as structurally deficient, primarily due to corrosion of steel and steel reinforcement. The annual direct cost of corrosion for highway bridges is estimated to be $8.3 billion. In addition, the consequences of this problem are numerous, including reduced safety, serviceability and service life, which lead to increased risk of injuries and fatalities; and increased maintenance costs and user costs. In summary, corrosion of steel reinforcements is the foremost cause of damage and early failure of reinforced concrete structures, leading to huge costs for inspection, maintenance, rehabilitation and replacement of the infrastructure worldwide. The repair and maintenance of reinforced concrete structures is becoming increasingly important and extensive. In order to increase the reliability of the structure and to reduce maintenance costs, eliminating or at worst impeding the corrosion problem is very important. Also, to design new concrete structures and to repair existing deteriorated concrete structures requires an understanding of the various causes and mechanisms of corrosion in reinforcing and prestressing steel along with their performance in the varying aggressive environments.

The main reason associated with the deterioration of reinforced concrete due to steel bar corrosion is not the reduction in mechanical strength of the reinforcing bar itself, but rather than that the pressure exerted from the expansion of the corrosion products which cannot be supported by the limited tensile strength of concrete. Therefore, this weakens

the bond between steel and concrete which immediately affects the serviceability and ultimate strength of reinforced concrete structures (Cabrera 1996).

The concrete cover acts as a physical barrier to the access of aggressive agents because of its strength and resistance to wear and tear, and to permeation of fluids containing harmful compounds. Normally the steel in reinforced concrete is protected from corrosion because of the high alkalinity of the concrete; when the pH of the pore water is greater than 12.5, a passive layer forms on the steel surface which naturally protects it from corroding**.** However when the pH of the concrete reduces from 12.5 to 9.5 due to carbonation or increase of the chloride ions' concentration near the steel, the passive layer gets destroyed and can no longer protect the embedded steel from corrosion attack. Furthermore, the concrete made through using low water-cement ratios and good curing practices have a low permeability that minimizes the penetration of the corrosion inducing ingredients. In addition, low permeability increases the electrical resistivity of the concrete to some degree, thus helping in reducing the rate of corrosion by retarding the flow of the electrical current within the concrete that accompanies the electrochemical corrosion process. Consequently, corrosion of the embedded steel requires the breakdown of its passivity.

Concrete is relatively weak in tension, and it cracks when the tensile strength is exceeded in a reinforced member. Cracking is an important phenomenon specific to reinforced concrete, and it can have a significant influence on the durability of a concrete structure. The influence of new materials and new technologies being used presently, on the concrete tensile strength and the bond characteristics is not well established; the examples are the use of high-strength concretes, the use of fiber-reinforced plastic rebars, and the use of epoxy-coated rebars. Concrete tensile strength and toughness are fundamental properties that ensure bond efficiency at the steel-concrete interface, as relatively low values of the bond stress-tensile strength ratio (τ / f_{ct} = 0.5 to 0.8) can exhibit a complex local stress and strain state (Gambarova and Rosati, 1996).

When the embedded reinforcement corrodes, the strength of a reinforced concrete member is damaged in a variety of ways. The expanded volume of corrosion products on the steel bar surface develops internal pressure at the steel-concrete interface which causes high tensile stresses in the concrete member. When the tensile stress in the concrete exceeds its tensile strength, cracks will form in the surrounding concrete. Also, with the increase of corrosion, existing fine and micro cracks in the surrounding concrete tend to enlarge and form a network of interconnected cracks, providing increased ionic transport between the surface of the concrete and the surface of the reinforcing steel, effectively promoting the corrosion process. Crack growth decreases concrete stiffness and tensile strength, while the formation of a network of cracks increases concrete permeability. Thus, the holding capacity and confinement of the concrete member is decreasingly compromised as cracking progresses. As corrosion increases, the normal contact pressure at steel-concrete interface is reduced, causing a considerable amount of deterioration of bond between the reinforcing steel and concrete. In addition to the bond deterioration and with the increase of corrosion, the cross sectional area of the steel reinforcement reduces significantly and hence, it can no longer withstand the load and leads to the collapse of the structure. Hence, it is essential to prevent the premature failure of reinforced concrete structures by appropriate controlling and monitoring of reinforcement corrosion.

In spite of the well understanding of the electrochemical processes induced by corrosion, the effects of corrosion on bond capacity, and the determination of residual bond strength, which is an important factor in predicting the service life of structures, are not well established. Bond between the reinforcing steel and the concrete is dependent on cohesion and adhesion at the steel-concrete interface and the mechanical interlocking between the lugs or deformations of the reinforcing bar and the surrounding concrete. Corrosion results in an early loss of both cohesion and adhesion. As steel corrodes, the corrosion products at first improve bond by a slight amount, however, the increasing levels of corrosion can result in longitudinal and transverse cracking which causes a release in the “hold” of the concrete on the bar and decreases the bond capacity at the steel-concrete interface.

In summary, the reinforcing steel is provided in reinforced concrete structures to resist the tensile forces, and to produce controlled cracking within that zone. In reinforced concrete members, concrete forms the body of the member and provides stiffness and resistance to compression loads. While the steel reinforcing bars (rebar) are placed where tensile loads are expected, so that once the concrete cracks, the steel is present to resist the tension. However, corrosion not only deteriorates the steel bar and its function of transferring the tensile forces, but also it deteriorates the concrete through spalling of the cover. Therefore, corrosion of the reinforcement has a strong influence on the bond behaviour at the interface between the steel reinforcement and the concrete. As corrosion of the reinforcing steel progresses, the bond strength between the reinforcing steel and the concrete diminishes progressively, and major repairs or replacement are needed. While considerable research has been undertaken about the problem, and numerous reports have discussed how this corrosion can be controlled, only limited data are available about its influence on the bond behaviour at the steel-concrete interface. Some researchers have proposed analytical models to study the bond behavior of corroded reinforcement (Coronelli (2002), Wang and Liu (2004), Bharagava et al. (2007)); However, considerable variations in the prediction of bond loss have been reported. Hence, a better understanding of the mechanism through which corrosion affects bond is necessary to enable the controlling factors to be better understood, to resolve the apparent inconsistencies between different studies, and to enable effective models to be developed.

1.2 Scope and objective of the study

The purpose of this research is to model the contact pressure at steel- concrete interface by combining the action of confining and corrosion pressure using a frictional model, and assuming the concrete as anisotropic material in the crack zone. The main objectives of the research are:

1. to develop an analytical model for corrosion pressure at steel-concrete interface, assuming the concrete in the cracking zone as anisotropic material,
2. to develop an analytical model for confining pressure at steel-concrete interface,

3. to add the affect of adhesion to the developed model, and

finally, verification, and calibration of the model for reinforced concrete systems of increasing complexity.

1.3. Thesis layout

This thesis is composed of six chapters. Chapter one addresses the scope and objective of the present study. Chapter two presents fundamentals of bond and corrosion at steel-concrete interface. Chapter three reviews some of the latest models of bond behavior for corroded reinforcing steel. Chapter four presents the analytical modeling of bond stress at the interface between concrete and reinforcing steel due to corrosion. Chapter five illustrates an analytical example, with results, including a discussion of the analysis. Finally, Chapter six presents a brief summary of the analytical observations, as well as the conclusions and recommendations for further research and development on the influence of corrosion on bond behavior.

Chapter 2

FUNDAMENTALS OF BOND AND CORROSION BETWEEN STEEL AND CONCRETE

The behaviour of a reinforced concrete structure is influenced by the bond at steel-concrete interface. This chapter presents some basic information on bond behaviour between the concrete and the reinforcing steel such as bond mechanisms, failure modes of bond, cracking behaviour and factors affecting the bond strength. It also presents some basic information on corrosion and the effects of corrosion on bond behaviour at steel-concrete interface.

2.1 Fundamentals of Bond

2.1.1 Introduction

Bond between reinforcing steel bar and surrounding concrete is necessary to ensure composite action of the two materials, and the load transfers between steel and concrete is required to maintain this composite action. This load transfer is named *bond* which is idealized as a continuous stress that develops in the vicinity of steel concrete interface. Raymond and Henry (1965) defined bond as "that property which causes hardened concrete to grip an embedded steel bar in such a manner as to resist forces tending to slide the bar longitudinally through the concrete". At the steel-concrete interface, bond failure will prevent the tensile force to be developed in the steel bar, thus influencing the resistance of the structural element. In reinforced concrete structures, an interaction between the steel bar and the surrounding concrete is essential to transfer a force between the two materials. Therefore, bond is fundamental because it influences many aspects of the behaviour of reinforced concrete such as cracking, deformability, and instability.

2.1.2 Bond Stress

Bond stress is defined as the shear stress at the steel-concrete interface which modifies the steel stress by transferring the load between the steel and the surrounding concrete (ACI Committee 408, 1966). Bond stress can be calculated as the stress per nominal unit area of the bar surface. Also, bond stress can be measured by the rate of change of steel stress in the bar. Thus, there will not be any change in bar stress without bond stress or vice versa.

2.1.2 Bond Mechanisms

According to ACI Committee 408 (1992), an efficient and reliable force transfer from the reinforcement to the surrounding concrete depends on three mechanisms; namely, adhesion, friction and mechanical interlocking as shown in Fig. 2.1 where V_a is the adhesion, V_b is the mechanical anchorage due to bearing of the lug and V_f is the frictional resistance.

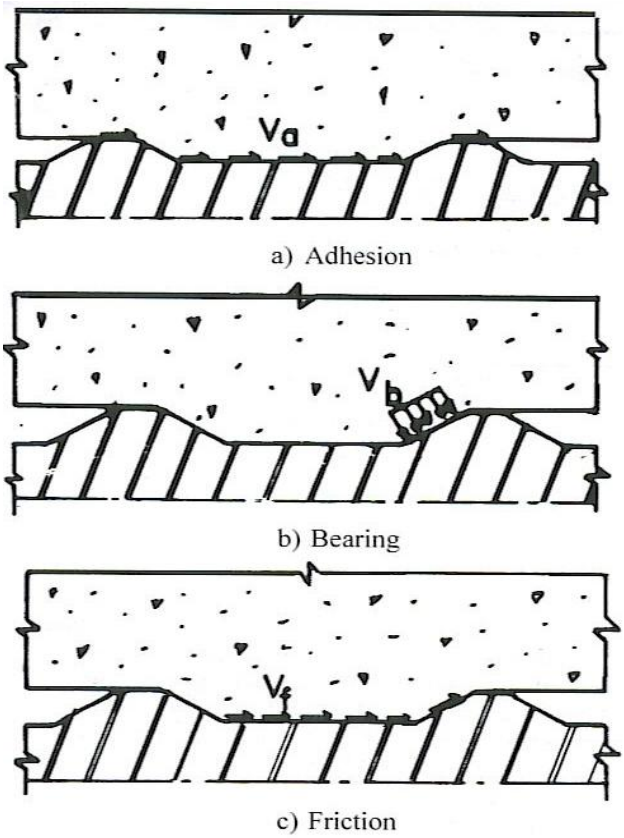

Figure 2.1 Idealized force transfer mechanism (ACI Committee 408, 1992)

Adhesion: Adhesion is the chemical bond between the bar and the concrete which is related to the shear strength at the steel-concrete interface. For a small load, the basic resisting mechanism is the chemical adhesion; however when a deformed bar moves with respect to the surrounding concrete due to increase in the loads, the chemical adhesion along the bar surface is lost.

Treece and Jirsa (1989) studied the adhesion mechanism for both uncoated and epoxy coated steel reinforcing bars. They found that there was no evidence for chemical adhesion between the epoxy coated and the concrete while the uncoated bar was adhered to the concrete. Similarly, Cairns and Abdullah (1994) studied the bond characteristics at the steel-concrete interface for uncoated and epoxy coating steel plates. They noted that the uncoated steel plates were covered with a layer of crushed mortar after failure, while the coated plates were observed to be clean after failure.

Friction: Friction is the force resisting the parallel displacement between two surfaces sliding against each other. Friction plays a significant role in force transfer between the concrete and the steel bar. Based on the work of Treece and Jirsa (1989), the ACI Committee 408 (1992) suggested that friction can contribute up to 35% of the ultimate strength governed by the splitting of the concrete cover.

Mechanical interlocking: For deformed steel bars, bond depends primarily on mechanical interlocking between the ribs and the concrete keys. In addition, the mechanical interlocking of the deformed steel bar depends on the geometry of the ribs along the steel bar. As the ultimate bond strength is reached, shear cracks begin to form in the concrete between the ribs as the interlocking forces induce large bearing stresses around the ribs, and slip occurs. Therefore, the bar ribs restrain the slip movement by bearing against the concrete keys. The slip of a deformed bar may occur in two ways, either through pushing the concrete away from the bar by the ribs, i.e. wedging action, or through crushing of the concrete by the ribs.

Perfect bond for reinforced concrete members provides complete compatibility of strains between concrete and steel. However, in reality, perfect bond occurs only in the regions where negligible stress transfers between concrete and steel. Whereas, in the regions where high stress transfers along the steel concrete interface, such as in the vicinity of cracks, the bond stress is related to the relative displacement between reinforcing steel and the surrounding concrete. Therefore, strain compatibility does not exist between reinforcing steel and surrounding concrete near cracks. The relation between bond stress and the relative displacement between reinforcing bar and concrete is due to strain incompatibility and the crack propagation is known as bond-slip as shown in Fig 2.2.

Initially, with uncracked concrete, bond stress τ is assured by the chemical adhesion between the steel and the concrete up to the point A as shown in Fig. 2.2 where the slip is relatively negligible. As mentioned earlier, once a deformed bar moves with respect to the surrounding concrete, surface adhesion is destroyed as a consequence of the wedging action of the ribs which pushes the concrete away from the steel.

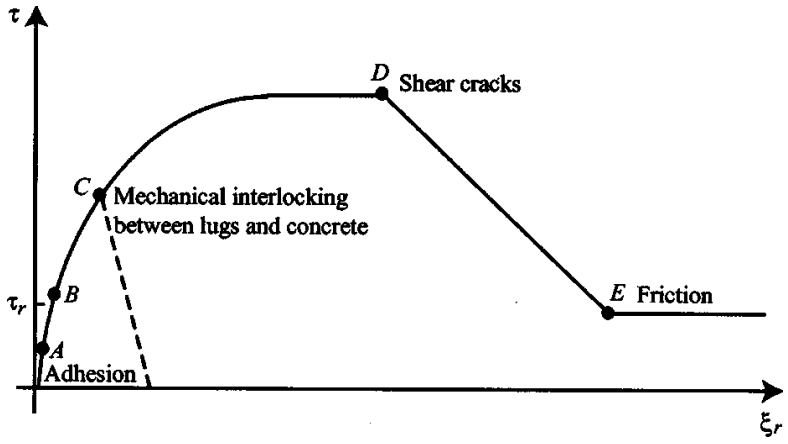

Figure 2.2 Typical bond stress-slip relationship (Girard and Bastien, 2002)

With the onset of slippage between the reinforcing steel and the concrete, bond resistance will be developed by friction and mechanical interlocking between the bar and the surrounding concrete. However, the bearing of the lugs become significant for the bond

between steel and concrete. The concentrated bearing forces in front of the lugs will split into two directions: Parallel components to the bar axis represents the bond stresses and the radial (perpendicular) components to the bar axis represents the circumferential tensile stresses. When these tensile stresses exceed the tensile strength of the concrete τ_r, internal cracks develop around the bar, and the deformation of concrete resulting from generated stresses tend to pull the concrete away from the reinforcing bar in the vicinity of a major crack as shown in Fig. 2.3. Therefore, at point B in Fig. 2.2, the stiffness of the concrete is reduced and longitudinal splitting cracks are initiated by the inclined compressive forces spreading from the lugs into concrete. The internal cracks reach the concrete surface at point C, and the bond resistance will drop to zero if sufficient confinement is not provided. Thus bond failure due to splitting occurs (Lundgren, 2005). However, with the presence of sufficient confinement, the load can be increased further and pull out failure will occur instead of splitting failure. At point D, shear cracks will initiate in the concrete keys between ribs which correspond to the point of maximum bond resistance. The bond resistance is decreased with the increasing slip due to spreading of shear cracks through the concrete. Hence the frictional resistance of concrete along the failure surface remains the only mechanism that exists at point E.

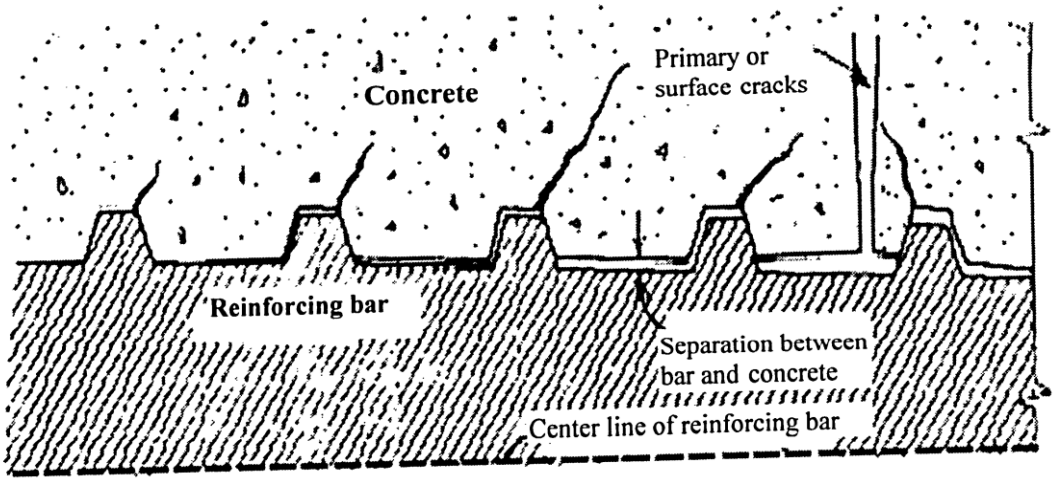

Figure 2.3 Separation between the reinforcing bar and concrete near primary crack (Lutz and Gergely, 1967)

When the tensile stress at a given location exceeds the tensile strength of concrete, crack develops around the bar, and it is manifested by a separation of the concrete at this location. Further loading will lead to loss of adhesion near the crack, and different secondary internal cracks will form close to the main crack which may not propagate to the external surface of the concrete. Steel stresses at the crack will reach a local peak while between the cracks; the steel stress is lower than that due to the concrete contribution.

The separation between steel and concrete in plain bars leads to complete loss of bond stresses in the vicinity of the crack. However, in the deformed bars, separation does not lead to complete loss of bond, and bond forces are transmitted by the rib bearing in the vicinity of main cracks, as shown in Fig. 2.4.

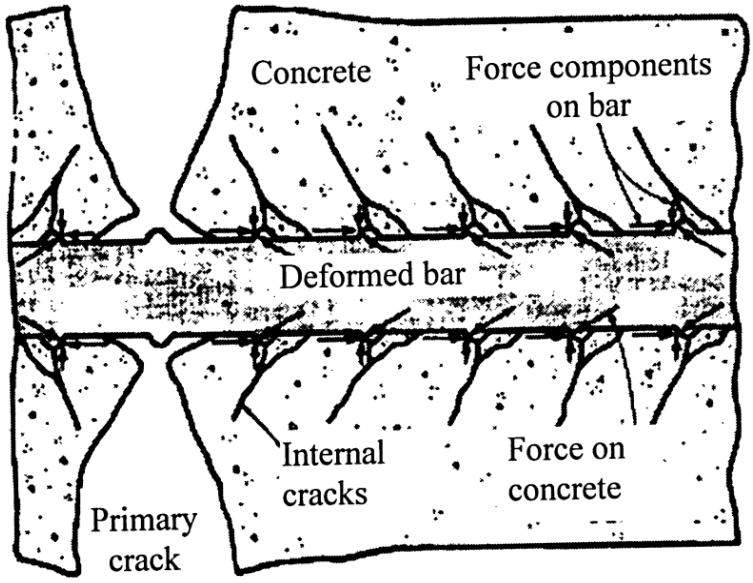

Figure 2.4 Formation of internal cracks (Goto, 1971)

2.1.3 Bond Failure Modes

Principally, the bond failure between steel and concrete can be described by two modes: pull-out and splitting failures. If the concrete is well confined or the ratio of concrete cover to bar diameter is more than three (Cairns and Abdullah, 1996), splitting does not

occur and bond failure is caused by bar pullout due to the shearing off of the concrete keys between the bar ribs. The mechanism of force transfer changes from rib bearing to friction along the vertical line between the tops of the ribs as shown in Fig. 2.5a. In the case of medium confinement where a sufficient amount of transverse reinforcement is provided, crushing or shearing-off of the concrete below the ribs accompanied by longitudinal cracks will occur through the entire cover thickness as shown in Fig. 2.5b. If the concrete cover to bar diameter ratio is less than three (Cairns and Abdullah, 1996) or the steel bars are closely spaced, the longitudinal cracks accompanied by slip on the rib face break out through the entire cover thickness as shown in Fig. 2.5c.

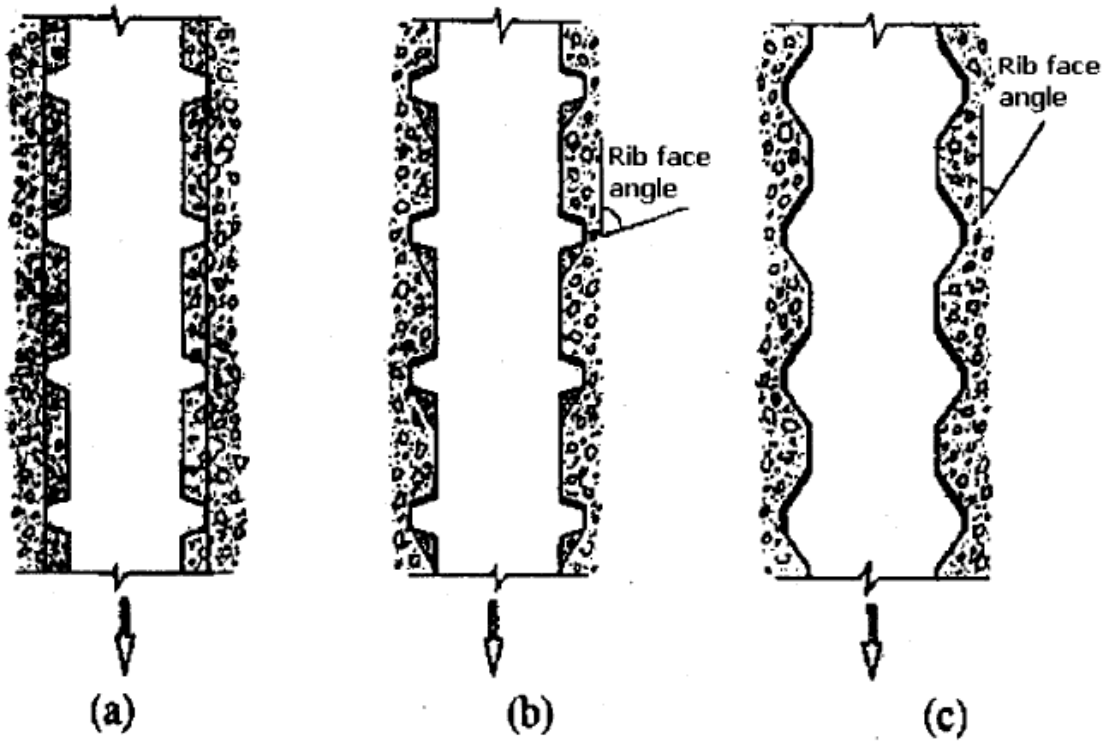

Figure 2.5: Modes of bond failure
(a) heavy confinement pull-out; (b) medium confinement, splitting induced pull-out accompanied by crushing and/or shearing-off in the concrete below the ribs; and (c) light confinement splitting accompanied by slip on the rib face
(Task group bond model, 2000)

Slipping of the deformed bars can occur due to crushing of the concrete in front of the ribs, and splitting of the concrete by wedging action (Rehm (1968) and Lutz and Gregely (1967)). Rehm (1968) related the bond failure modes to the ratio of rib height to rib spacing. When the ratio is greater than 0.15, the bond failure occurs due to the shearing off of the concrete keys between the bar ribs and the bar will pull out as shown in Fig. 2.6a. When the ratio is less than 0.15, the bond failure occurs due to crushing of the concrete in front of the ribs, and the deformed bar will split from the surrounding concrete as shown in Fig. 2.6b

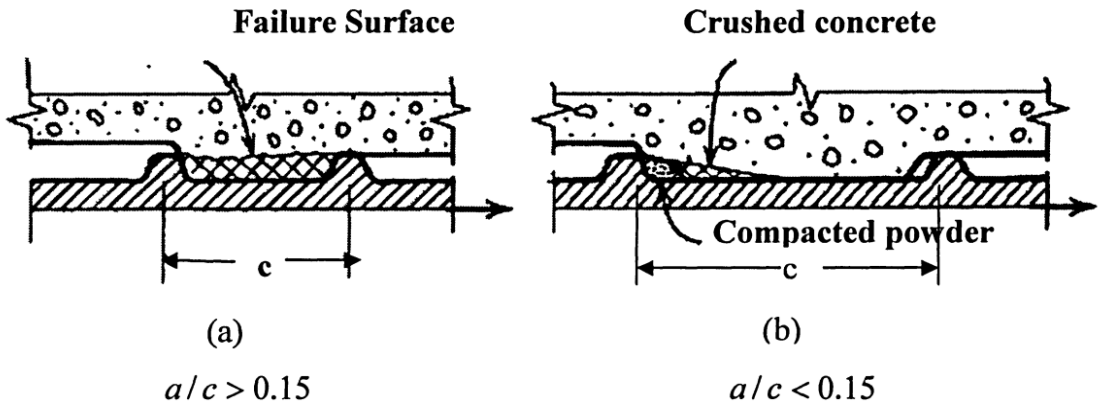

Figure 2.6 Failure mechanisms at the ribs of deformed bars (Rehm, 1968)

Longitudinal splitting cracks develop when the concrete separates from the reinforcing bar at a primary crack due to an increase in the circumferential tensile stresses. Tepfers (1973) studied the circumferential stress distribution over a thick walled cylinder confining the reinforcing bar as described later on in section 4.1. Tepfers assumed three stages of bond response of the concrete cylinder: the uncracked stage, partially cracked stage and the plastic stage. Tepfers (1979) derived equations for the three stages by assuming short anchorage lengths, and found good agreement between the measured values of the short anchorage tests with the partially cracked theory. According to the

cracked elastic behaviour, the bond strength, τ_c at the cracking of the concrete cover, is given by equation 2.1.

$$\tau_c = 0.6(0.5 + c/d_b) f_{ct} \quad (2.1)$$

For larger concrete cover thickness, the assumption of a plastic behaviour at the steel-concrete interface, gives:

$$\tau_c = 2(c/d_b) f_{ct} \quad (2.2)$$

Where,

τ_c = Bond strength when concrete cracks

c = minimum concrete cover thickness

d_b = diameter of the steel reinforcing bar

f_{ct} = concrete tensile strength

2.1.4 Factors Affecting the Bond Strength

Bond strength between the steel and concrete depends on several factors such as concrete and steel strengths; bar size and profile; concrete cover thickness; embedment length of steel; spacing of bars; stirrups; temperature; corrosion etc. A brief description of some of these factors that influence the bond strength at steel-concrete interface is presented in the following sections.

2.1.4.1 Concrete Strength

Compressive strength is considered to be a significant parameter in bond behaviour because the force between steel and concrete is transferred mainly by bearing and bond (Orangun et al. 1977). Tepfers (1973) showed that the slope of the bond stress distribution varies considerably over the splice length with a higher concrete strength

when compared to that with lower concrete strengths. Since bond failure can occur by tensile splitting and shearing off of the concrete, the compressive strength is considered to be a significant key in bond behavior (ACI Committee 408, 1992).

It has been found that the bond of high strength concrete is proportional to the compressive strength of concrete (Alavi-Fard and Marzouk, 2002). However, test result indicates that the square root has proven to be adequate as long as concrete strengths remain below about 55 MPa (ACI Committee 408, 1992), while for high strength concrete, it is observed that $f_c'^{1/4}$ provides the best fit for the effect of compressive strength on the concrete contribution to bond strength for bars not confined by transverse reinforcement (Zuo and Darwin 1998, 2000). Zuo and Darwin (1998, 2000) found that $f_c'^{3/4}$ provides a good fit for the effect of compressive strength on the concrete contribution to bond strength for bars confined by transverse reinforcement.

The tensile and compressive stresses of concrete contribute to the development of bond stresses. For example, micro cracks are controlled by the tensile stresses of the concrete, while bearing stresses induce high compressive stresses in front of the ribs.

Martin (1982) observed that for a slip range of 0.01 to 1 mm, the bond stress is proportional to the concrete compressive strength, based on the pullout test results, with concrete strengths varying from 16 to 50 MPa; However, for very small slip less than 0.01 mm, and for high slip larger than 1 mm, the effect of the concrete compressive strength is less important and proportional to $f_c'^{2/3}$.

2.1.4.2 Concrete Cover Thickness and Bar Spacing

Bond strength increases with increasing cover thickness and bar spacing (ACI Committee 408, 2003). Tepfers (1973), Orangun el al., (1977), and Eligehausen (1979) observed that the concrete cover and the bar spacing significantly influence the type of bond failure. Splitting tensile failure occurs with small concrete cover and bar spacing, while pullout

failure occurs with large concrete cover and bar spacing. For most structural members, splitting failure is expected and can occurs between the bars, between the bars and the free surface, or both, while pullout failure can occurs with some splitting if the member has significant transverse reinforcement to confine the anchored steel (ACI Committee 408, 2003).

2.1.4.3 Transverse Reinforcement

The amount and distribution of transverse reinforcement influences the type of bond failure (Tepfers, 1973; Orangun et al., 1977; Eligehausen, 1979). The increase in the transverse reinforcement increases the concrete confinement which results in an increase in bond force, and converts the splitting failure to a pullout failure. Additional transverse reinforcement, above that needed to convert the splitting failure to a pullout failure becomes less effective, eventually providing no increase in bond strength (Orangun et al., 1977).

2.1.4.4 Bar Size

The relationship between bar size and bond strength is not always appreciated due to the following reasons (ACI Committee 408, 2003):

1. The increase in the bar size increases the length of development.
2. For a certain development length, larger bars achieve higher bond forces than smaller bars for the same degree of confinement.

Therefore, it is desirable to use several of the small bars instead of using a few large bars and maintain a reasonable clear distances between the bars (ACI Committee 408, 2003).

The bar size also plays an important role in the contribution of confining transverse reinforcement to bond strength. When the larger bars slip, higher stresses are mobilized in the transverse reinforcement, thus better confinement for concrete is provided.

Therefore, the effect of transverse reinforcement on the bond strength is the same as the bar size effect (ACI Committee 408, 2003).

2.1.4.5 Bar Profile

The stress transfer between the reinforcing bar and the surrounding concrete depends on the resistance to relative motion or slippage between the concrete and the surface of the embedded steel bar due to the bond at steel-concrete interface. It is well known that this mechanism of stress transfer is the base of the theory of reinforced concrete.

The geometry of the bar rib has great influence on the bond strength due to the importance of the mechanical interlocking to the bond strength. Previous studies (Rehm, 1961; Lutz et al., 1966; Darwin and Eheneze, 1993) indicate that the geometry of the lugs affect the bond strength of anchored bars. It was concluded from their studies that bond strength of deformed bars would improve with an increase in the rib bearing area (projected rib area normal to the bar axis) to the rib shearing area (bar perimeter times center-to-center distance between ribs) ratio. This ratio is known today as the relative rib area R_r.

Lutz et al. (1966) showed that slip occurs due to the crushing of the concrete in front of the ribs when the rib face angle (the angle between the face of the rib and the longitudinal axis of the bar) is greater than 40 degrees producing a face angle between 30 to 40 degrees from crushed concrete, and when rib face angle is less than 30, no crushing of the concrete occurs in front of the rib. In addition, if the face of the rib formed an angle of 90 degree with the axis of the bar, all of the bond strength will be carried out by the direct bearing of the rib against the concrete key. In this case, friction between the concrete and steel will not contribute to the bond strength, but this case can not be achieved due to insufficient compaction of the concrete in front of the rib which oppositely affects the bond strength. However, if the rib face angle is zero degree as in a plain bar, the friction caused by adhesion between the concrete and steel will be the only bond component, and loss of this adhesion will destroy the bond.

As a result from the crushing of the concrete in front of the rib, Choi and Lee (2002) found that the range of the effective rib face angle was between 25 and 35 degrees, which is lower than the actual rib face angle, and when the bars are not confined by transverse reinforcement, the relative rib area has a little effect on the bond strength of deformed bars.

2.1.4.6 Steel Yield Strength

The bond stress is related to the force in the steel. When the strain in the bar exceeds the yield strain, the interlocking effect between the bar ribs, and the concrete is decreased due to the influence of the effect of lateral bar contraction on the friction mechanism; Therefore, the bond stress decreases significantly after steel yielding (Task Group Bond Models, 2000). According to the ACI Committee 408 (2003) report, the average bond stress for bars that yielded before bond failure is significantly lower than that of the bars with high strength steel.

Studies show that when the concrete is not confined by transverse steel reinforcement, 2% of the bars yielded before bond failure produce average bond stresses, and 10% yielded after bond failure produce average bond stresses when confined by transverse reinforcement, compared to similar bars with the same bonded lengths made of higher strength steel that does not yield (Darwin et al. 1996a; Zuo and Darwin 1998, 2000).

2.1.4.7 Bar Casting Position

It was observed that bar casting position plays an important role in the bond strength between concrete and reinforcing steel. Top-cast bars have lower bond strengths than bottom cast bars (Jeanty, Mitchell, and Mirza 1988).

Luke et al. (1981) studied the affect of casting position on the bond strength; they found that the bond strength decreases with increasing the depth of concrete below the bar as shown in Fig. 2.7. It can be noted from Fig. 2.7 that bond strength decreases with

increasing slump. However; this decrease is mostly for top-cast bars while for bottom cast bars, slump appears to have little effect. The reason for that is the water and air trapped will be greater under top bars. In addition, the relative downward movement of the surrounding concrete caused by settlement of the fresh mixture increases with the increase of the depth of concrete below the bar.

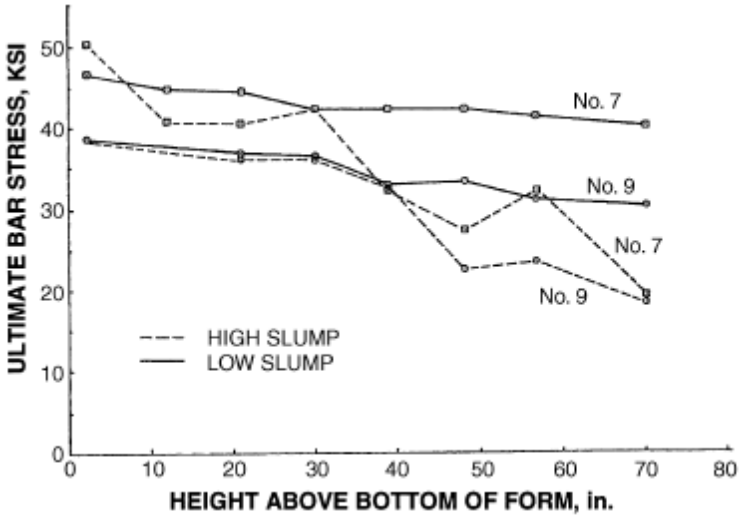

Figure 2.7 Bond strength as a function of bar location within a wall specimen High slump = 8-1/2 in. (215 mm). Low slump = 3 in. (75 mm) (Luke et al., 1981)

2.1.4.8 Effects of Corrosion

For very low levels of corrosion, when there is no longitudinal cracking; the corrosion products have a beneficial effect of improving the bond characteristics at the steel-concrete interface because it increases the surface roughness and hence the frictional force. While at high levels of corrosion, the steel bars display localized pitting and loss of some of the ribs over the bar length, result in the weakening of mechanical interlocking mechanism at the steel-concrete interface.

When reinforcement corrodes, the strength of a reinforced concrete member is undermined in a variety of ways. The expanded volume of corrosion products on the steel bar surface develops internal pressure at the steel-concrete interface which causes high tensile stresses in the concrete specimen. When the tensile stresses in the concrete exceed its tensile strength, cracks will form in the concrete. With the increase of corrosion,

existing fine and micro cracks in the surrounding concrete tend to enlarge and form a network of interconnected cracks, providing increased ionic transport between the surface of the concrete and the surface of the reinforcing steel, effectively promoting the corrosion process. Crack growth decreases concrete stiffness and tensile strength, while the formation of a network of cracks increases concrete permeability. Thus, the holding capacity and confinement of the concrete member is decreasingly compromised as cracking progresses. As corrosion increases, the crack width increases, and this results in the breakdown of cohesion, adhesion and friction at the steel-concrete interface.

Amleh and Mirza, (1999) examined the affect of the corrosion on the number and spacing of the transverse cracks. They found that as the level of corrosion increases, the transverse crack spacing increases, reflecting the deterioration of bond characteristics at the steel-concrete interface.

2.1.5 Measurement of Bond

Many different methods have been used to investigate the bond characteristics of the steel reinforcement in the concrete. According to Nawy (1996), bond tests can be classified into three groups: pull-out tests, embedded bar tests and beam tests. This classification includes the pullout tests (both the concentric and the eccentric), variety of bond beam tests (the National Bureau of Standards beam, the University of Texas beam), semi beam specimen test, and the standard tension specimen. A good overview of the current tests used to determine the bond characteristics of reinforcing bar can be found in ACI Committee 408 (1992), Park and Paulay (1975), and MacGregor (1997), Ferguson (1988),. The main aim of the bond test is to determine the stresses transferred from steel to concrete and vice versa under service conditions.

2.1.5.1 Pullout Tests

Pullout test is the most widely used by researchers because of its simplicity. In this test, a bar is embedded in the centre of a concrete cylinder or prism, and the force required to

pull out the bar or make it slip excessively is measured, as illustrated in Fig. 2.8. In this type of test, a small load causes a slip and develops a high bond stress near the loaded end, leaving the upper part of the bar totally unstressed as shown in Fig. 2.9. However, this test appears useful where relative bond resistance is compared rather than real bond resistance is obtained (Ferguson 1988). The slip at the loaded end increases when the applied load is increased which leads to the high bond stress and the slip extends deeper into the concrete specimen. If the embedment is long enough, the bond strength is higher than tensile strength of bar, and failure occurs due to bar rupture, while if the bar is very short, or light weight aggregates were used, the bond strength is less than the tensile strength of the bar, and failure occurs due to bar pullout. In case longitudinal splitting of the concrete occurs, failure is initiated due to concrete cracking.

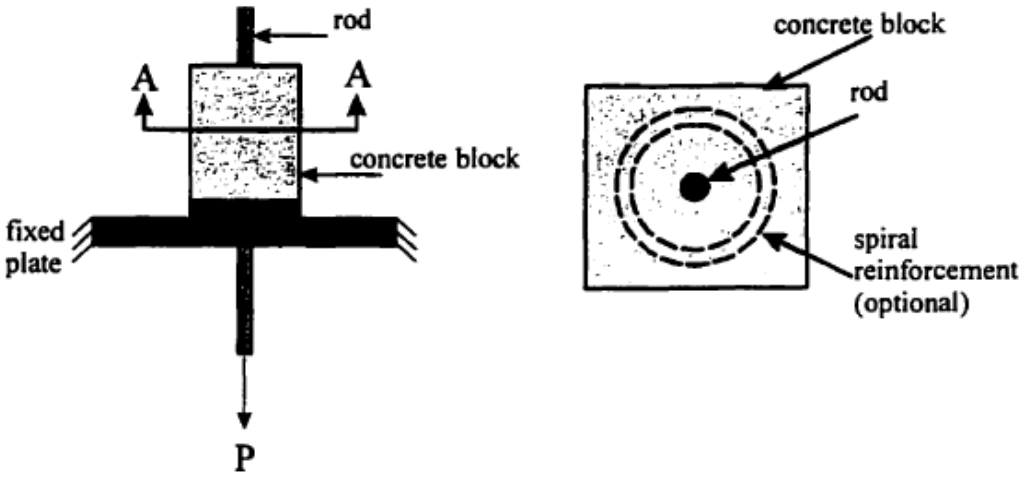

Figure 2.8 Schematic diagram of a pullout test (Amleh, 2000)

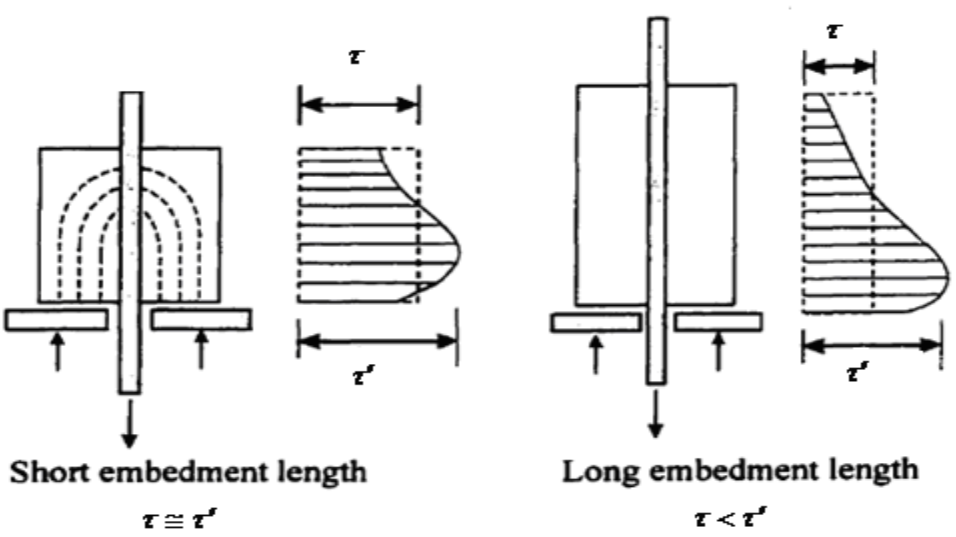

Figure 2.9 Effect of embedment length on the distribution of bond (Leonhardt, 1964)

This method is not intended for establishing bond strength values for structural design purposes because in reinforced concrete beams or slabs, the concrete surrounding the tensile reinforcement is in tension, whereas the concrete in this test is in compression, which not only increases the bond strength but also eliminates tension cracks in the specimen. Furthermore, this type of test is not subjected to external shear or bending moments, which are present in the actual structures. Therefore, the failure patterns in the pullout test are not realistic (Almusallam et al. 1996).

2.1.5.2 Tension Tests

Modification to concentric pull out test to eliminate compression on the concrete specimen is called the tension pullout test (Ferguson 1988). However, the interaction between spaced splices and crack pattern introduces problems in this test (Ferguson 1988). Goto (1971) performed this type of test to clarify the pattern of cracks around the tensile reinforcing bars.

In this test, a steel bar is embedded in the centre of a concrete cylinder, and subjected to applied loads at its ends as shown in Fig. 2.10. When the applied forces at the specimen

ends on the steel bar are increased, the bond stresses at the steel-concrete interface increase gradually; this leads to an increase in the force transmitted to the concrete until it reaches the tensile capacity T_C at which the section cracks. The tensile capacity of concrete at a section can be obtained from equation (2.4).

$$T_C = f_{ct}.A_{ct} \tag{2.4}$$

Where f_{ct} is the tensile strength of the concrete, and A_{ct} is the concrete area subjected to tension. Note that just before the crack forms, the force transferred from the steel to the concrete is dependent on the bearing of the lugs because the adhesion between the steel bar and the concrete is exhausted. The concrete section with the tensile force T_C leads to redistribution of the stresses in the steel and the concrete, and the bond stresses. At the section where the crack formed, the steel force is equal to T, while the applied force at the end of the specimen, and the resultant concrete force is zero. The redistribution of the various stresses is shown in Fig. 2.10. If the cracks are widely spaced, this redistribution can lead to increase the tensile force in the concrete somewhere between the crack and the free end to T_C, which in turn leads to form a crack at this section, and the steel, concrete and the bond stresses will be redistributed as shown in Fig. 2.10. Fig. 2.11 is showing the free body diagram of the steel bar for different conditions of cracks. This process will be repeated as long as stress in the concrete between the cracks will reach T_C, otherwise, the cracking process will stabilize, and no further cracking will occur in the specimen.

Once the cracks have stabilized, any further increase in the load applied to the specimen will cause only an increase in the steel force at the crack section, until finally the bar yields, and will not result in any additional cracks. According to that, the bond stress between the cracks remains almost constant. Therefore, the spacing between the cracks will be increased as a result of corrosion at the steel-concrete interface.

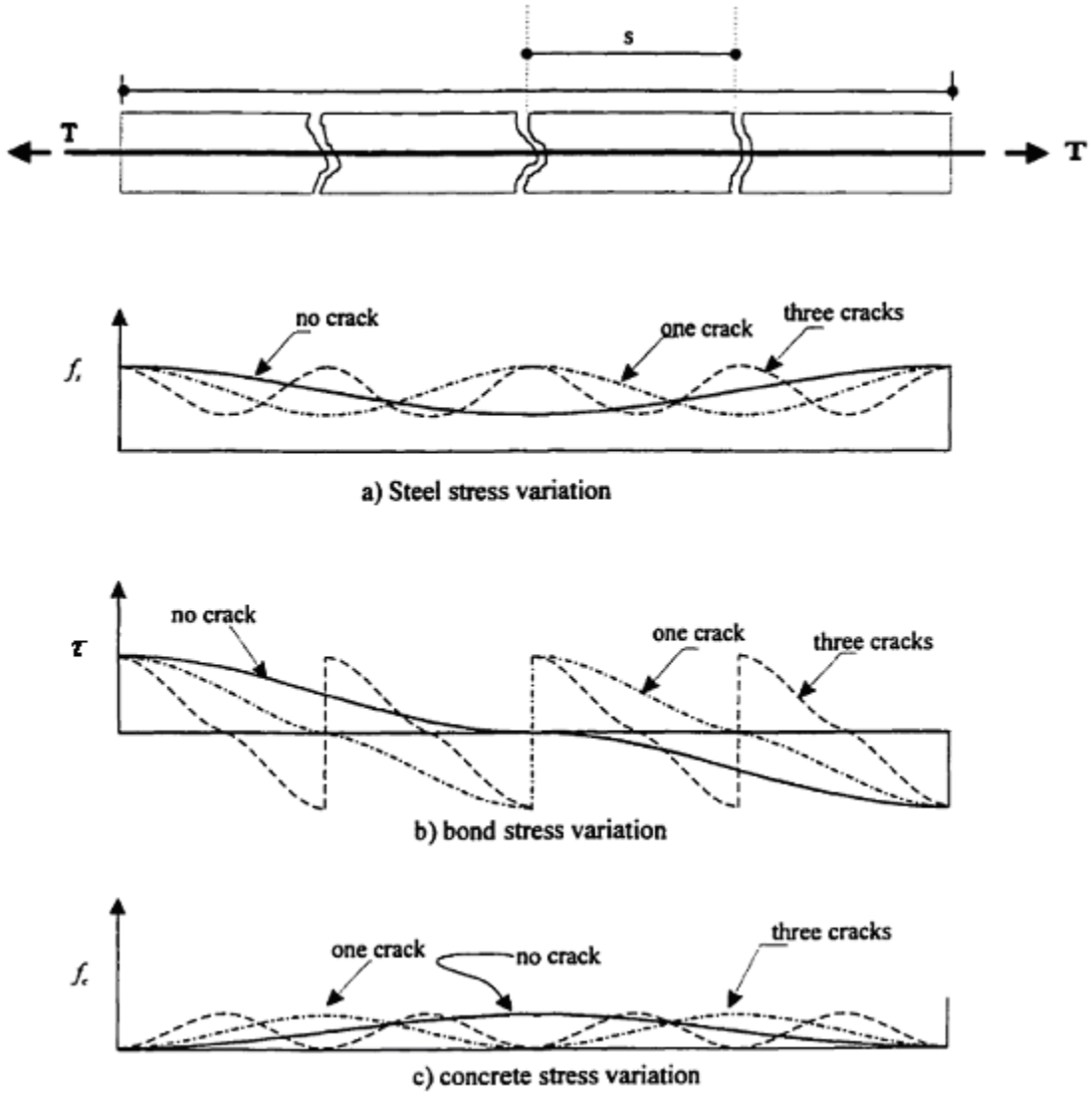

Figure 2.10 Variation of steel, bond and concrete stresses in a tension specimen (Amleh, 2000)

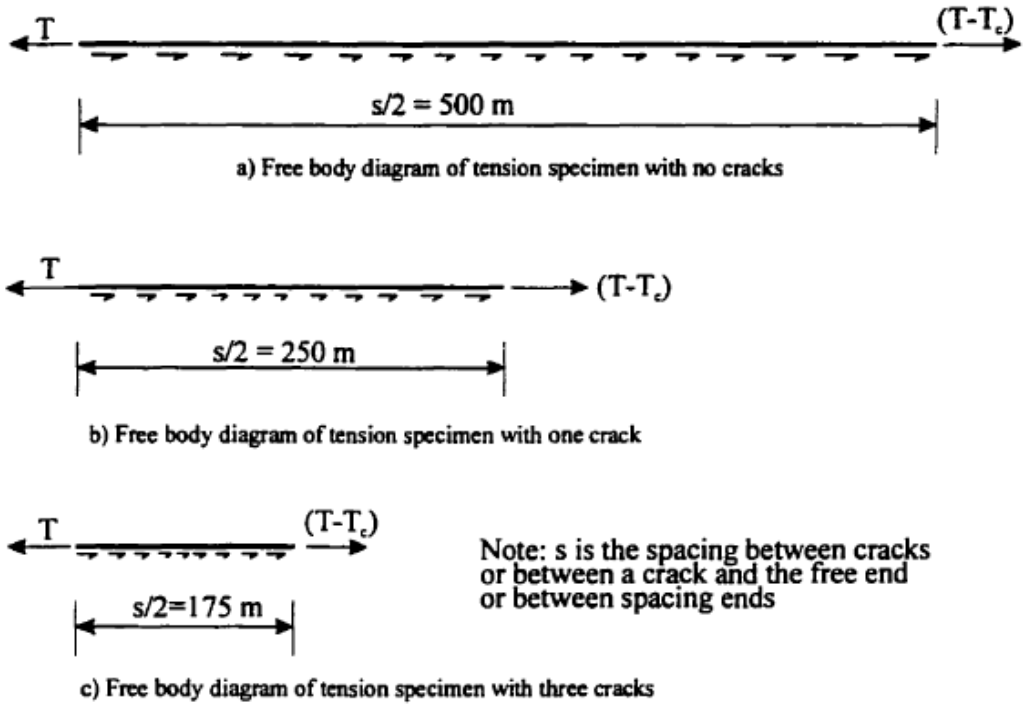

Figure 2.11 Free body diagrams showing forces on the steel bar in a tension specimen with no, one and three cracks (Amleh, 2000)

2.1.5.3 Beam Tests

The influence of flexural tension cracks is included in beam tests, therefore they are considered more reliable than other bond tests (Ferguson 1988). Beam tests can be divided into two types: National Bureau of Standards beam test as shown in Fig, 2.12, and the University of Texas beam test as illustrated in Fig. 2.13.

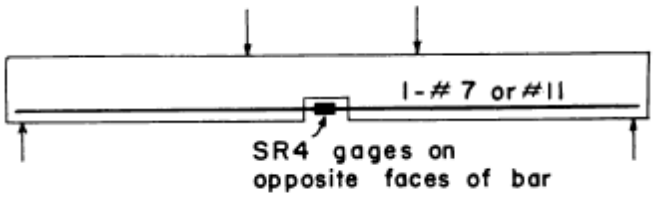

Figure 2.12 Bond beam test – National Bureau of Standard bond test beam (Ferguson, 1988)

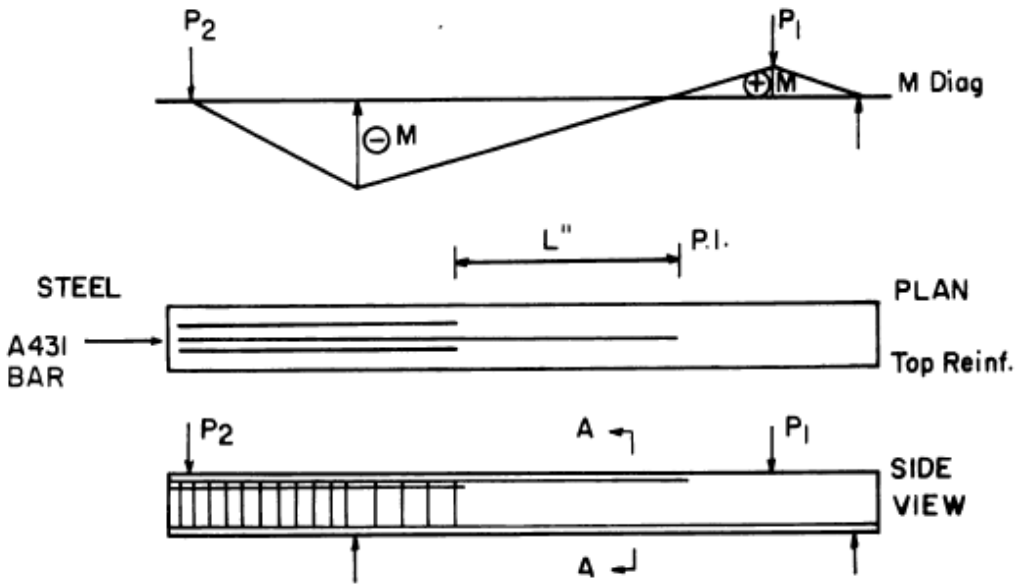

Figure 2.13 Bond beam test- University of Texas (Ferguson, 1988)

The results of this type of test are considered more reliable because the tests truly represent the actual bond stress conditions encountered in the flexural members. However, the major concern in the bond beam test is the reaction restraint that might increase the confining of the concrete over the bar at the supports by increasing the splitting resistance (Ferguson 1988).

Semi-beam specimen or cantilever beam tests have been used to reduce the specimen size and its cost. This test was developed by Kemp et al. (1968) to overcome some of the disadvantages in the pullout test as shown in Fig. 2.14. Some of the advantages of this test are (Kemp et al., 1968):

1. The bond stress obtained from this test is similar to that in the actual flexural members because of the presence of both external shear and bending moments in the test specimen.
2. The tensile strains in the steel bar and concrete are similar to those occurring in actual structures
3. Different types of failure can be produced

The disadvantages of this test are the confining pressure on the steel bar, which increases the beam length to overcome the splitting resistance, and the low ratio of shear to bond stress (Ferguson 1988).

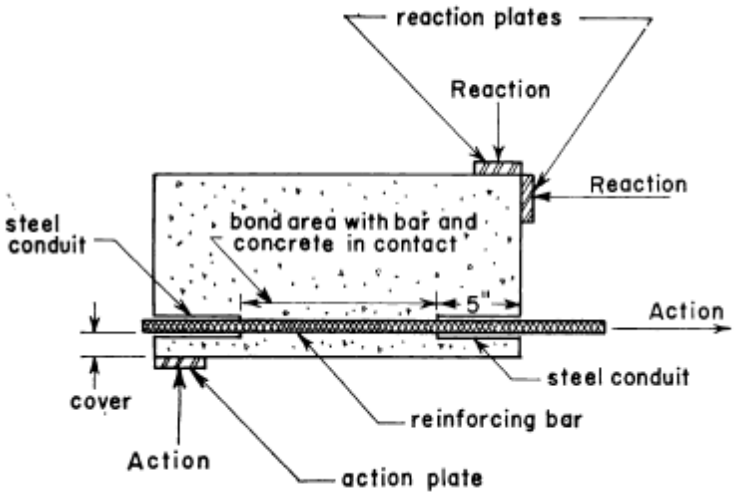

Figure 2.14 Schematic bond test (Kemp et al., 1968)

2.2 Fundamental of Corrosion

2.2.1 Mechanism of Reinforcement Corrosion

Corrosion of steel embedded in concrete is an electrochemical process of the transformation of a metal towards its "natural" form which is its ore state. This transformation occurs because the metal in its ore state such as the oxides contain less energy than pure metals; therefore, they are more thermodynamically stable. The corrosion process takes place as a series of electrochemical reactions with the passage of an electric current only when both anodic and cathodic reactions are possible. Corrosion depends on the type and nature of the metal, the immediate environment, temperature and other related factors.

The steel bar embedded in concrete is normally protected from corrosion as a result of the high alkalinity of the concrete; the pH of the pore water can be greater than 12.5, which protects the embedded steel against corrosion. At this high pH level, a microscopic oxide layer known as the `passive' film, forms on the steel surface during the early stages of cement hydration which naturally protects the embedded steel from corroding. However, when the pH of the concrete changes from 12.5 to 9.5 due to carbonation or increase of the chloride ions concentration near the steel, this layer is destroyed and can no longer protect the embedded steel from corrosion attack.

Carbonation refers to the reaction between the carbon dioxide, present in the air, penetrates into the concrete and the calcium hydroxide which is a primary hydration product that provides the pore solution with its alkalinity. As a result of these reactions, pH in the pores of the cement paste decreases to about 9.5 (Kyle et al, 1999). The penetration of the carbon dioxide depends on the quality of the concrete such as water-cement ratio, and hydration and the degree of saturation of the pores in the cement paste.

The presence of the chloride ions, either in the concrete mix or due to the ingress from the immediate environment, also breaks down the passive layer, when the chloride ions reach a threshold value. Chloride ions react with the passive film to form a soluble iron chloride complex, $[FeCl]^{+}$ (Mindess, 2003). Subsequently this chloride complex reacts further with the hydroxyl groups in the solution resulting in the subsequent release of chloride ions. This release of chloride ions allows for the process to propagate itself, as well as simultaneously bonding free calcium hydroxide. As a result, the corrosion process focuses at local area instead of spreading along the bar, and this result in the formation of deep pits and local loss of bar cross sectional area. Therefore, the damage due to chloride ingress is so dangerous.

In order for corrosion to take place there are four criteria that must be met (Corrosion in reinforced concrete structures 2005):

1. An anodic reaction must be possible by the breakdown of the passive layer that protects the steel at high alkalinities because of lowered pH in pore water due to carbonation or ingress of chloride into concrete reaching a critical level. The anodic reaction is characterized by:

$$Fe \rightarrow Fe^{2+} + 2e^{-} \tag{2.5}$$

2. A cathodic reaction must be possible due to the presence of oxygen at the steel interface. The cathodic reaction is written as:

$$O_2 + 4e^{-} + 2H_2O \rightarrow 4OH^{-} \tag{2.6}$$

3. A flux of ions is possible. Within concrete the electrolyte pore solution serves as a bridge for the transport of ions from cathode to anode

4. A flux of electrons is possible. The reinforcement itself serves as the medium for the transport of electrons between the sites on anodic and cathodic reactions.

Anodic and cathodic reactions take place at the surface of the corroding steel which functions as a mixed electrode that is electrically connected through the body of steel itself.

Reactions at anodes and cathodes are referred to as “half-cell reactions”. The ‘anodic reaction’ is the oxidation process, which results in dissolution or loss of metal (loss of electrons) while the ‘cathodic reaction’ is the reduction process which results in the reduction of dissolved oxygen forming hydroxyl ions. At anodic area, the arrived hydroxyl ions OH^{-} electrically neutralize the Fe^{+2} ions dissolved in pore water and form a solution of ferrous hydroxide at the anode:

$$Fe^{2+} + 2OH^{-} \rightarrow Fe(OH)_2 \tag{2.7}$$

This compound $Fe(OH)_2$ reacts further with additional hydroxide and available oxygen, to form the water insoluble red rust (ferric hydoxide):

$$4Fe(OH)_2 + O_2 + H_2O \rightarrow 4Fe(OH)_3 \tag{2.8}$$

Anodic and cathodic sites are electronically connected as they exist on the same rod and they are ionically connected by concrete pore water functioning as a complex electrolyte as shown in Fig. 2.15.

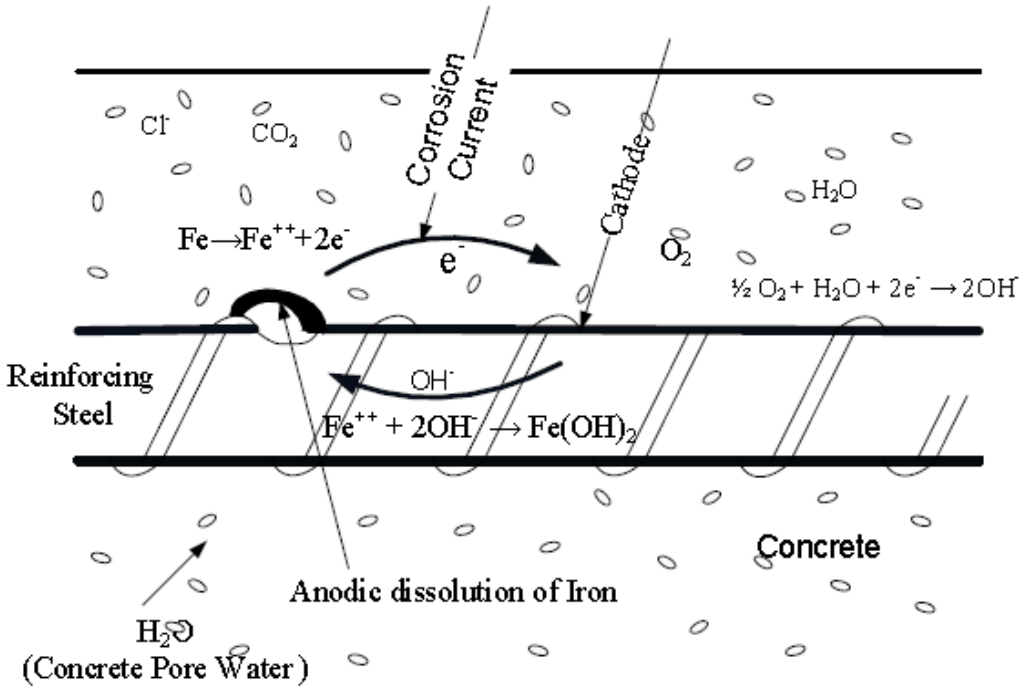

Figure 2.15 Micro-corrosion cell formations in reinforced concrete (Azher, 2005)

Red rust is not the only corrosion product of steel in concrete. Other compounds such as black rust, Fe_3O_4, green rust, $FeCl_2$, and other ferric and ferrous oxides, hydroxides, chlorides, and hydrates are also formed. Their composition depends on the availability of the pore water, its pH and composition, and oxygen supply. Fig. 2.16 shows the relative

increase in the volumes of the various oxides and hydroxides of iron, which increases considerably when water molecules combine with them.

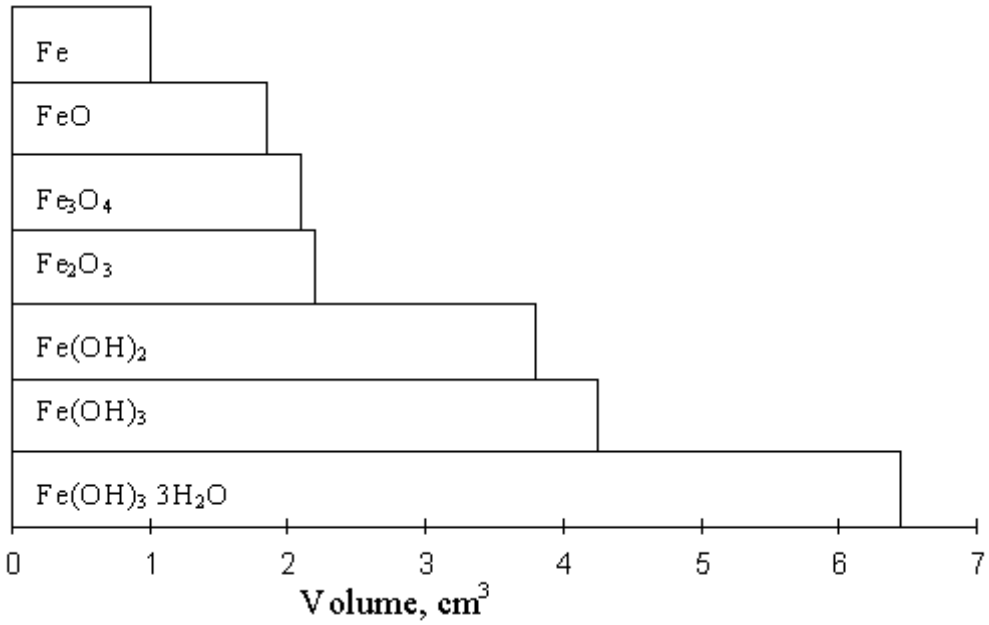

Figure 2.16 The relative volumes of iron and its corrosion reaction products (Nielsen, 1985)

This rust can have a volume two to six times that of the parent iron from which it is formed. The rust product can exert large pressures (similar to bursting pressures in pipes) and cause cracking of the concrete cover leading to its eventual spalling. In addition to loss of cover concrete, a reinforced concrete member may be damaged due to the loss of bond between steel and concrete and loss of rebar cross section. Therefore, it can be noted that oxygen and moisture are the most important elements for reinforcement corrosion to occur and the ingress of these components through the concrete must be controlled to avoid corrosion.

According to the different spatial locations of anode and cathode, corrosion of steel in concrete can occur in two forms:

1. As microcells, where anodic and cathodic reactions are adjacent to each other, and the distance between them may be a micron. Microcell corrosion leads to a

uniform iron dissolution over the whole surface which is generally caused by carbonation of concrete or by very high chloride content at the steel surface.

2. As macrocells, where anodic and cathodic reactions are separated by a finite distance, which may be centimeters or meters. The anode and cathode may occur at the same bar or on different bars with electrical continuity.

Macrocell corrosion is more important because the reduction in cross-sectional area of the rebar may be extremely accelerated due to the large cathode to anode area ratio which may lead to structural safety problems.

2.2.2 Effects of Corrosion on Reinforced Concrete

When the reinforcing bar corrodes, the properties of concrete can be affected in a variety of ways depending on the environment, length of exposure, and concrete type. Corrosion results in the loss of strength, loss of stiffness, loss of bond strength, loss of serviceability, and cracking and spalling of reinforced concrete which can perform individually in combination with each other in order to provide a large variety of potential effects. Spalling of concrete leads to a reduction in the ultimate capacity, and more significantly, a reduction in the stiffness and ductility of the reinforced concrete section due to the loss or breakdown of the bond at steel-concrete interface. Cracking of concrete results in reduction in stiffness of the material, and increases the permeability of the concrete that leads to more critical environmental effects.

When reinforcement corrodes, the formation of ferric hydroxide $Fe(OH)_3$ is accompanied by a large expansion of volume. The expanded volume of corrosion products on the steel bar surface exerts an outward pressure on the concrete and as the pressure builds, the tensile stresses of the concrete may be exceeded the tensile strength of concrete caused through build-up of even a microscopically thin layer of corroding reinforcement (Richardson, 2002). The ultimate result is cracking of the concrete, which in turns results in delamination and spalling stages as illustrated in Fig. 2.17. The first sign of distress could be pop outs or long thin cracks along the line of the reinforcement.

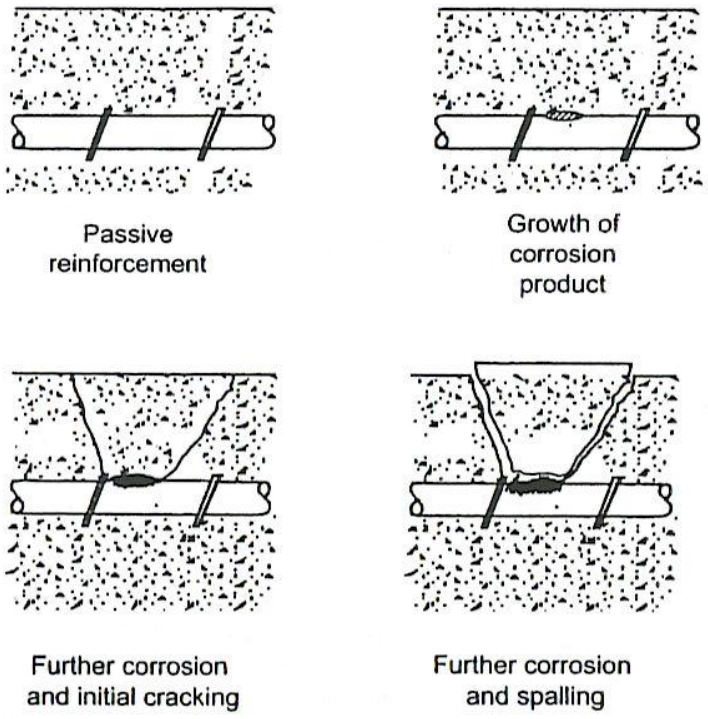

Figure 2.17 Stages in Corrosion-induced damage (Richardson, 2002)

At initial stage, the formation of small amounts of corrosion products increases the bond strength by reducing the concrete porosity (Kyle et al, 1999). However, further increase in the corrosion level develops internal pressure at the steel-concrete interface which causes high tensile stresses in the concrete specimen that leads to concrete cracking. Cracks can reduce the overall strength and stiffness of the concrete structure. In addition, these cracks can increase the ingress of aggressive ions which result in concrete deterioration. The formation of large quantities of corrosion products may result in local expansions. Thus, cracking, spalling and delamination of the concrete take place, resulting in failure of the structure as shown in Fig. 2.18 (Zhou et al, 2005).

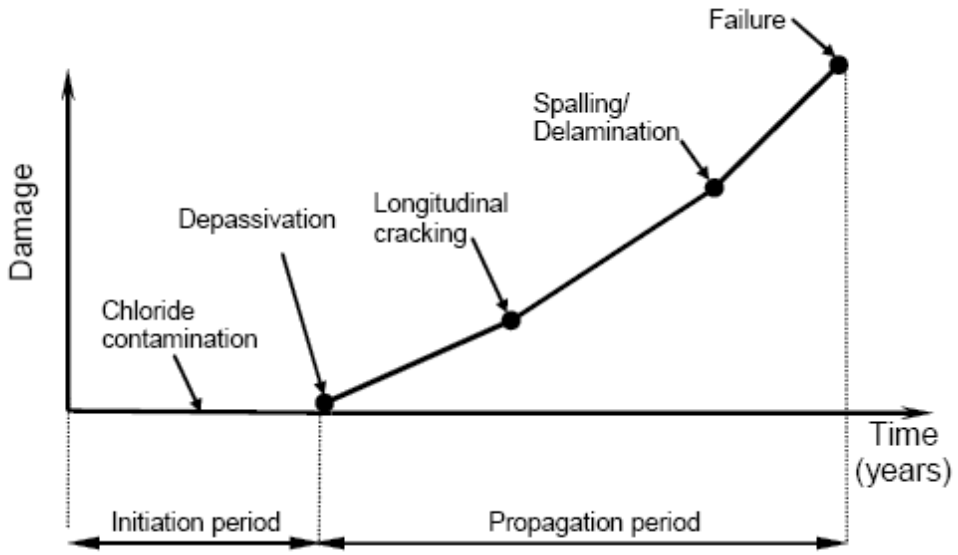

Figure 2.18 Corrosion induced damage of RC structures (Zhou et al., 2005)

The bond strength increases in the beginning up to a certain level of corrosion then decreases when corrosion is very high. The reason for that is the increases in the roughness of the reinforcing bar surface with the growth of a firm layer of corrosion, whereas the loss in bond with further corrosion is due to the severe degradation of bar ribs, the lubricating effect of the flaky corroded metal on the bar surface, and the reduced concrete confinement of the bar due to the widening of the longitudinal corrosion crack (Al-Sulaimani et al. 1990). Similarly, Almusallam et al. (1996) showed that the ultimate bond strength increases with corrosion level from 0 to 4% of mass loss. The reason for that is the increase in the confinement pressure due to the pressure exerted from the expansive corrosion products on the surrounding concrete as well as an increase in the bar roughness in the initial stage. The ultimate bond strength initially increased with an increase in the degree of corrosion until it attained a maximum value of 4% rebar corrosion after which there was sharp decrease in the ultimate bond strength up to 6% rebar corrosion. Beyond the 6% rebar corrosion level the ultimate bond strength did not vary much even up to 80% corrosion as shown in Fig. 2.19. Almusallam et al. concluded that the significant reduction in the bond strength due to significant degradation which reduced the mechanical interlocking of the ribs of the lugs causing the deformed bar to act as a plain bar. In addition, a reduction in the friction

between the bar and the concrete due to accumulated rust layer around the bar**,** and the reduction of the confinement of the concrete around the steel bar due to the formation of the crack was observed.

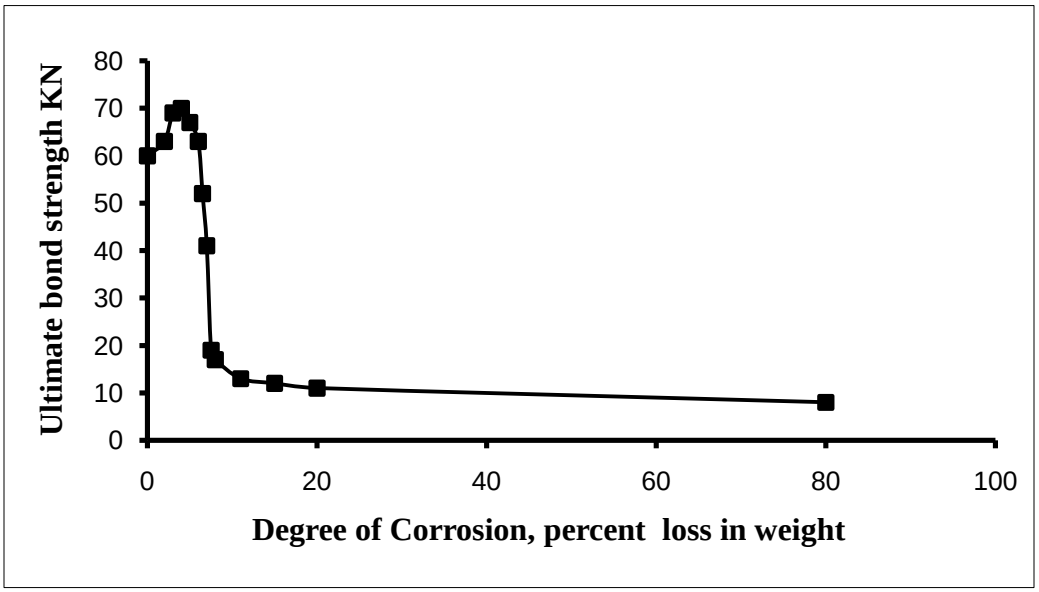

Figure 2.19 Relationship between the ultimate bond strength and different degrees of corrosion for cantilever beam test (Almusallam et al., 1996)

Another effect is the loss of steel area; corrosion is one of the important causes of steel area loss which appears uniformly along the length of the reinforcement. In general, corrosion has two effects: firstly, it will reduce the cross-sectional area of the steel and secondly, it will create local discontinuities in the steel surface. These effects reduce the tensile capacity of the steel due to the loss of its cross-sectional area. Thus, the cross-sectional area of steel decreases as long as the corrosion products increase; therefore, the ultimate moment capacity of structure also decreases, in addition to the bond deterioration, till the area of the steel becomes so small that it can no longer withstand the load and leads to the collapse of the structure.

Yoon et al. (2000) stated that the corrosion reduces the cross sectional area of the reinforcing steel that may cause some stress concentrations in the reinforcing steel, which results in decreasing the ductility of the structure especially when pitting corrosion occurs.

It was determined that corrosion not only affects the bond strength, but it can change the mode of failure as well. Rodrigues et al. (1997) noticed that with corrosion, the failure mode was shifted from bending to shear failure. This change in mode of failure was attributed to the reduction of concrete section due to spalling of top concrete cover and reduction of stirrup section due to pitting. The failure mode in beams with low tensile reinforcement was in bending while the beams with high ratio of shear reinforcement and low uncorroded tensile reinforcement failed by bending in concrete. Fig. 2.20 shows the different types of failure modes that were observed by Rodriguez et al. as detailed below:

Type 1 - occurred in both corroded and un-corroded beams with a low tensile reinforcement ratio.

Type 2 - occurred in beams with high ratio of un-corroded tensile reinforcement and most corroded beams with a high ratio of shear reinforcement.

Type 3 - occurred in almost all the beams with high ratio of corroded tensile bars and large stirrup spacing.

Type 4 - occurred in corroded and un-corroded beams with curtailed tensile reinforcement.

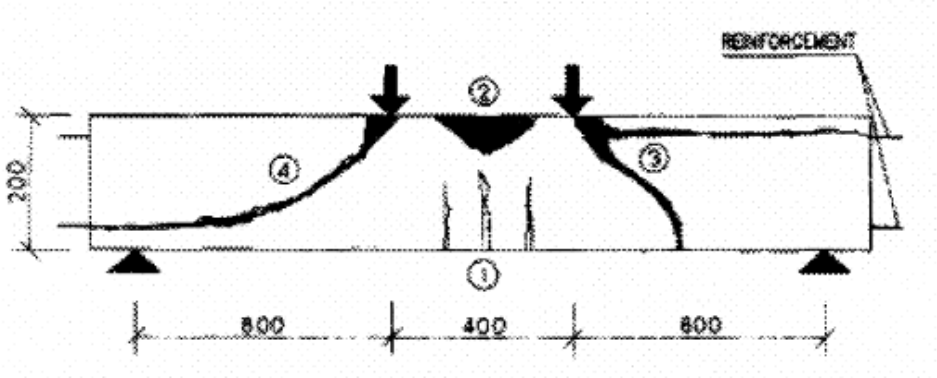

1) Failure by bending (yielding of tensile reinforcement).
2) Failure by bending (crushing of concrete).
3) Failure by shear.
4) Failure by both shear and bond splitting.

Figure 2.20 Different types of failure modes (Rodrigues et al., 1997)

It was also observed that the corrosion increases the crack width and deflections at service load, leading to a decrease in the bond strength, and an increase in both spacing and cracking width at ultimate load (Rodrigues et al. 1997).

Jin and Zhao (2001) observed that the failure mode of corroded reinforced concrete beams changed from ductile mode to brittle mode and was similar to that of plain concrete with the increase of the bar corrosion as shown in Fig. 2.21. Both beams BD1, and BD10 failed in flexure; however, with the slightly corroded beam BD1, there are several main cracks that appeared at the bottom of the beam while in highly corroded beam BD10; the cracks appeared only in one place. They found that the distribution of cracks of corroded reinforced concrete beams became concentrated instead of scattered.

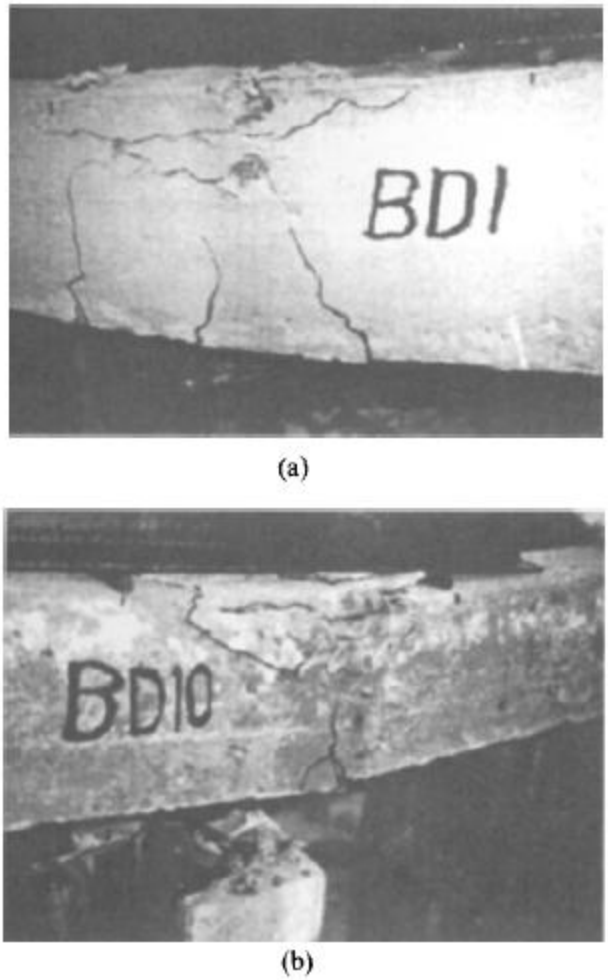

Figure 2.21 Different Failure forms of beam specimens (a) BD1 (b) BD10 (Jin and Zhao, 2001)

2.3 Summary of Research at Ryerson

The following is a brief description of the research projects that were conducted at Ryerson University in the field of corrosion of reinforced concrete. Several detailed investigations dealing with accelerated electrochemical corrosion of reinforced concrete and the modeling of the effect of corrosion on reinforced concrete structures have been completed at Ryerson University:

Yan Lan (2003) conducted an analytical study based on fracture mechanics to investigate the behavior of three different types of specimens. The nonlinear finite element program ATENA with the nonlinear material models for concrete, reinforcement bar and bond-slip was used to analyze cracking propagation and bond failure process. The influence between corrosion and bond slip in RC structure was also studied.

Assem Hassan (2005) studied the influence of corrosion on three different types of steels embedded in four types of concrete. The four used concrete types were; Sundance fly ash concrete mix, Silica fume concrete mix, normal concrete mix with 0.32 w/c ratio, and high w/c ratio concrete mix with (0.52). Each type of these concretes has three different steel types embedded, namely: normal steel bars, stainless steel bars, and pre-damaged epoxy coated steel bars.

Zahir Aldulaymi (2007) studied the influence of increasing levels of corrosion on the progressive deterioration of bond between the steel and concrete and determined the extent to which the various water to cement (w/c) ratio, 0.47 and 0.37, with two concrete cover thicknesses, 40 mm and 65mm, influence the corrosion of the steel reinforcement as well as the chloride ion penetration.

Timothy Joyce and Rogers Smith carried out experimental investigations to study the effect of reinforcement corrosion on the flexural strength of reinforced concrete beams. They observed that the flexural capacity of reinforced concrete beams decreased as the rate of corrosion increased. In addition, a relationship between the reduction of load-carrying capacity and the residual bond strength was identified. Nabil Al-Bayati studied

the effect of corrosion on shear behavior in both NC and SCC beams. In this study, the use of NC and SCC showed minor influences on failure mode, while corrosion showed a higher degree of influence on failure mode and the structural capacity of beams made from both types of concrete.

Alaka Ghosh modeled the bond stress at steel concrete interface for uncorroded and corroded reinforcing steel using nonlinear finite element program ABAQUS. Ghosh modeled the loss of contact pressure and the decrease of friction coefficient with the mass loss of reinforcing steel. Sini Bhaskar developed an analytical model of contact pressure between the reinforcing bar and concrete in a reinforced concrete member.

Chapter 3

REVIEW OF BOND MODELS

A variety of models have been proposed to predict the bond behavior at the steel-concrete interface due to corrosion of reinforcing steel, which can be divided into three groups: empirical, analytical and numerical models. This chapter discusses some of the recent analytical and numerical models of bond in corroded steel bars.

3.1 Lundgren's model (2002)

Lundgren and Gyltoft (2000) developed a bond model at the steel-concrete interface for uncorroded bars using a three dimensional analyses. In this model, the bond stress depends on the slip and on the radial deformation between the bar and the concrete taking into account the effect of cyclic loading with varying slip directions. This model uses the elastic-plastic theory to describe the relationship between the stresses and the deformations; the relationship between the traction, t, and the relative displacement, u, where it is expressed in equation 3.1 and shown in Fig. 3.1

$$\begin{bmatrix} t_n \\ t_t \\ t_r \end{bmatrix} = \begin{bmatrix} D_{11} & \frac{u_t}{|u_t|} D_{12} & 0 \\ 0 & D_{22} & 0 \\ 0 & 0 & D_{33} \end{bmatrix} \begin{bmatrix} u_n \\ u_t \\ u_r \end{bmatrix} \tag{3.1}$$

where t_n = normal splitting stress,

t_t = bond stress,

t_r = stress in direction around the bar,

u_n = relative normal displacement at the interface, and

u_t = slip

The stiffness D_{12} in equation 3.1 is normally negative and leads to negative, t_n, that is, the compressive forces directed outwards in the concrete. The stiffness D_{33} prevents the bar from rotating in the concrete and the traction, t_r, has no influence on the yield lines.

Figure 3.1 shows the physical interpretations of the variables t_n, t_t, u_n and u_t at the surface between the reinforcement bars and the concrete. The initial values of these interface elements have a thickness of zero.

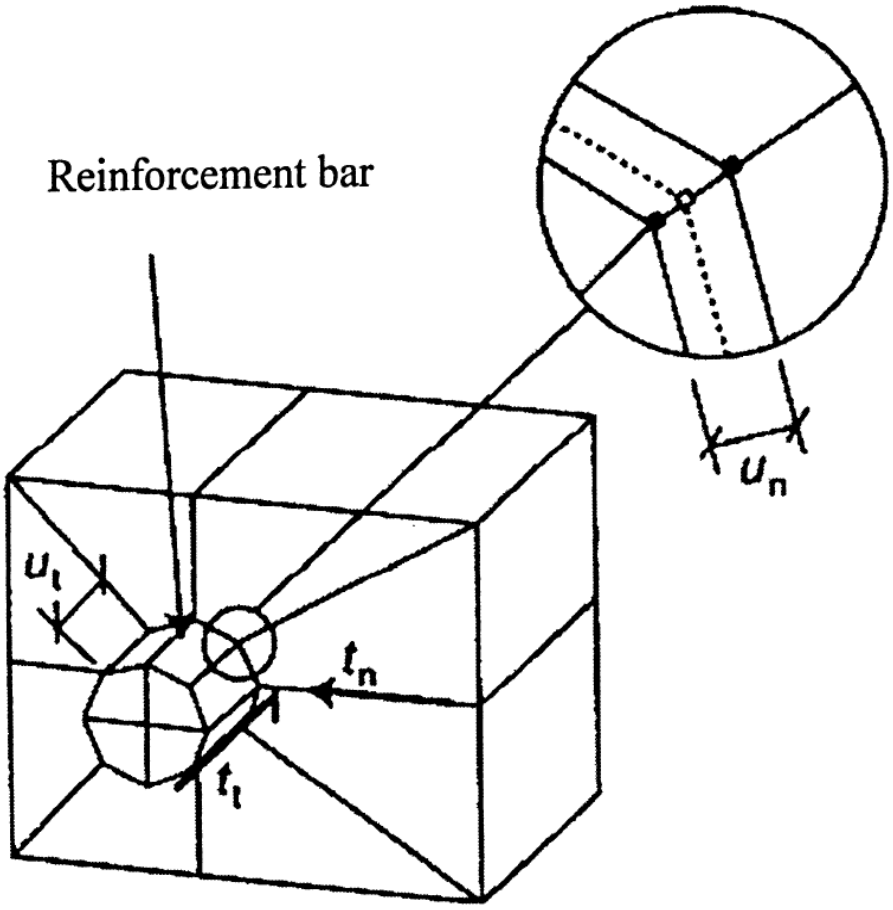

Figure 3.1 Physical interpretation of variables t_n, t_t, u_n and u_t (Lundgren and Gylltoft, 2000)

This model has two yield line functions; the first one, F_1 describes the friction by assuming that the adhesion is negligible:

$$F_1 = |t_t| + \mu t_n = 0 \tag{3.2}$$

The second yield line function, F_2 describes the upper limit at a pullout failure which is determined from the stresses in the inclined compressive struts that result from bond action as shown in Fig 3.2. From the equilibrium in Fig. 3.2:

$$\sqrt{t_t^2 + t_n^2}.dl.rd\varphi = c.dl \sin\alpha.rd\varphi \tag{3.3}$$

and

$$\sin\alpha = \frac{-t_n}{\sqrt{t_t^2 + t_n^2}} \tag{3.4}$$

Therefore,

$$F_2 = t_t^2 + t_n^2 + c.t_n = 0 \tag{3.5}$$

Figure 3.3 shows the yield lines. A flow rule is assumed along the yield function describing the upper limit F_2 for plastic loading and another flow rule is assumed for the yield function describing the friction F_1 for which the plastic part of the deformations is

$$\begin{aligned} du^p &= d\lambda \frac{\partial G}{\partial t}, \\ G &= \frac{|u_t|}{u_t} t_t + \eta t_n = 0 \end{aligned} \tag{3.6}$$

where $d\lambda$ is the incremental plastic multiplier. For the hardening rule of the model, a hardening parameter κ is established as

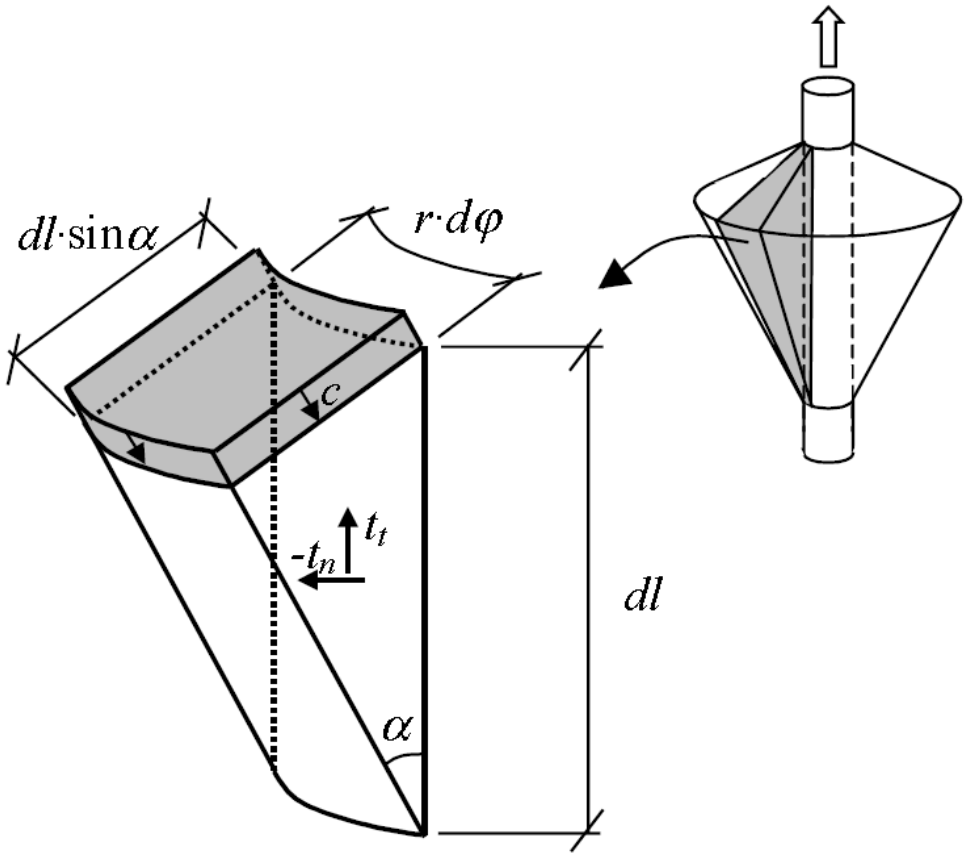

Figure 3.2 The stress in the inclined compressive struts determines the upper limit (Lundgren and Gylltoft, 2000)

$$dk = \sqrt{du_n^{p^2} + du_t^{p^2}} \tag{3.7}$$

The variables μ and *c* in the yield functions are assumed to be functions of k.

The bond stress in this model will increase when the pressure around the bar is lost.

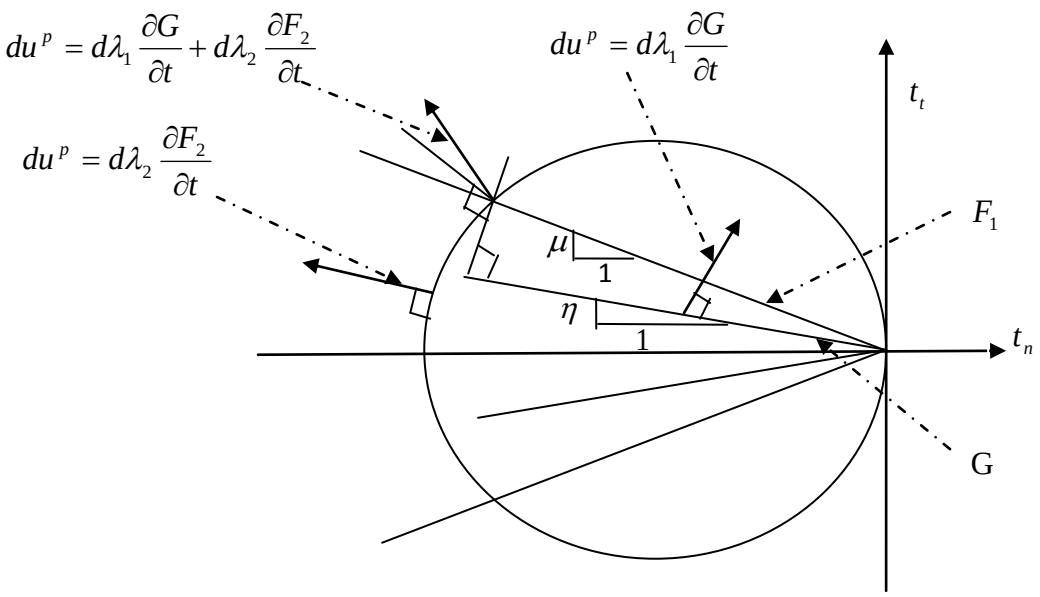

Figure 3.3 The yield lines (Lundgren and Gylltoft, 2000)

In addition, Lundgren (2002) modeled the effect of corrosion on bond between reinforcing steel and concrete. The mechanical behaviour of the corrosive products (stiffness increases with the stress level) was, together with the volume of the rust relative to the uncorroded steel, given as input for a corrosion layer. This corrosion layer was combined with the above mentioned earlier developed model of the bond mechanism, and implemented as a user-supplied subroutine in the finite element program DIANA. Corrosion of reinforcement leads to a volume increase; thus, splitting stresses are induced in the concrete.

Lundgren calculates the free increase of radius a when the normal stresses are zero using the following equation as showing in Fig. 3.4 (Lundgren 2002):

$$a = -r + \sqrt{r^2 + (\upsilon - 1)(2xr - x^2)} \tag{3.8}$$

where,

υ = ratio of rust volume to the volume of original steel bar

x = corrosion penetration depth, and

r = radius of the original steel bar

Figure 3.4 shows the volume increase of the corrosive products compared with the virgin steel. The thickness 'x' is the depth of corrosion attack, which is considered as a function of time. However, due to the strain in the rust, the real increase of the radius is u_{ncor}, which can be calculated from the following equation:

$$\varepsilon_{cor} = \frac{u_{ncor} - a}{x + a} \tag{3.9}$$

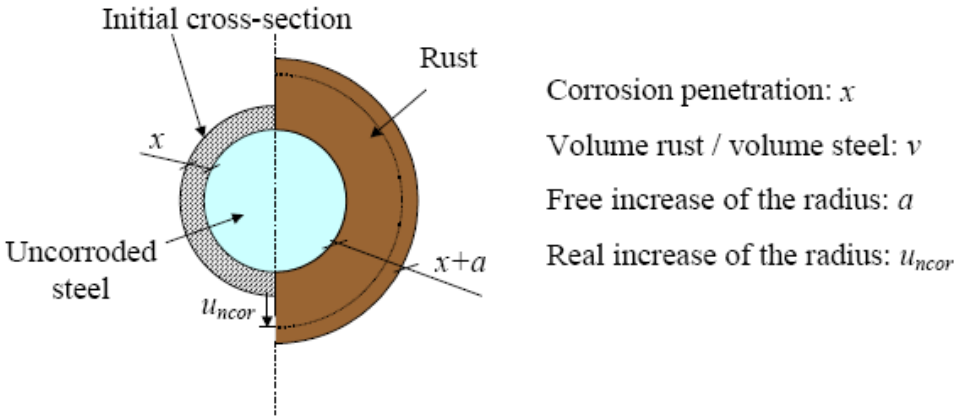

Figure 3.4 Physical interpretation of the variables in the corrosion model (Lundgren's model, 2002)

The normal stresses in the layer are determined from the strain in the rust. This corrosion layer was combined with the model of bond mechanism for uncorroded bar and the deformations are related as:

$$u_n = u_{ncor} + u_{nbond} \tag{3.10}$$

$$u_t = u_{tcor},\ u_{tcor} = 0 \tag{3.11}$$

where, u_{ncor} is the normal deformation of corrosion layer, and u_{nbond} is the normal deformation of bond layer.

The corrosion of reinforcement was assumed to influence the coefficient of friction. The coefficient of friction is calculated by introducing a function k(x/r) as described in the equation given below.

$$\mu(k) = k(x/r).\mu_0(k), \text{ but } \mu(k) \geq 0.4 \tag{3.12}$$

where, $\mu_0(k)$ = function of friction for uncorroded reinforcement, and the function $k(x/r)$ was chosen as shown in Fig. 3.5.

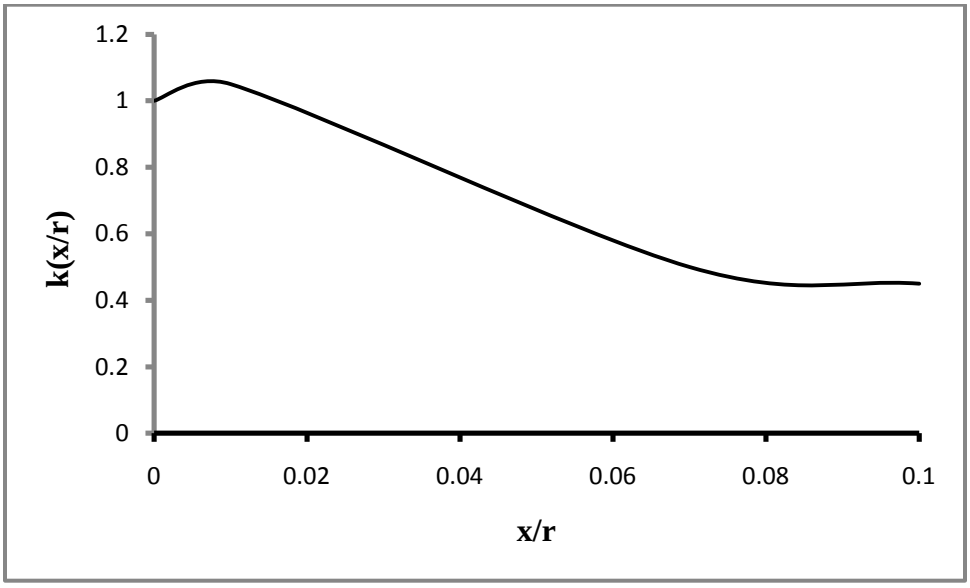

Figure 3.5 The function k(x/r) vs x/r (Lundgren's model, 2005)

3.2 Coronelli's model (2002)

Coronelli (2002) developed a model which predicted the bond strength for corroded bars in reinforced concrete structures by studying the interface pressure caused by the expansion of corrosion product at different confinement stages. For this purpose Coronelli used the relation between the depth x of the corrosion attack and the total crack width W_{cr} was established by modifying the relationship proposed by Molina et al. (1993) as shown in Fig. 3.6.

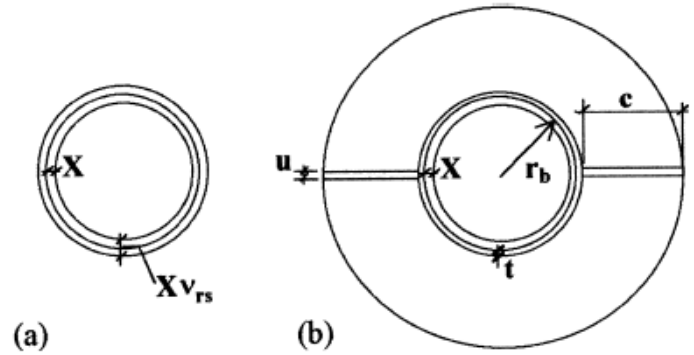

Figure 3.6 Corrosion depth (x) and bar expansion (t) (Coronelli's model, 2002)

The crack width W_{cr} is:

$$W_{cr} = \sum_i w_i^{cor} = 2\pi * t \tag{3.13}$$

With

$$t = (\upsilon_{rs} - 1)x \tag{3.14}$$

Where,

t = thickness of corrosion product

υ_{rs} = ratio between the volumes of the corroded and virgin steel (υ_{rs} = 2)

x = corrosion depth at the onset of primary cracking

w_i^{cor} = opening of each single radial crack

Equation 3.14 assumed that the corrosion products accumulate around the corroded bar and without taking into account that the corrosion products tend to penetrate into the cracks and reach the external surface of the cover; therefore Coronelli modified the equation 3.14 to equation 3.15 by equating the total volume of the oxides formed per unit length of the bar to that of the layer around the bar (thickness $x + t$) plus that within the cracks as shown in Fig. 3.7

$$t = (\upsilon_{rs} - 1)\frac{r_b}{r_b + c}x \tag{3.15}$$

And

$$w = 2\pi.t \tag{3.16}$$

Where,

r_b = bar radius,

c = cover thickness

The pressure due to the expansion of corrosion products cracks the smaller cover first as shown in Fig 3.7 (a); with further corrosion or with increase of loading the final splitting cracks propagate, and correspond to the cracking of the thickest cover. When the bar is confined by equal cover on both sides, this occurs for corner bars or when the bar is placed in a central position in the cross section as shown in Fig. 3.7(b) in which the primary crack pattern coincides with that of the final cracks. When these cracks reach their full propagation, the crack width corresponding to a given corrosion level is evaluated by Eq. (3.15) and (3.16), this quantity is used to calculate the corresponding pressure at the bar concrete interface.

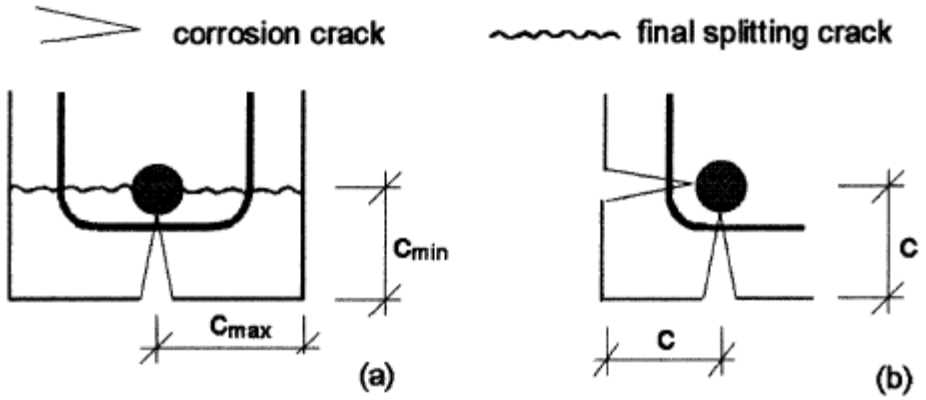

Figure 3.7 Corrosion crack patterns: (a) corrosion cracks smaller cover; and (b) corrosion cracks both sides (Coronelli's model, 2002)

Coronelli (2002) modified the proposed model of Cairns and Abdullah model (1996) for non-corroded reinforcing bars to include the effects of corrosion of reinforcement including changes in rib angle, rib area, rib shape, and the accumulation of expansive corrosion products at the steel-concrete interface which affect friction and adhesion stresses acting on the inclined rib face. He described the ultimate bond strength, $\tau_{bu}(xp)$, for corroded reinforcing bars by the following expression:

$$\tau_{bu}(xp) = K(xp)P^{\max}(xp) + \tau_{AD}(xp) + \varphi(xp)P_{cor}(xp) \tag{3.17}$$

where,

$P^{\max}(xp)$ = maximum pressure at anchorage bond failure,

$\tau_{AD}(xp)$ = cohesive bond strength contribution,

$P_{cor}(xp)$ = pressure developed by corrosion product expansion, and

xp = the corrosion level

The friction 'μ' and adhesion 'f_{coh}' between the corroded reinforcing bar and cracked concrete are proposed by Coronelli (2002) to consider the influence of accumulated rust products on the bar surface.

$$\mu = \tan\varphi = 0.3 - 0.2(x - x_{cr}) \tag{3.18}$$

$$f_{coh} = 2 - 10(x - x_{cr}) \tag{3.19}$$

where,

x = the corrosion penetration depth,

x_{cr} = the corrosion penetration depth associated with through-cracking of cover concrete.

Furthermore a 5% reduction is adopted for the tangent of the angle δ + φ in equation 3.16 for a corrosion depth equal to 100 mm: This follows

$$\tan(\delta + \varphi) = 1.57 - 0.785x \tag{3.20}$$

3.3 Wang-Liu model (2004)

Wang and Liu (2004) developed a new analytical model to predict the bond strength of corroded reinforcing bars without stirrups as shown in Fig. 3.8. To calculate the corrosion pressure before corrosion cracking ($x \le x_{cr}$), the thickness of the rust layer t_r calculated from equation 3.21 developed by Wang and Liu (2004).

$$t_r = \frac{\upsilon_{rs}(2R_i x - x^2) + x(R_c - R_i + x)}{R_c + R_i} \tag{3.21}$$

where,

R_c = the radius of crack front; R_i = the initial radius of the bar; x = the corrosion depth;

υ_{rs} = the ratio between the volume of the rust products and virgin steel.

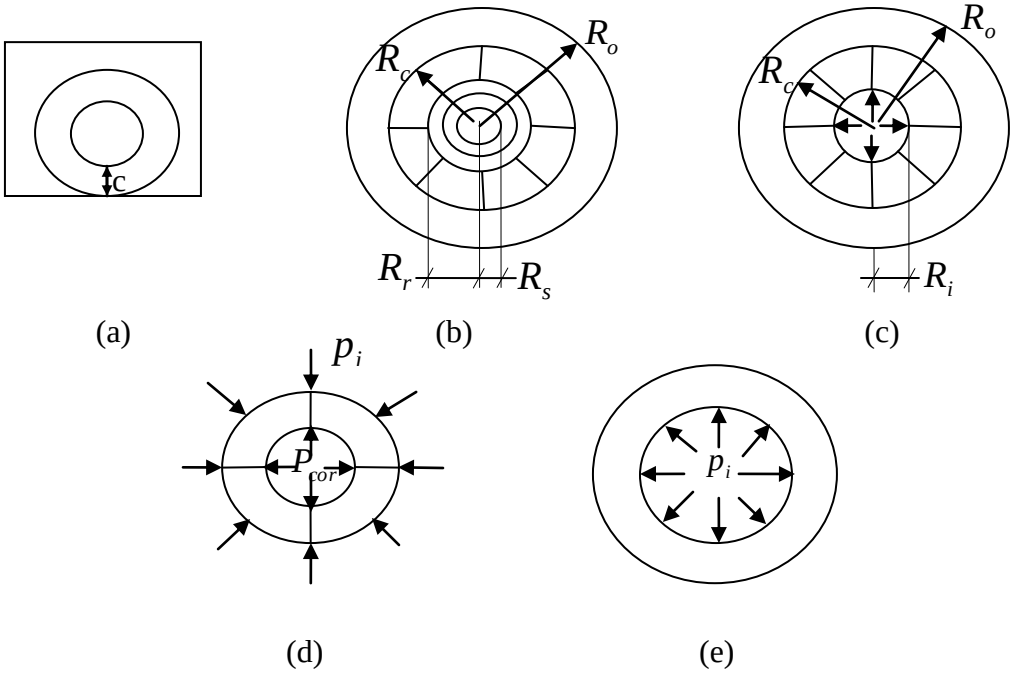

Figure 3.8 Wang and Liu Model
(a) Cylinder model; (b) A thick-walled cylinder undergoes a radial displacement ur = Ri at the inner boundary; (c) A thick-walled cylinder undergoes an equivalent pressure pcor of ur = Ri at the inner boundary; (d) The cracked inner part; (e) The elastic outer part (Wang and Liu, 2004).

When the hoop stresses of the thick-walled cylinder reach the tensile strength of concrete, f_{ct} , at r = R_c, cracking in concrete in the inner part of the thick-walled cylinder is modeled as a process of softening that begins with the exceeding of the tensile strain capacity of concrete at a smeared hoop strain $\varepsilon_\theta > \varepsilon_{ct}$ as shown in Fig. 3.9

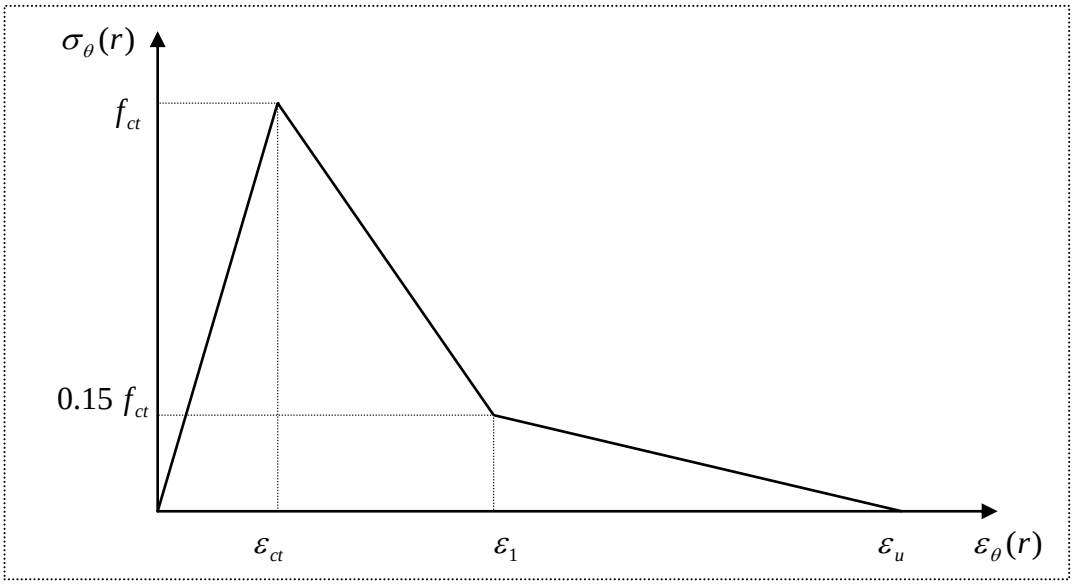

Figure 3.9 Average stress– strain relationship of concrete in tension (Wang and Liu, 2004)

The radial displacement u_r is assumed to be linear elastic and can be calculated from equation 3.22

$$u_r = \frac{f_{ct}.r.(R_o/r)^2 + 1}{E_0.(R_o/R_c)^2 + 1} \tag{3.22}$$

where,

E_o = the young modulus of concrete,

R_o = the outer radius of thick wall cylinder which is equal to $R_i + C$ (the cover thickness)

By equating equation 3.21 to equation 3.22 and assuming r = R_i, the value of different crack penetration depth x can be obtained at different values of the radius of crack front R_c. To obtain the corrosion pressure, P_{cor}, in Fig. 3.8 (d), the equilibrium conditions along any radially cracked section was considered as following:

$$P_{cor}.R_i = pi.R_c + \int_{Ri}^{Rc} \sigma\theta(r)dr \tag{3.23}$$

where $pi = f_{ct}.\dfrac{R_o^2 - R_c^2}{R_o^2 + R_c^2}$ (3.24)

To estimate $\sigma\theta(r)$ in the cracked inner part (Fig. 3.8d), the following equations that describe the relationship between average hoop stress $\sigma\theta(r)$ and strain $\varepsilon\theta(r)$ of concrete in tension were used (Fig. 3.9):

$$\sigma\theta(r) = E_0.\varepsilon\theta(r) \qquad \varepsilon\theta(r) \le \varepsilon ct \qquad (3.25a)$$

$$\sigma\theta(r) = f_t.\left[1 - 0.85.\frac{\varepsilon\theta(r) - \varepsilon ct}{\varepsilon 1 - \varepsilon ct}\right] \qquad \varepsilon ct \le \varepsilon\theta(r) \le \varepsilon 1 \qquad (3.25b)$$

$$\sigma\theta(r) = 0.15 f_t.\frac{\varepsilon u - \varepsilon\theta(r)}{\varepsilon u - \varepsilon 1} \qquad \varepsilon 1 \le \varepsilon\theta(r) \le \varepsilon u \qquad (3.25c)$$

where, $\varepsilon 1 = 0.0003$ and $\varepsilon u = 0.002$ in Fig. 3.9, while to calculate the corrosion pressure after corrosion cracking ($x \ge x_{cr}$), the thickness of the rust layer t calculated from equation (3.26)

$$t = \frac{(\upsilon_{rs} - 1).(2R_i x - x^2)}{R_o + R_i} \qquad (3.26)$$

Similar to the equilibrium condition of equation (3.23), equation (3.27) was used to obtain the corrosion pressure P_{cor} after corrosion cracking:

$$P_{cor}.R_i = \int_{Ri}^{Ro} \sigma\theta(r)dr \tag{3.27}$$

And to estimate $\sigma\theta(r)$ in equation (3.27), the radial displacement distribution in the whole cracked range between R_i and R_o was considered and the corresponding hoop strain $\varepsilon\theta(r)$ at position r ($R_i \le r \le R_o$) can be given as the following:

$$\varepsilon\theta(r) = \varepsilon\theta c.\frac{(R_o / r)^2 + 1}{2} \tag{3.28}$$

where $\varepsilon\theta c$ = the hoop strain at R_o, and $\sigma\theta(r)$ can be found from equation 3.25.

To calculate the bursting and friction forces produced by the bond action of ribbed bars; the geometry of a ribbed bar and the mechanical interactions between the bar and concrete under splitting failure will be used, see Fig 3.10. The core diameter $d_0 = 0.96d_b$, where d_b is the nominal diameter of the uncorroded reinforcing bar; the rib spacing l_r was taken as $l_r = 0.6d_b$. When the corrosion penetration depth reaches x, the nominal diameter becomes d_x, where $d_x = d_b - 2x$, while the average ribs height of uncorroded bar is $0.07\,d_b$; hence, with corrosion the average rib height becomes h_x , where $h_x = 0.07d_x$, see Fig. 3.10. The splitting bond anchorage strength, τ_{crx}, is defined by the following equations and is shown in Figure 3.10:

$$\tau_{crx} = \left[\sin\alpha - f(x).\cos\alpha\right].P_x.\frac{\pi.(d_0 + h_x).h_x}{\pi.l_r.d_x.\sin\alpha} \tag{3.29}$$

where, $$f(x) = 0.6.(1.0 - \frac{t}{h_x}) \tag{3.30}$$

, and the angle of the face of crushed concrete was taken as $\alpha = 25^{\circ}$. P_x and fP_x are the normal compressive force and friction force of the bearing face; where *f* is the friction coefficient of crushed concrete, and P_{crx} is the average radial force.

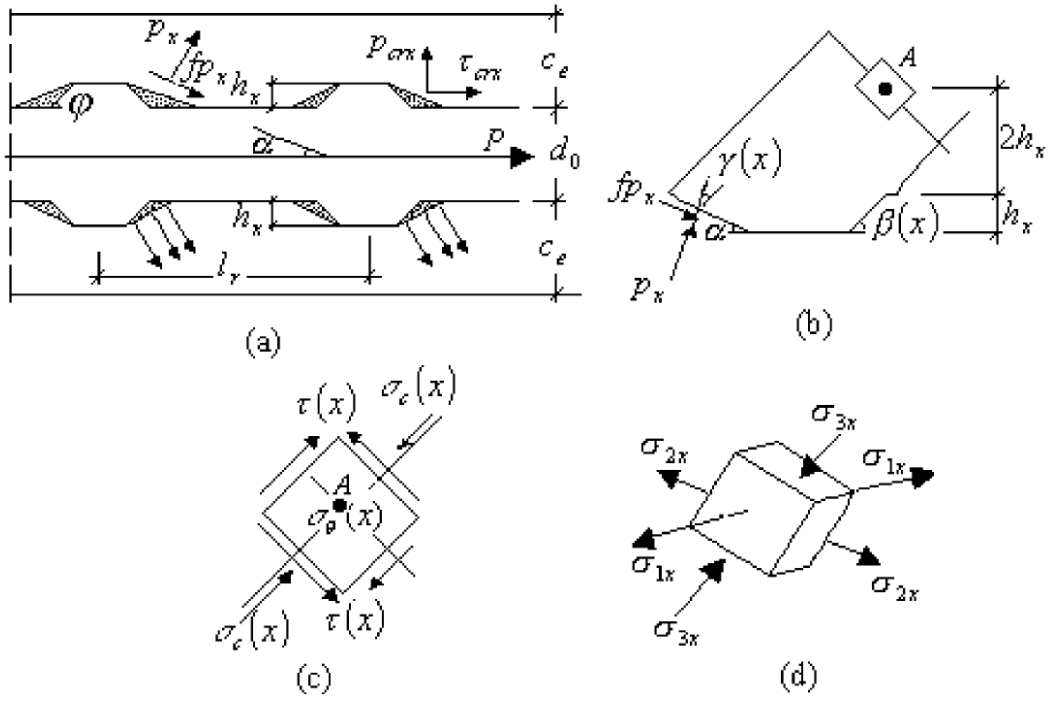

Figure 3.10 (a) Geometry of a ribbed bar and the mechanical interaction between bar and concrete; (b) Point A at the end of concrete key; (c) Stresses of Point A; (d) Principal stresses of Point A (Wang and Liu 2004)

The ultimate bond strength of corroded reinforcements under splitting failure can be obtained from equation 3.31.

$$\tau_{bu}(x) = \tau_{crx} + \tan\alpha.P_{cor} \tag{3.31}$$

3.4 Ghosh-Amleh model (2006)

Ghosh and Amleh (2006) developed a nonlinear finite element model to account for the effect of corrosion on the ultimate bond strength. For this purpose, the non linear finite

element program ABAQUS was used to model the bond stress at steel-concrete interface for different levels of corrosion with different concrete strengths and cover thicknesses.

The developed equation which shows the relationship between the contact pressure and the concrete cover thickness is given by:

$$p^0 = 0.128c + 1.5 \tag{3.32}$$

where p^0 is the contact pressure, and c is the cover thickness.
To calculate the loss of contact pressure at different levels of corrosion for different types of concrete mixtures and cover thickness, a general equation is developed as:

$$L = [(-0.00024 f_c^{'} - 0.0028)c + 4.3]M \tag{3.33}$$

where

L= percentage loss of contact pressure,
$f_c^{'}$ = compressive strength of concrete,
c = concrete cover thickness, and
M = percentage mass loss of steel rebar

They used equation 3.34 to calculate the friction coefficient, u, at the uncorroded steel rebar-concrete interface, while equation 3.35 was used for corroded steel bars:

$$\mu = \mu_k + (\mu_s - \mu_k)e^{-\mathbf{d_c}\gamma_{\mathbf{eq}}} \tag{3.34}$$

$$\mu = \mu_k + [(\exp - 0.035M) - \mu_k]\exp - [(0.0261M + 0.45)]\gamma_{eq} \tag{3.35}$$

They investigated and modeled the radial force and the vertical component of reaction at the rebar lug which cause the contact pressure at the steel-concrete interface as shown in

Fig. 3.11. For both the uncorroded and the corroded bar, the bond stress was calculated by modeling the normal contact pressure and the friction at the steel-concrete interface. To express the non-linear behaviour of the steel and concrete, both elastic and plastic properties were assigned. Eight noded solid elements were used for both the concrete and steel bar and the interface between the steel bar and the concrete was simulated by using a surface-based interaction with an exponential decay friction factor. A monotonic load was applied on the top surface of the reinforcement, and the top concrete surface of the cylinder was prevented from translating. For each load increment, the slip was computed at the loaded end of the reinforcing steel.

It was found that the corrosion of reinforcing steel increases the hoop and radial stresses due to the increase in the volume of the expanded corrosion products, the deterioration of the ribs and the reduction of the effective cross-sectional area of the steel bar. In addition to that, the friction force between the reinforcing steel and the concrete is also reduced due to the lubricating effect of flaky corroded layer. Therefore, the contact pressure at the steel-concrete interface decreases rapidly with an increase in the corrosion level, especially in the case of any severe localized corrosion.

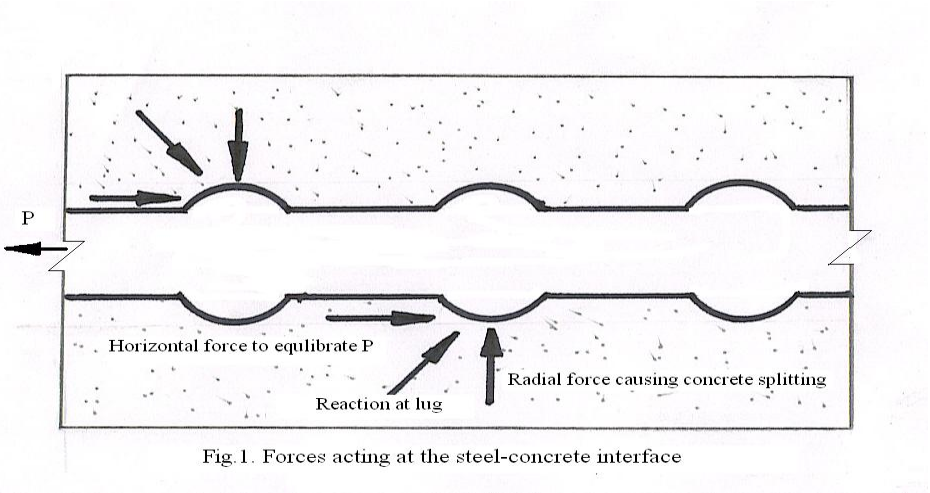

Figure 3.11 Forces acting at the steel concrete interface (Amleh-Ghosh model, 2006)

3.5 Bhargava-Ghosh-Mori-Ramanujam model (2007)

Bhargava et al. (2006) developed a new model to calculate the radial corrosion pressure in corroded bars caused by the expansive corrosion products before and after through-

thickness cracking of the cover concrete as shown in Fig. 3.12. In this model, the thick walled cylinder was divided into two zones; zone 1 is the cracked concrete and zone 2 is the uncracked concrete. The cracking in the concrete cover thickness was modeled as a process of tension-softening according to CEB-FIP, 1990. The concrete was assumed to be linear-elastic before cracking, and was assumed contribute to tension-softening once a crack occurred. The corrosion pressure P_{cor} was calculated from the following equations:

$$u_C = \frac{d_C.E_{ef1}\left[(1-\nu_{C2})R_C^2 + (1+\nu_{C2})R_0^2\right]\left[2R_iR_C\right]}{E_{ef2}\left[(1-\nu_{C2})R_C^2 + (1+\nu_{C2})R_0^2\right]\left[(1-\nu_{C1})R_i^2 + (1+\nu_{C1})R_C^2\right] - E_{ef2}(R_C^2 - R_i^2)(R_C^2 - R_0^2)(1-\nu_{C1}^2)} \tag{3.36}$$

$$R_C = \sqrt{\frac{1}{\dfrac{f_{ct}(1+\nu_{C2})}{E_{ef2}\left[\dfrac{(1+\nu_{C2})u_C R_C R_0^2}{(1+\nu_{C2})R_0^2 + (1-\nu_{C2})R_C^2}\right]} - \dfrac{1}{R_0^2}}} \tag{3.37}$$

$$P_{cor} = \frac{E_{ef1}}{(1-\nu_{C1}^2)}\left[\left\{\frac{u_C R_C - d_C R_i}{R_C^2 - R_i^2}\right\}(1+\nu_{C1}) - \frac{R_C}{R_i}\left\{\frac{d_C R_C - u_C R_i}{R_C^2 - R_i^2}\right\}(1-\nu_{C1})\right] \tag{3.38}$$

where,

u_C = radial displacement at R_c; E_{ef1}, E_{ef2} = effective modulus of elasticity for zone 1 and zone 2 respectively including the effect of creep = $\dfrac{E}{1+\varphi_c}$ and φ_C = creep coefficient of concrete = 2; ν_{C1}, ν_{C2} = Poisson's ratio for zone 1 and zone 2 respectively; d_c = radial displacement at R_i which is equal to the thickness of corrosion products; f_{ct} = residual tensile strength of the cracked concrete.

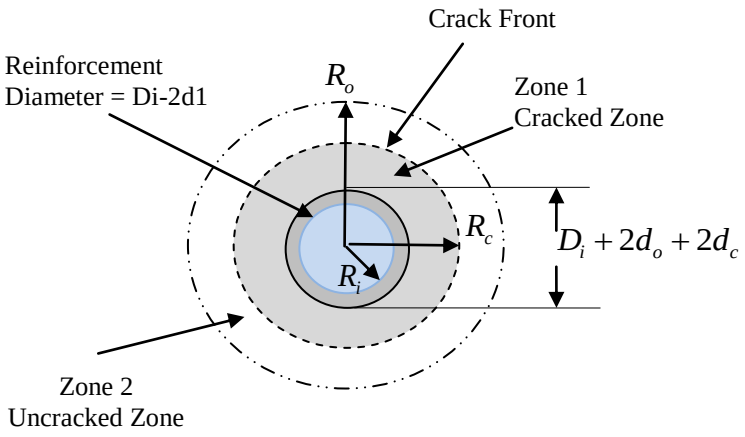

Figure 3.12 Two zones for cover concrete due to corrosion cracking process (Bhargava et al., 2006)

Bhargave et al. (2007) slightly developed the relationship (Equation 3.17) for ultimate bond strength $\tau_{bu}(xp)$ given by Coronelli (2002) to account for the corrosion products. The proposed $\mu(xp)$ and $f_{coh}(xp)$ are based on the range values suggested by Coronelli (2002) and take into consideration the influence of accumulated rust products between the corroded reinforcing bar and cracked concrete. The proposed relationships for bond strength due to adhesion are as follows:

$$\tau_{AD}(xp) = \frac{nA_r(xp) f_{coh}(xp)[\cot\delta(xp) + \tan(\delta+\varphi)(xp)]}{\pi D_r(xp) S_r} \tag{3.39}$$

$$\mu(xp) = \tan\varphi(xp) = 0.37 - 0.26(x - x_{cr}) \tag{3.40}$$

$$f_{coh}(xp) = 3.68 - 22.08(x - x_{cr}) \tag{3.41}$$

where x is the corrosion penetration depth corresponding to corrosion level xp ; x_{cr} is the corrosion penetration depth associated with through-cracking of cover concrete. In the proposed model the relationship for $\tan(\delta+\varphi)(xp)$ has been modified after considering initial values for δ and $\tan\varphi$ as 45° and 0.3, respectively for uncorroded reinforcing bar and a 5% reduction in $\tan(\delta+\varphi)(xp)$ for a corrosion penetration depth of about 100 μm.

$$\tan(\delta+\varphi)(xp) = 1.857 - 0.9285x \tag{3.42}$$

Bhargava et al (2007) modified the original relationship of Giuriani et al. (1991) that consider the confining actions due to the residual tensile strength of the cracked concrete and the stirrup legs to incorporate the effect of corrosion products. The maximum pressure at bond failure at any corrosion level *xp* is proposed to be evaluated as follows:

$$P_{\max c}(xp) = \left[\frac{b}{n_b\{D_r(xp)+2d_c(xp)\}} - 1\right] f_t(xp) \tag{3.43}$$

$$P_{\max s}(xp) = \left[\frac{n_s A_s}{n_b\{D_r(xp)+2d_c(xp)\}s_v}\right] \times E_{st}\sqrt{\frac{a_2 w(xp)^2}{D_s^2\alpha^2} + \frac{a_2 w(xp)}{D_s\alpha} + a_0} \tag{3.44}$$

$$P_{\max}(xp) = P_{\max c}(xp) + P_{\max s}(xp) \tag{3.45}$$

where b = width of member; n_b = number of reinforcing bars; w = fictitious splitting crack opening; n_s = number of legs of the stirrups in the cross section width b; A_s = cross sectional area of the stirrup leg; S_v = spacing of the stirrups; E_{st} = modulus of elasticity of the stirrup steel; a_0, a_1, a_2 = coefficients taken from the reference (Giuriani et al., 1991); α = shape factor characterizing stirrup bar = 2.

Chapter 4

ANALYTICAL MODELING OF BOND STRESS AT STEEL-CONCRETE INTERFACE DUE TO CORROSION

An analytical model, which describes the contact pressure at the steel-concrete interface in a reinforced concrete, is developed. The effect of corrosion is considered in the model to determine contact pressure due to corrosion. Also, this chapter illustrates the procedure involved in developing the expression for the contact pressure at the bar-concrete interface for the proposed model.

4.1 Introduction

The bond between steel and concrete is the critical feature of reinforced concrete that makes the use of concrete as a structural material possible. It has been established that with corrosion of the reinforcement the bond strength decreases rapidly with an increase in the corrosion level, especially in the case of any severe localized corrosion. The bond behaviour is influenced by the deterioration of the reinforcing bar ribs, and by the reduced adhesion at the reinforcing bar surface due to the widening of the splitting cracks resulting from corrosion. Corrosion, especially with severe localized corrosion, causes a significant reduction of the interlocking phenomenon between the ribs and the concrete keys due to the deterioration of the reinforcing bar ribs. This reduction of the interlocking between the reinforcing bar and the concrete, retards the primary mechanism of the bond in deformed bars, which is the transfer of forces by mechanical interlocking of the ribs, and hence, the bond strength decreases significantly.

Several theoretical and analytical models have been developed, to predict the loss of bond strength as a result of corrosion, however, considerable variations in the prediction of bond loss have been reported. Hence, a better understanding of the mechanism through which corrosion affects bond is necessary to enable the controlling factors to be better

understood, to resolve the apparent inconsistencies between different studies, and to enable effective models to be developed.

The analytical modeling of engineering contact problems is one of the most difficult and demanding tasks in computational mechanics. As was mentioned earlier, bond behavior depends on many phenomena that occur at the steel concrete interface, such as the transverse microcracking that develops at the very early load phase, the local crushing of the porous concrete layer around the rib of the reinforcing bar, and the splitting of surrounding concrete when the wedge action of the steel reinforcing ribs radial stresses exceeds the tensile strength of the concrete. Theoretical expressions for the bond strength between steel and concrete may be developed by equating the bursting force generated by bond action to the splitting resistance of the concrete section (together with any confining reinforcement if present). In general, once the main parameters have been identified, analytical and theoretical models are conceived on the basis of a few fundamental assumptions, which aim at describing the dominant resistant mechanism or the local bond stress/bar slip relationship.

4.2 Modeling bond-stress at steel-concrete interface

The majority of research efforts have been directed to the side of the equation dealing with splitting resistance; such as the study done by Tepfers (1973), and many other researchers. At this stage, reference is made locally, generally to a portion of an embedded bar, and not to the entire anchorage or splice length: a typical case is the thick-walled concrete ring subjected to an inner hydrostatic pressure simulating the wedging action of a reinforcing bar, which have been introduced since the mid seventies by Tepfers (1973 and 1979).

Tepfers (1979) studied the stress distribution over the thick-walled cylinder, subjected to internal shear and pressure, confining the reinforcing bar, who assumes the radial components of the bond forces (the confinement forces) are balanced against concrete rings in tension, which resist the tensile hoop stresses. In this contrast the internal shear

and pressure correspond respectively to the bond and radial stresses developed at the concrete-steel interface, where the radial force transfer at the concrete-steel interface determines the tensile hoop stress developed in the concrete surrounding the bar and thus the critical load. In other words, the transfer of forces between the steel and concrete is achieved by the bearing of ribs on the concrete when the bond failure is approached. The resultant compressive forces exerted by the rib make an angle α with the reinforcing bar axis. These forces create circumferential tensile stresses in the concrete around the bar as shown in Fig. 4.1. The radial components of the bond forces are balanced by the tangential stresses in the concrete, Fig. 4.2 shows the forces exerted by the concrete on a deformed bar in the reinforced concrete.

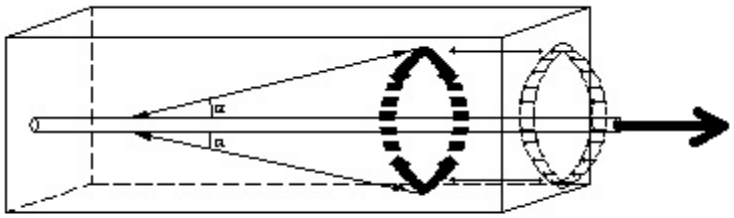

Figure 4.1 Tensile stress in concrete ring due to the force transfer between steel and concrete (Tepfers, 1979)

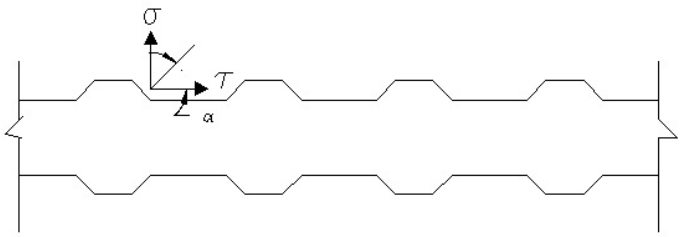

Figure 4.2 Forces exerted by the concrete on a ribbed bar in a reinforced concrete (Tepfers, 1979)

As shown in Fig. 4.2, the radial bond stress component, σ, is balanced by tangential tensile stresses in the concrete then:

$$\sigma = \tau \tan\alpha \tag{4.1}$$

Giuriani et al. (1991), stated that the radial pressure of the bond stresses equilibrates by the confining action arises from the following:

1. The tensile strength of the uncracked part of the surrounding concrete
2. The residual tensile strength transferred by the faces of the splitting cracks, and
3. The transverse reinforcement

In the present work, the confining action from transverse reinforcement is neglected for simplicity. However, it should be noted that the surface conditions of a bar might influence bond strength, an aspect again neglected by the "hydraulic pressure" analogy. Hence, both sides of the equilibrium equation should be considered in equal depth to obtain a balanced analysis of bond strength. In addition, a balanced study of the local bond behavior should also consider the splitting crack opening (crack width) that is related to the confining action that is present along the reinforcing bar (Gambarova and Giuriani, 1985).

Pantazopoulou and Tastani (2002) used the simple friction model to explain the relationship between bond-stress, τ, normal contact pressure, P, and coefficient of friction, μ, at the steel-concrete interface as shown in Fig. 4.3.

$$\tau = \mu P \tag{4.2}$$

According to Fig. 4.3, the bond stress depends on the normal contact pressure. When the normal contact pressure is large, higher frictional force will be required for the splitting failure to occur. Three mechanisms contribute to normal contact pressure: the hoop

tensile stresses in the concrete cover, the transverse reinforcement crossing the splitting crack path, and transverse compressive stress fields existing in the anchorage region (Pantazopoulou and Tastani 2002).

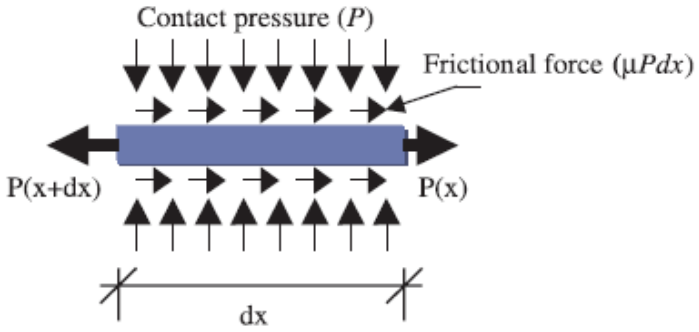

Figure 4.3 Frictional model for bond (Pantazopoulou and Tastani, 2002)

Based on the same methodology mentioned above, thick-walled cylinder analogy and equation 4.2 will be used in the present work to determine the bond stresses due to the confining action, and the corrosion pressure exerted from the expansion of corrosion products.

4.3 Proposed analytical model for contact pressure

4.3.1 Assumption for the study

In the proposed model the corrosion is assumed to be uniformly distributed along the reinforcing steel bar. The analogy of a thick-walled cylinder is adopted. Figure 4.4 shows the sketch of the model. The concrete surrounding the corroding reinforcing bar is considered as a thick-walled hollow cylinder with the wall thickness equal to the minimum concrete cover thickness (Coronelli 2002). According to Fig. 4.4(b), σ_θ and σ_r are the tangential (hoop or circumferential) and the radial stresses, respectively, at any internal point of the thick-walled cylinder cross-section. The radial pressure, σ_r, due to bond action on the concrete is regarded as hydraulic pressure acting on a thick-walled concrete cylinder as shown in Fig. 4.4(a).

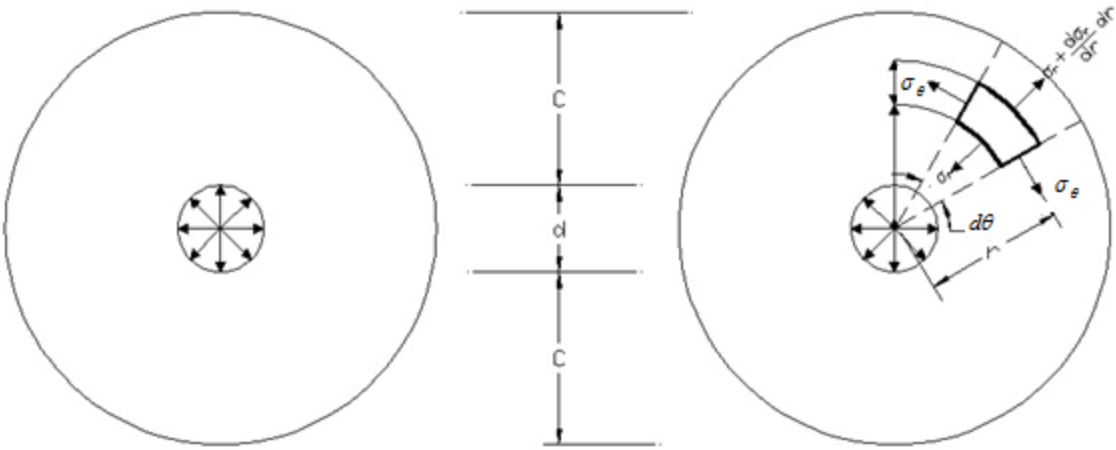

(a) (b)

Figure 4.4 Interaction between concrete and steel at the interface: (a) thick-walled cylinder approach of the prism cross-section, and (b) stresses in concrete

4.3.2 The expression for ultimate bond strength

Coronelli (2002) modified the model for non-corroded reinforcing bars proposed by Cairns and Abdullah (1996) for splitting bond-failure, to consider corroded bars as was explained in Chapter 3 and given in Equation 3.17. The modifications of the model included changes in rib angle, rib area, rib shape and the accumulation of corrosion products at the steel-concrete interface which interns affects the friction and adhesion stresses acting on the inclined rib face. The ultimate bond strength for corroded reinforcing bars will be adopted in the proposed model; therefore, Equation 3.17 can be written as following:

$$\tau_{bu}(xp) = \tau_{CP}(xp) + \tau_{COR}(xp) + \tau_{AD}(xp) \tag{4.3}$$

where, xp refers to the corrosion level, τ_{bu} = ultimate bond strength for corroded reinforcing bar; τ_{CP} = bond strength contribution of maximum confining pressure at

anchorage bond failure; τ_{AD} = bond strength contribution due to adhesion between corroded steel and cracked concrete; τ_{COR} = bond strength contribution of corrosion pressure.

4.3.3 Derivation of the expression for Adhesion

Bhargava et al. (2007) slightly modified the Coronelli (2002) equation to account for the effect of corrosion products as shown in equation 4.4

$$\tau_{AD}(xp) = \frac{n.A_r(xp).f_{coh}(xp)\left[\cot\delta(xp) + \tan(\delta+\phi)(xp)\right]}{\pi D_r(xp).S_r} \tag{4.4}$$

where, n = the number of transverse ribs at a section; $A_r(xp)$ = the rib area in plane at right angles to the bar axis; $f_{coh}(xp)$ = the adhesion strength; $D_r(xp)$ = reduced diameter of the corroded reinforcing bar; s_r = the rib spacing which is equal to $0.6D_i$ (Wang and Liu 2004); and D_i = initial diameter of the reinforcing bar. The rib area A_r can be calculated from equation 4.5 (Bhargava et al. 2007).

$$A_r(xp) = \pi D_r(xp)h_r(xp) \tag{4.5}$$

where, $h_r(xp)$ = the rib height and equal to $0.07D_r(xp)$ (Wang and Liu 2004). Based on the values suggested by (Coronelli 2002), $f_{coh}(xp)$ can be obtained from equation 4.6.

$$f_{coh}(xp) = 3.68 - 22.08(x - x_{cr}) \tag{4.6}$$

where x is the corrosion penetration depth; x_{cr} is the corrosion penetration depth associated with through-cracking of cover concrete. Based on the initial values that were proposed by Coronelli for the relationship for tan ($\delta + \varphi$)(xp) after considering initial values for δ and tanφ as 45° and 0.3, respectively for uncorroded reinforcing bar and a 5% reduction in tan ($\delta + \varphi$)(xp) for a corrosion penetration depth of about 100 µm.

$$\tan(\delta+\varphi)(xp) = 1.857 - 0.9285x \tag{4.7}$$

4.3.4 Derivation of the expression for confining pressure

The original relationship of Giuriani et al. (1991) has been modified to incorporate the effect of corrosion products and exclude the effect of transverse reinforcement. Equation 4.8 shows the original relationship by Giuriani et al. (1991), without the effect of confinement due to transverse reinforcement.

$$\sigma_n = B\sigma_{rc} \tag{4.8}$$

where, σ_n = radial pressure produced by principal bar ribs on surrounding concrete; σ_{rc} = residual tensile stress in cracked concrete; B= concrete index of confinement, which is defined as the ratio between the net concrete split area, B_c, and the area of the longitudinal section of the anchored bars in the splitting plane, B_s, $= B_c / B_s$

$$B_c = \frac{b - nd_b}{b} \tag{4.9}$$

$$B_s = \frac{nd_b}{b} \tag{4.10}$$

and the residual tensile stress of the cracked concrete has been suggested by Giuriani and Rosati (1986) as a function of crack opening and aggregate size:

$$\sigma_{rc} = \frac{f_{ct0}}{k\frac{w}{\phi_a} + 1} \tag{4.11}$$

where, f_{ct0} = maximum residual strength of cracked concrete at onset of cracking (w=0); b = width of the member; n = number of reinforcing bars; d_b = diameter of the reinforcing bar; w = fictitious splitting crack width; k = coefficient of the curve; ϕ_a = maximum aggregate size.

As shown in Fig. 4.5(a), for thick walled cylinder; $b = 2R_0$; n = 1; $d_b = 2R_i$.

Substituting equations 4.9 and 4.10 into equation 4.8:

$$\sigma_n = \left(\frac{2R_0 - 2R_i}{2R_i}\right).\sigma_{rc} = \left(\frac{R_0}{R_i} - 1\right).\sigma_{rc} \tag{4.12}$$

For corroded bars, the expansion of corrosion products reduces the concrete confinement through reducing the net split area, B_c , and increasing the area of the longitudinal section of the anchored bars in the splitting plane, B_s ; Thus, this effect could be implemented in the change of the diameter of the reinforcing bar, d_b, by adding the thickness of the

accumulated rust products around the reinforcing bar to the original bar diameter, d_b, $d_b = 2(R_i + d_c)$, where, d_c is the thickness of effective rust layer . Therefore equation 4.12 with the effect of corrosion becomes:

$$\sigma_n = \left(\frac{R_0}{R_i + d_c} - 1 \right) . \sigma_{rc} \tag{4.13}$$

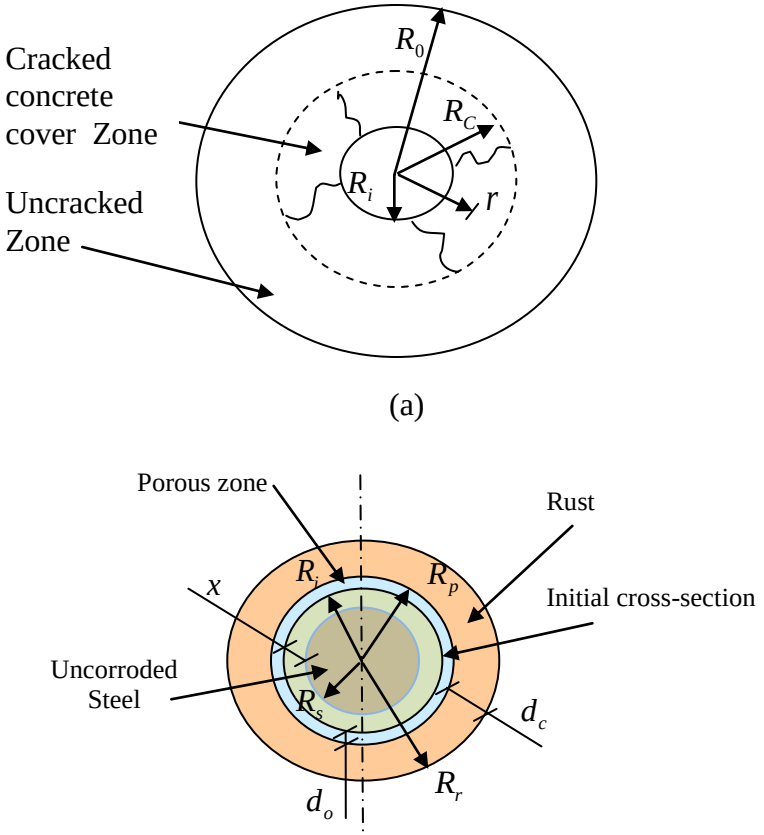

Figure 4.5 Schematic of proposed corrosion model

In the proposed model let $P_{conf} = \sigma_n$, where P_{conf} = maximum confining pressure at bond failure due to cracked concrete, hence, equation 4.13 becomes:

$$P_{conf} = \left(\frac{R_0}{R_i + d_c} - 1 \right) \cdot \left(\frac{f_{ct}}{k \frac{w}{\phi_a} + 1} \right) \tag{4.14}$$

The fictitious splitting crack width, w, proposed by Molina et al. (1993) is modified to take into account the thickness of porous zone, which is:

$$w = 2\pi((v_{rs} - 1)x - d_o) \tag{4.15}$$

where, υ_{rs} = ratio between the volumes of the corroded and virgin steel, x = the corrosion penetration depth, and d_0 = thickness of porous zone.

Using the simple friction model, bond strength contribution of maximum confining pressure at anchorage failure can be expressed as:

$$\tau_{CP}(xp) = \mu . P_{conf}(xp) \tag{4.16}$$

where μ = coefficient of friction and can be calculated from equation 3.38 (Bhargava et al. 2007)

$$\mu(xp) = \tan\varphi(xp) = 0.37 - 0.26(x - x_{cr}) \tag{4.17}$$

4.3.5 Derivation of the expression for corrosion pressure

To assess the mechanical damage resulting from the expansion of the corrosion products around the corroding reinforcing bars, the uniform internal pressure that is induced by the corrosion products around the steel/concrete interface, and the resulting state of stress in the surrounding concrete is evaluated by means of an elastic analysis. In this approach, the concrete cover is again treated as a thick-walled cylinder subjected to the internal pressure build-up of expansive corrosion products. The thick walled cylinder is shown schematically in Fig 4.5(b), where, R_i is the original radius of the steel bar before corrosion, R_S is the radius of the bar after corrosion, R_r is the total radius with the rust layer, and R_p is the radius of the porous zone (Liu and Weyers 1998).

Liu and Weyers (1998) assumed a porous zone around the reinforcing bar at the interface between the reinforcing bar and the concrete. This porous zone is formed due to several factors such as, the transition from cement past to steel, entrapped/entrained air voids, and corrosion products diffusing into the capillary voids in the cement paste. The volume of the porous zone is related to the surface area of the reinforcement, water-cement ratio, degree of hydration, and degree of consolidation (Liu and Weyers 1998). When the steel bar corrodes, the density of the corrosion products is lower than that of the steel; therefore, the volume of the corrosion products is higher than that of the steel. This increase in the volume will gradually fill the porous zone with corrosion products, and if the total volume of corrosion products is less than the volume of porous zone then the formation of corrosion products will not create any stress on the surrounding concrete, however, when the volume of corrosion products exceeds the volume of the porous zone, the formation of the corrosion products starts to create expansive pressure on the surrounding concrete, and this pressure increases with the increase of corrosion products; this pressure is the corrosion pressure P_{cor}. Due to this corrosion pressure cracks will be formed at the steel-concrete interface.

The effective thickness of the corrosion layer that causes the corrosion pressure can be modeled using Fig. 4.5(b), $d_o = R_p - R_i$, where $d_o =$ the thickness of the porous zone,

which is normally it ranges between 10 and 20 μm, in the present model d_o = 12.5 μm (Liu and Weyers 1998); $d_C = R_r - R_p$, where d_c = effective rust layer; $x = R_i - R_s$, x = corrosion depth of the bar.

By taking a unit length of the thick walled cylinder, the volume of the corroded reinforcing steel bar (after reduction) is $\Delta v_s = \pi(R_i^2 - R_s^2)$; and the volume of the corrosion products is $\Delta v_r = (v_{rs} - 1).\Delta v_s$. The volume of the corrosion products Δv_r can be calculated using equation 4.18

$$\Delta v_r = \Delta v_1 + \Delta v_2 + \Delta v_3 \tag{4.18}$$

where,

$\Delta v_1 = \pi(R_p^2 - R_i^2)$, $\Delta v_1 =$ volume filled by porous zone

$\Delta v_2 = \pi(R_r^2 - R_p^2)$, $\Delta v_2 =$ volume of expansive corrosion products causing pressure

$\Delta v_3 =$ volume of corrosion products penetrated into corrosion cracks

$\Delta v_3 = \sum w.(\frac{R_c - R_r}{2})$, $\sum w =$ total crack width at steel-concrete interface = $2\pi.d_C$ (Pantazapoulou and Papoulia 2001); Therefore, $\Delta v_3 = \pi(R_r - R_p)(R_c - R_r)$. Substituting $\Delta v_1, \Delta v_2$, and Δv_3 into equation 4.18 and simplifying it, the effective rust layer can be obtained from equation 4.19

$$d_c = \frac{(v_{rs} - 1).(2R_i x - x^2) - d_0(2R_i + d_0)}{R_c + R_i + d_0} \tag{4.19}$$

The growth of corrosion products exerts an outward pressure on the concrete at the interface between the rust band (corrosion products) and concrete. Under this expansive pressure, when the tangential stress, σ_θ, exceeds the tensile strength of concrete, f_{ct}, cracks initiate at the steel-concrete interface. After initiation, the cracks propagate along

the radial direction and stop arbitrarily at R_c which varies between the radii R_i and R_o to reach a state of self-equilibrium. This stage is called partial cracked and the cracks in this stage divide the thick walled cylinder into two zones: inner cracked zone and outer uncracked zone as shown in Fig. 4.5. The cover is assumed to be fully cracked when $R_c = R_o$ as shown in Fig. 4.6

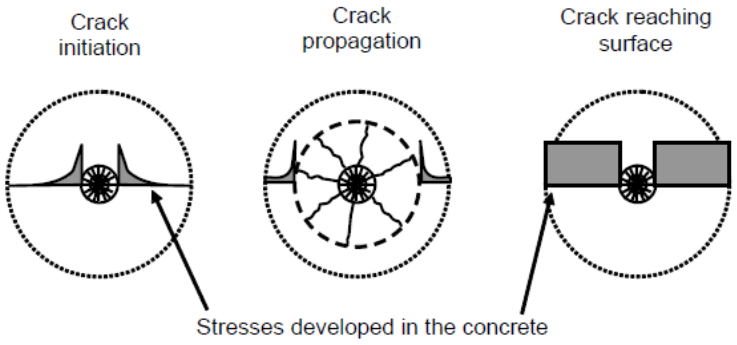

Figure 4.6 Models for crack initiation and propagation through the concrete cover

For the inner cracked concrete cylinder, the cracks assumed to be smeared and uniformly distributed on the circumference of the cracked cylinder (Pantazapoulou and Papoulia 2001); therefore the formulation is written in terms of average stresses and strains. This means that the problem is axisymmetric so that there is no tangential displacement in the cylinder. Chernin et al. (2009) showed that the stiffness of concrete in the radial direction remains practically unchanged while in the tangential direction it decreases significantly as shown in Fig. 4.7. Thus, the concrete in the inner cylinder is an anisotropic material with the modulus of elasticity in the tangential direction is a function of the radial coordinate, r. Similar to Li et al. (2006), in this study, the residual tangential stiffness will be assumed to be constant along the crack between R_i and R_c, therefore, $E_{\theta,ef} = \alpha.E_{r,ef}$, where $\alpha \leq 1$ and referred as a tangential stiffness reduction factor (Li et al. 2006), $E_{\theta,ef}$ is the effective modulus of elasticity in the tangential direction, and $E_{r,ef}$ is the effective modulus of elasticity in the radial direction.

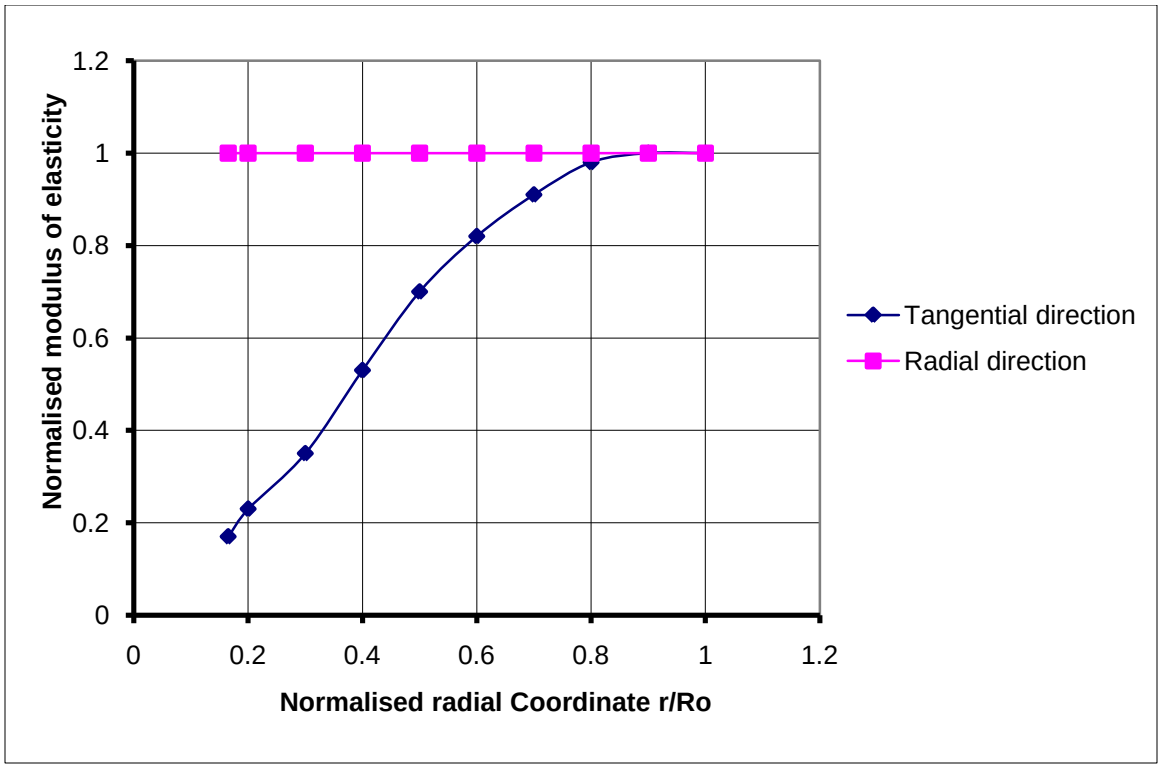

Figure 4.7 Residual stiffness of partially cracked thick-walled concrete cylinder (FE analysis) (Chernin et al. 2009)

Following Timoshenko and Goodier (1970) proposed solution for the radial displacement, $u(r)$, for the uncracked concrete cylinder, Li et al. (2006) developed further their equation for the cracked concrete cylinder zone by using the tangential stiffness reduction factor, α. Hence, the governing radial displacement, $u(r)$, equation in the cracked concrete cylinder zone should satisfy the following equation (Li et al. 2006):

$$\frac{d^2u(r)}{dr^2} + \frac{1}{r}.\frac{du(r)}{dr} - \alpha\frac{u(r)}{r^2} = 0 \qquad (4.20)$$

where r is the radial distance from the center of the thick walled cylinder to any point between R_i , and R_c as shown in Fig. 4.5(a).

The solution to equation 4.20 is:

$$u(r) = a_1.r^{\sqrt{\alpha}} + \frac{b_1}{r^{\sqrt{\alpha}}} \tag{4.21}$$

where, a_1 and b_1 are functions of R_c. Thus the radial and tangential stresses can be obtained as follows (Li et al. 2006):

$$\sigma_r = \frac{\sqrt{\alpha}E_{ef}}{1-\nu^2}\left[(1+\nu).a_1.r^{\sqrt{\alpha}-1} - \frac{(1-\nu).b_1}{r^{\sqrt{\alpha}+1}}\right] \tag{4.22}$$

$$\sigma_\theta = \frac{\alpha E_{ef}}{1-\nu^2}\left[(1+\nu).a_1.r^{\sqrt{\alpha}-1} + \frac{(1-\nu).b_1}{r^{\sqrt{\alpha}+1}}\right] \tag{4.23}$$

where $\nu = \sqrt{\nu_1\nu_2}$, ν_1 and ν_2 are the Poisson's ratios in the radial and tangential directions, respectively. This assumption is based on anisotropic requirement given by Lekhnitskii (1963) and its approximation given by Sheng et al. (1991), as stated in Li et al. (2006).

As was mentioned earlier, for the outer uncracked concrete zone, the theory of elasticity still applies. According to Timoshenko and Goodier (1970), the radial displacement, $u(r)$,in the uncracked zone should satisfy the following equation:

$$\frac{d^2u(r)}{dr^2} + \frac{1}{r}.\frac{du(r)}{dr} - \frac{u(r)}{r^2} = 0 \tag{4.24}$$

The solution of equation 4.24 is:

$$u(r) = a_2.r + \frac{b_2}{r} \tag{4.25}$$

where, a_2 and b_2 are functions of R_c. Thus the radial and tangential stresses can be obtained as follows:

$$\sigma_r = \frac{E_{ef}}{1-\nu^2}\left[(1+\nu).a_2 - \frac{(1-\nu).b_2}{r^2}\right] \tag{4.26}$$

$$\sigma_\theta = \frac{E_{ef}}{1-\nu^2}\left[(1+\nu).a_2 + \frac{(1-\nu).b_2}{r^2}\right] \tag{4.27}$$

The coefficients a_1, b_1, a_2, and b_2 in the above equations can be established from the boundary conditions for the concrete cylinder, which are:

1. The radial stress at the outer uncracked cylinder $\sigma_r = 0$ at $r = R_0$
2. The compatibility requirement for the displacement at the crack front $u_{r1} = u_{r2}$ at $r = R_c$
3. The compatibility requirement for the stress at the crack front $\sigma_{r1} = \sigma_{r2}$ at $r = R_c$
4. The compatibility requirement for the stress at the crack front $\sigma_{\theta 1} = \sigma_{\theta 2} = f_{ct}$ at $r = R_c$

From the first boundary condition,

$$a_2(1+\nu) - \frac{b_2(1-\nu)}{R_o^2} = 0 \tag{4.28}$$

and from equation 4.28,

$$a_2 = \frac{b_2(1-v)}{R_o^2(1+v)} \tag{4.29}$$

From the second boundary condition,

$$a_1 R_c^{\sqrt{\alpha}} + b_1 R_c^{-\sqrt{\alpha}} = a_2 R_c + \frac{b_2}{R_c} \tag{4.30}$$

From the third boundary condition,

$$(1+v)a_2 - \frac{(1-v)b_2}{R_c^2} = \sqrt{\alpha}\left[(1+v)R_c^{\sqrt{\alpha}-1}a_1 - b_1(1-v)R_c^{-\sqrt{\alpha}-1}\right] \tag{4.31}$$

From the fourth boundary condition,

$$\frac{E_{ef}}{1-v^2}\left[(1+v)a_2 - \frac{(1-v)b_2}{R_c^2}\right] = f_{ct} \tag{4.32}$$

now by substitute equation 4.28 into 4.32,

$$\frac{E_{ef}}{1-v^2}\left[(1+v).\frac{b_2(1-v)}{R_o^2(1+v)} - \frac{(1-v)b_2}{R_c^2}\right] = f_{ct} \tag{4.33}$$

From equation 4.33, b_2 can be obtained:

$$b_2 = \frac{f_{ct}(1+\nu)R_c^2 R_o^2}{E_{ef}(R_c^2 + R_o^2)} \tag{4.34}$$

Substituting equation 4.34 in equation 4.29, a_2 can be obtained

$$a_2 = \frac{f_{ct}(1-\nu)R_c^2}{E_{ef}(R_c^2 + R_o^2)} \tag{4.35}$$

At $r = R_c, u_{r2} = u_c$ thus:

$$u_c = a_2 R_c + \frac{b_2}{R_c} \tag{4.36}$$

Substituting a_2, and b_2 in equation 4.36, u_c can be obtained from equation 4.37

$$u_c = \frac{f_{ct}R_c\left[(1-\nu)R_c^2 + (1+\nu)R_o^2\right]}{E_{ef}(R_c^2 + R_o^2)} \tag{4.37}$$

Substituting a_2, and b_2 in equation 4.30

$$a_1 R_c^{\sqrt{\alpha}} + b_1 R_c^{-\sqrt{\alpha}} = \frac{f_{ct}(1-\nu)R_c^2}{E_{ef}(R_c^2 + R_o^2)}.R_c + \frac{f_{ct}(1+\nu)R_c^2 R_o^2}{E_{ef}(R_c^2 + R_o^2)}.\frac{1}{R_c} \tag{4.38}$$

and simplifying equation 4.38, it will be

$$a_1 R_c^{\sqrt{\alpha}} + b_1 R_c^{-\sqrt{\alpha}} = \frac{f_{ct}R_c\left[(1-\nu)R_c^2 + (1+\nu)R_o^2\right]}{E_{ef}(R_c^2 + R_o^2)} \tag{4.39}$$

Therefore, a_1 can be obtained from equation 4.39:

$$a_1 = \frac{u_C}{R_c^{\sqrt{\alpha}}} - \frac{b_1}{R_c^{2\sqrt{\alpha}}} \tag{4.40}$$

Now, by substituting a_1, a_2, and b_2 in equation 4.31, b_1 can be obtained:

$$b_1 = \frac{f_{ct} R_c^{\sqrt{\alpha}+1}}{2\sqrt{\alpha} E_{ef} (R_c^2 + R_o^2)} \left[\sqrt{\alpha}(1+\nu)m - (1-\nu^2)(R_c^2 - R_o^2) \right] \tag{4.41}$$

where $m = (1-\nu)R_c^2 + (1+\nu)R_0^2$ (4.42)

E_{ef} = effective modulus of elasticity = $\frac{E_0}{1+\varphi_c}$ (Bazant 1979), and

φ_C = creep coefficient of concrete = 2 in this proposed model (Liu and Weyers 1998, Bhargava et al. 2006).

Therefore, the corrosion pressure at steel concrete interface P_{cor} can be obtained from equation 4.43 by substituting ($r = R_i$), and $P_{cor} = -\sigma_r$ into equation 4.22:

$$P_{cor} = -\sigma_r = -\frac{\sqrt{\alpha} E_{ef}}{1-\nu^2} \left[(1+\nu).a_1.R_i^{\sqrt{\alpha}-1} - (1-\nu) b_1 R_i^{-\sqrt{\alpha}-1} \right] \tag{4.43}$$

The total bond strength contribution to corrosion pressure τ_{COR} can be obtained from equation 4.44.

$$\tau_{COR}(xp) = \mu.P_{cor}(xp) \tag{4.44}$$

Therefore, the ultimate bond strength, τ_{bu} in equation 4.3 can be obtained as following:

$$\tau_{bu}(xp) = \mu P_{total}(xp) + \tau_{AD}(xp) \tag{4.45}$$

where $P_{total}(xp) = P_{conf}(xp) + P_{cor}(xp)$ is the total contact pressure and steel-concrete interface.

When the concrete cylinder is fully cracked, the boundary conditions are:

1. The radial stress at the outer cylinder $\sigma_r = 0$ at $r = R_o$
2. The radial displacement d_c at $r = R_i$ can be found from equation 4.19 by assuming x and $R_c = R_o$

Equation 4.20 is the governing equation; the solution for equation 4.20 is (Li et al. 2006):

$$u(r) = a_3.r^{\sqrt{\alpha}} + \frac{b_3}{r^{\sqrt{\alpha}}} \tag{4.46}$$

where,

$$a_3 = \frac{(1-v)R_i^{\sqrt{\alpha}} d_c}{(1-v)R_i^{2\sqrt{\alpha}} + (1+v)R_o^{2\sqrt{\alpha}}} \tag{4.47}$$

$$b_3 = \frac{(1-v)R_i^{\sqrt{\alpha}} R_o^{2\sqrt{\alpha}} d_c}{(1-v)R_i^{2\sqrt{\alpha}} + (1+v)R_o^{2\sqrt{\alpha}}} \tag{4.48}$$

Now, substituting a_3 and b_3 into equation 4.43 to solve for corrosion pressure P_{cor}

4.3.6 Stiffness reduction factor α

Chernin et al. (2009) developed a relationship for α as a power function of the radial coordinate as shown in equation 4.49.

$$\alpha = (\frac{r}{R_c})^n \tag{4.49}$$

where $n = 1.5$ for $f_{ct} \le 3.07MPa$ and $n = 0.081\exp(0.95 f_{ct})$ for $f_{ct} \ge 3.07MPa$.

While Li et al. (2006) derived an equation to calculate α depending on the average tangential strain, ε_θ, over the cracked surface; equation 4.50 shows the simplified form of the Li et al. (2006) equation to calculate α.

$$\alpha = \frac{f_{ct}\exp(\left[\frac{-u_C(R_c^{\sqrt{\alpha}} - R_i^{\sqrt{\alpha}})}{\sqrt{\alpha}(R_c - R_i)R_c^{\sqrt{\alpha}}}\left\{1 + \frac{S(R_c^{\sqrt{\alpha}} - R_i^{\sqrt{\alpha}})}{2\sqrt{\alpha}R_i^{\sqrt{\alpha}}}\right\} + \frac{u_c}{R_c}\right])}{E_{ef}\left[\frac{-u_C(R_c^{\sqrt{\alpha}} - R_i^{\sqrt{\alpha}})}{\sqrt{\alpha}(R_c - R_i)R_c^{\sqrt{\alpha}}}\left\{1 + \frac{S(R_c^{\sqrt{\alpha}} - R_i^{\sqrt{\alpha}})}{2\sqrt{\alpha}R_i^{\sqrt{\alpha}}}\right\}\right]} \tag{4.50}$$

Where, $S = \sqrt{\alpha} + \frac{R_c^2 - R_i^2}{R_c^2 + R_i^2}$ (4.51)

In addition, Zhong et al. (2010) proposed a stiffness degradation factor(damaged variable) to model the stiffness degradation of the cover concrete subjected to cracking based on an energy principle applied to fracture reinforced concrete structure. Figure 4.8 shows the stress- strain diagram curve for concrete. The left chart shows the stress-strain

curve for concrete subject to tensile stress where E_r is the initial stiffness of the concrete, and E_θ is the secant stiffness of the cracked concrete. The right chart in Fig. 4.8 shows the softening curve extracted from the right branch of the stress-strain curve shown in the left chart. The stiffness reduction factor α in cracked concrete is the ratio between the secant stiffness and the initial stiffness ($\alpha = E_r / E_\theta$). Equation 4.52 shows the proposed stiffness degradation factor α.

$$\alpha = \frac{\phi(\varepsilon^f_{\max}(t))}{E_r \varepsilon^f_{\max}(t) + \phi(\varepsilon^f_{\max}(t))} \tag{4.52}$$

where, $\phi(\varepsilon^f_{\max}(t))$ is a function representing the softening stress-strain curve, and $\varepsilon^f_{\max}(t)$ is the maximum cracking strain achieved before loading as shown in Fig. 4.8.

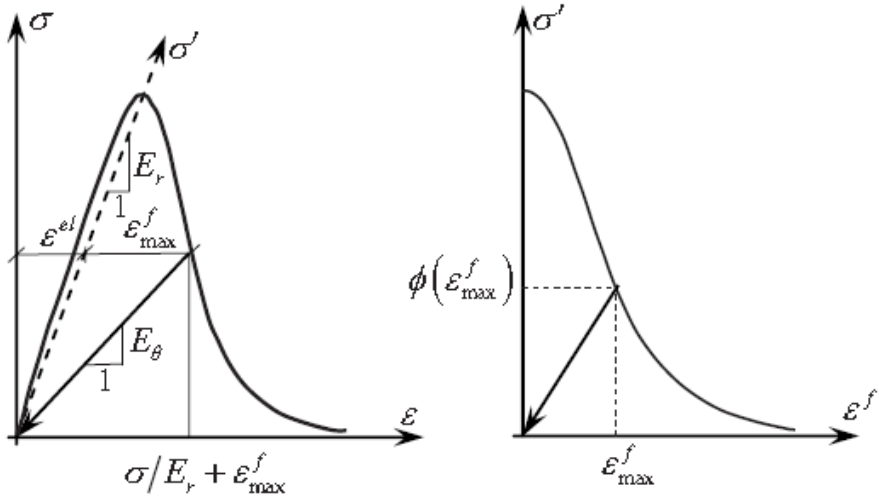

Figure 4.8 Typical stress-strain softening curve for concrete subject to tensile stress (Zhong et al., 2010)

Figure 4.9 shows both Li et al. (2006), Chernin et al. (2009), and Zhong et al. (2010) models to determine α .

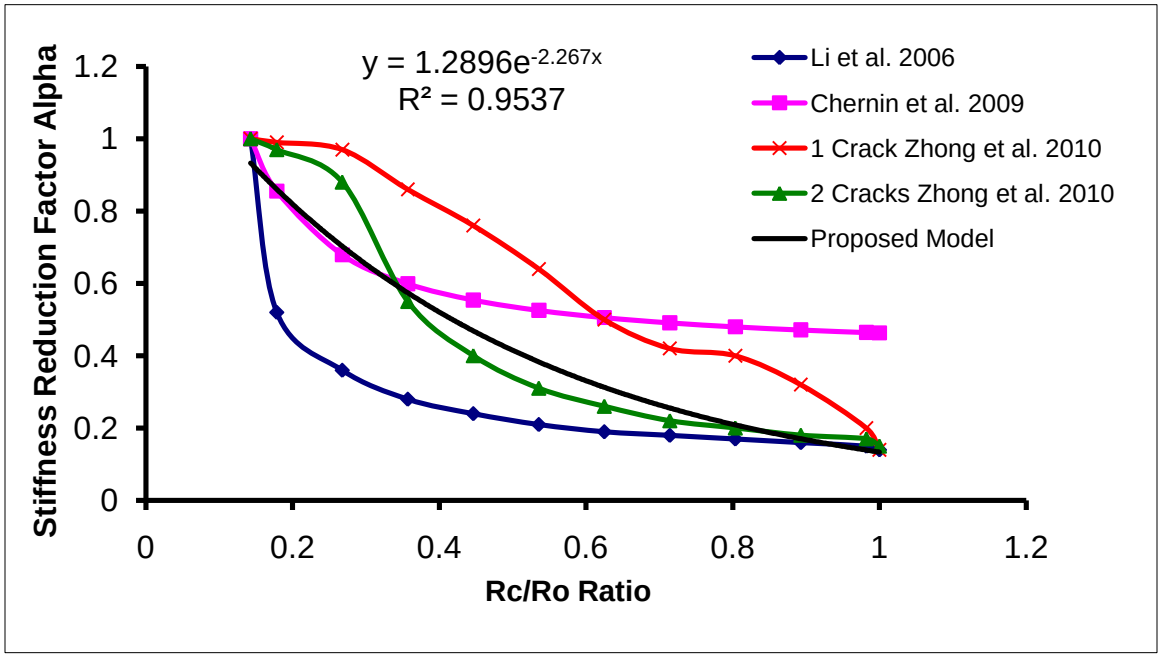

Figure 4.9 Stiffness reduction factor of partially cracked thick-walled cylinder

The difference between the aforementioned models is shown in Fig. 4.9. The exponential trend for 2 cracks Zhong et al is showing in equation 4.53.

$$\alpha = 1.29 \exp(-2.267 * \frac{R_c}{R_o}) \tag{4.53}$$

According to Bazant and Planas (1998), the average tangential stiffness reduction factor is dependent on the average tangential strain $\bar{\varepsilon}_\theta$ over the cracked surface and can be determined as follows:

$$\alpha = \frac{f_{ct} \exp\left[-\gamma(\bar{\varepsilon}_\theta - \bar{\varepsilon}_\theta^c)\right]}{E_{ef}\,\bar{\varepsilon}_\theta} \tag{4.54}$$

where, $\bar{\varepsilon}_{\theta}^{c}$ is the average tangential cracking strain and γ is a material constant. According to Nelson and Bicanic (2002), the radial displacement for the concrete cover is:

$$u(r) = \frac{f_{ct}.r.\left[(R_o / r)^2 + 1\right]}{E_o\left[(R_o / R_c)^2 + 1\right]} \tag{4.55}$$

To account for creep and shrinkage E_{ef} will be used in Equation 4.55 instead of E_o. Therefore, the average tangential cracking strain $\bar{\varepsilon}_{\theta}$ for concrete cover between R_i, and R_c can be determined from equation (4.56):

$$\bar{\varepsilon}_{\theta} = \frac{1}{R_c - R_i}\int_{R_i}^{R_c} \frac{f_{ct}.\left[(R_o / r)^2 + 1\right]}{E_{ef}\left[(R_o / R_c)^2 + 1\right]}.d_r \tag{4.56}$$

By equating equation 4.53 with equation 4.54, and simplifying it; α can be determined from equation 4.57.

$$\alpha = \frac{f_{ct} * F}{E_{ef}\bar{\varepsilon}_{\theta}} \tag{4.57}$$

where, $F = 5.77 * \exp(-2.91 * \frac{R_c}{R_o}) * \frac{R_c}{R_o}$. The factor F in equation 4.57 is derived by assuming the relation $R_i / R_o = 0.25$ (the concrete cover is 3 times the bar radius), for any other relation R_i / R_o, a correction to this equation must be taken into account. In addition,

the reduction stiffness factor $\alpha \leq 1$. In this research, equation 4.57 will be used to calculate α for partially cracked cylinder.

For fully cracked cylinder, the radial displacement for the concrete cover given by Wang and Liu (2004) is modified to account for creep and shrinkage.

$$u(r) = \frac{\varepsilon_\theta^c * r * \left[(R_o / r)^2 + 1\right] * (\varphi_c + 1)}{2} \tag{4.58}$$

where ε_θ^c is the hoop strain at R_o. ε_θ^c can be obtained by equating equation 4.58 with equation 4.19 at $r = R_i$. The average tangential cracking strain $\bar{\varepsilon}_\theta$ for concrete cover between R_i, and R_o can be determined from equation 4.59:

$$\bar{\varepsilon}_\theta = \frac{1}{R_o - R_i} \int_{R_i}^{R_o} \frac{\varepsilon_\theta^c . (\varphi_c + 1)\left[(R_o / r)^2 + 1\right]}{2} d_r \tag{4.59}$$

Finally, α for fully cracked cylinder can be obtained by substituting equation 4.59 into 4.54.

4.4 Solution procedure

As can be noticed from section 4.3 and Fig. 4.5, the radius of the inner cylinder R_c (the location of crack front) is unknown, as well as the thickness of the rust layer d_c. The aim is to determine the internal pressure and the corresponding radial displacement. Thus, the following steps need to be carried out:

For Partial cracking:

1. Value of R_c is incrementally increased from R_i to R_o
2. For each value of R_c, u_c is calculated using equation 4.37
3. Find α using equation 4.57 as following:

   3.1 The average tangential cracking strain $\bar{\varepsilon}_\theta$ can be obtained from equation 4.56

   3.2 Find the value of the factor F

4 Find the corrosion pressure P_{cor} using equation 4.43, where the constants b_1, and a_1 can be obtained using equations 4.41, and 4.40 respectively

5 Find the confinement pressure P_{conf} using equation 4.14 as following:

   5.1 Find the radial displacement at R_i using equation 4.21

   5.2 Find the corrosion depth x using equation 4.19

   5.3 Find the crack width w using equation 4.15

6 Find the total contact pressure which is the sum of of the corrosion pressure and the confining pressure

7 Find the friction coefficient using equation 4.17

8 Find the bond strength due to adhesion using equation 4.4

9 Find the ultimate bond strength using equation 4.45

For fully cracked:

1. For a given value of x and $R_c = R_o$, d_c can be found using equation 4.19
2. Find α using equation 4.54
3. Find the corrosion pressure P_{cor} using equation 4.43, where the constants a_3 , and b_3 can be obtained using equations 4.47, and 4.48 respectively
4. Find the crack width w using equation 4.14
5. Find the confinement pressure P_{conf} using equation 4.13
6. Find the friction coefficient using equation 4.16
7. Find the bond strength due to adhesion using equation 4.4
8. Finally, find the ultimate bond strength using equation 4.45

Chapter 5

NUMERICAL EXAMPLE AND VERIFICATION OF PROPOSED MODEL

This chapter presents the application of the effect of corrosion on bond behavior between reinforcing steel and concrete through a numerical example of the proposed model described in Chapter 4. Also presented, by using the same numerical example, are comparisons with other models employed by other researchers. Finally, to evaluate the accuracy of the proposed model, the experimental results by Almusallam et al. (1996), Al-Sulaimani et al (1990), Lee et al. (2002), and Cabrera and Ghiddoussi (1992) are compared with the predicted results of the proposed model.

5.1 Numerical example for the proposed model

The utility of the proposed bond deterioration between reinforcing steel and concrete model can be demonstrated through the following example:

To calculate the ultimate bond stress with respect to corrosion depth x. Consider a reinforced concrete beam having 16 mm bar diameter and 60 mm thick concrete cover. Let the maximum size of the aggregate used be 15 mm and the experimentally determined coefficient related to fracture energy is 167. The concrete tensile strength before the crack begins is taken as 3.3 MPa, the modulus of elasticity is 24674 MPa, and the creep coefficient of concrete is 2. The volume of corrosion products formed is assumed to be v_{rs} times (here, v_{rs} is taken to be equal to 3) the volume of the original reinforcing steel that has corroded.

Solution:

Using the solution procedure outlined in Chapter 4, the steps are as follows:

1. Find R_c : The inner radius of the cylinder $R_i = 8mm$, and the outer radius of the cylinder $R_0 = 68mm$. Values of R_c will be from 8 mm to 68 mm. Assume the poisons' ratio $v = 0.2$. To illustrate the solution procedure in section 4.4, $R_c = 30mm$ will be taken as an example.

2. The displacement at crack front, u_c, at $R_c = 30mm$ can be calculated using equation 4.37

$$u_c = \frac{f_{ct} R_c \left[(1-v)R_c^2 + (1+v)R_o^2\right]}{E_{ef}(R_c^2 + R_o^2)}$$

However, from equation 4.42, $m = (1-v)R_c^2 + (1+v)R_o^2$

$$m = (1-0.2)*30^2 + (1+0.2)*68^2 = 6268.8$$

The effective modulus of elasticity $E_{ef} = \frac{E_0}{1+\varphi_c} = 8224.67MPa$.

Therefore, $u_C = \frac{3.3*30*6268.8}{8224.67*(30^2 + 68^2)} = 0.0136mm$

3. Find α by using equation 4.57: $\alpha = \frac{f_{ct} * F}{E_{ef}\bar{\varepsilon}_\theta}$

3.1. The average tangential cracking strain $\bar{\varepsilon}_\theta$ can be obtained from equation 4.56

$$\bar{\varepsilon}_\theta = \frac{3.3}{(30-8)*8224.67} * \left[\frac{1}{(68/30)^2 + 1} * ((68)^2 * (\frac{1}{8} - \frac{1}{30}) + (30-8))\right]$$
$$= 1.325E-03$$

3.2 Find the value of the factor F: The ratio $R_i / R_0 = 0.118$. But, the factor F in equation 4.57 is derived by assuming the ratio $R_i / R_0 = 0.25$; therefore a correction factor is needed. The correction to factor F is $0.25/0.118 = 2.125$.

$$F = 5.77 * \exp(-2.91 * \frac{30}{68}) * \frac{30}{68} * 2.125 = 1.498$$

Therefore, the stiffness reduction factor α is:

$$\alpha = \frac{3.3*1.498}{8224.67*1.325E-03} = 0.454$$

4. Find the corrosion pressure, P_{cor}, by using equation 4.43:

$$P_{cor} = -\frac{\sqrt{\alpha} E_{ef}}{1-\nu^2}\left[(1+\nu).a_1.R_i^{\sqrt{\alpha}-1} - (1-\nu)b_1 R_i^{-\sqrt{\alpha}-1}\right]$$

First, find the constants b_1, and a_1 can be calculated using equations 4.41, and 4.40 respectively

$$b_1 = \frac{3.3*30^{\sqrt{0.454}+1}}{2\sqrt{0.454}*8224.67*(30^2+68^2)}\left[\sqrt{0.454}(1+0.2)*6268.8 - (1-0.2^2)(30^2-68^2)\right]$$

$$b_1 = 0.138$$

$$a_1 = \frac{0.0136}{30^{\sqrt{0.454}}} - \frac{0.144}{30^{2\sqrt{0.454}}} = -3.221E-05$$

Therefore, the corrosion pressure P_{cor} is:

$$P_{cor} = -\frac{\sqrt{0.454} * 8224.67}{1-0.2^2}\left[(1+0.2)*(-3.221E-05)8^{\sqrt{0.454}-1} - (1-0.2)*0.138*8^{-\sqrt{0.454}-1}\right]$$

$$P_{cor} = 19.764MPa$$

5. Find the confinement pressure, P_{conf}, using equation 4.14:

$$P_{conf} = \left(\frac{R_0}{R_i + d_c} - 1\right).\left(\frac{f_{ct}}{k\frac{w}{\phi_a} + 1}\right)$$

5.1. The radial displacement at R_i can be calculated using equation 4.21

$$u(r) = a_1.r^{\sqrt{\alpha}} + \frac{b_1}{r^{\sqrt{\alpha}}}$$

$$u_i = (-3.221E-05)*8^{\sqrt{0.454}} + \frac{0.138}{8^{\sqrt{0.454}}} = 0.0343mm$$

5.2 Find corrosion depth, x, by equating the radial displacement, u_i, (the effective rust layer) to the effective rust layer, d_c:

$$d_c = 0.0343 = \frac{(3-1).(2*8x - x^2) - 0.0125(2*8 + 0.0125)}{30 + 8 + 0.0125}$$

Solving the above equation gives $x = 0.047$ mm

5.3 Find crack width w by using equation 4.15: $w = 2\pi((v_{rs} - 1)x - d_o)$

$$w = 2\pi((3-1)*0.047 - 0.0125) = 0.508mm$$

Therefore, the confinement pressure is:

$$P_{conf} = \left(\frac{68}{8 + 0.0343} - 1\right).\left(\frac{3.3}{167\frac{0.508}{15} + 1}\right) = 3.699MPa$$

6. Find the total contact pressure which is equal to the sum of the corrosion pressure and the confining pressure

Therefore, $P_{total} = P_{conf} + P_{cor} = 3.699 + 19.764 = 23.463MPa$

7. Find friction coefficient by using equation 4.17:

$$\mu(X_p) = \tan\varphi(X_p) = 0.37 - 0.26(X - X_{cr})$$

Corrosion depth at full cracking is $x_{cr} = 0.11\,mm$ which was calculated at

$R_c = 68mm$; Therefore, the coefficient of friction is:

$$\mu = 0.37 - 0.26(0.047 - 0.11) = 0.386$$

8. Find bond strength due to adhesion using equation 4.4:

$$\tau_{AD}(xp) = \frac{n.A_r(x).f_{coh}(xp)\left[\cot\delta(xp) + \tan(\delta+\phi)(xp)\right]}{\pi D_r(xp).S_r}$$

8.1. Equation 4.6 will be used to calculate the bond strength due to cohesion, f_{coh} .

$$f_{coh} = 3.68 - 22.08(x - x_{cr})$$

$$f_{coh} = 3.68 - 22.08(0.047 - 0.11) = 5.961MPa$$

8.2. Find tan (δ + φ) using equation 4.7: $\tan(\delta+\varphi)(xp) = 1.857 - 0.9285x$

Therefore, $\tan(\delta+\varphi)(xp) = 1.857 - 0.9285 * 0.047 = 1.813$

Now, substituting the above values into the bond strength due to adhesion equation:

$$\tau_{AD} = \frac{\pi * (8 - 0.35) * 0.07 * (8 - 0.35) * 5.961 * [1 + 1.813]}{\pi(8 - 0.35) * 0.6 * 8} = 1.945MPa$$

9. Find the ultimate bond strength, τ_u , using equation 4.45: $\tau_{bu}(xp) = \mu P_{total} + \tau_{AD}$

$$\tau_{bu} = 0.386 * 23.463 + 1.945 = 11.013MPa$$

Fully Cracked Section:

Again, following the same procedure outlined in Chapter 4:

1. When $R_c = 68mm$, the cylinder is fully cracked and the ultimate bond strength can be determined by calculating d_c at a given value of x greater than x_{cr}.

   For x = 0.40 mm, d_c can be calculated using equation 4.19

$$d_c = \frac{(3-1).(2*8*0.4-0.4^2)-0.0125(2*8+0.0125)}{68+8+0.0125} = 0.162mm$$

2. Find the stiffness reduction factor α by using equation 4.54 which is α = 0.052.
3. Find the constants a_3 , and b_3 using equations 4.47, and 4.48 respectively.

$$a_3 = \frac{(1-0.2)8^{\sqrt{0052}}*0.069}{(1-0.2)*8^{2\sqrt{0.052}}+(1+0.2)*68^{2\sqrt{0052}}} = 0.021$$

$$b_3 = \frac{(1-0.2)*8^{\sqrt{0.052}}*68^{2\sqrt{0.052}}*0.069}{(1-0.2)*8^{2\sqrt{0.052}}+(1+0.2)*68^{2\sqrt{0.052}}} = 0.137$$

Similarly, using the above-mentioned procedure to obtain the corrosion pressure and the confining pressure, it was found that the $P_{cor} = 7.087MPa$, and $P_{conf} = 0.431MPa$. Again, the total contact pressure is equal to the sum of the corrosion pressure and the confining pressure:

$$P_{total} = P_{conf} + P_{cor} = 0.431 + 7.087 = 7.517MPa$$

The coefficient of friction is: $\mu = 0.37 - 0.26(0.4 - 0.11) = 0.295$

The bond strength due to adhesion, f_{coh} is:

$$f_{coh} = 3.68 - 22.08(0.4 - 0.11) = -1.840 MPa$$

and $\tan(\delta + \varphi)(xp) = 1.857 - 0.9285 * 0.4 = 1.485$

f_{coh} is less than 0, therefore a zero value for the bond strength due to adhesion will be used and the ultimate bond strength is:

$$\tau_{bu} = 0.295 * 7.517 + 0 = 2.214 MPa$$

Similarly, the above calculations and equations were used to calculate the ultimate bond strength for different values of front cracks R_c for partially cracked cylinder and for different depths of corrosion attack, x, after the cylinder was fully cracked as shown in Tables 5.1 through 5.4.

Figure 5.1 shows the variation of confining, corrosion and total pressures with the increase in depth of corrosion attack 'x'. As can be seen from the figure, there is a non linear decrement in the confining pressure with the increase of the depth of corrosion attack, while the corrosion pressure increases in the beginning with the depth of corrosion attack up to a maximum pressure and then it decreases. The confining action arises from the tensile strength of concrete that equilibrate the radial pressure plays the most important role in the ultimate bond strength before cracking. At the onset of any crack in

the concrete, the confining action will be reduced due to the loss of tensile strength of concrete. Hence, it implies that as soon as the concrete cover cracks, the confining pressure does not play a significant role in the ultimate bond strength, while the corrosion pressure plays a significant role in the ultimate bond strength.

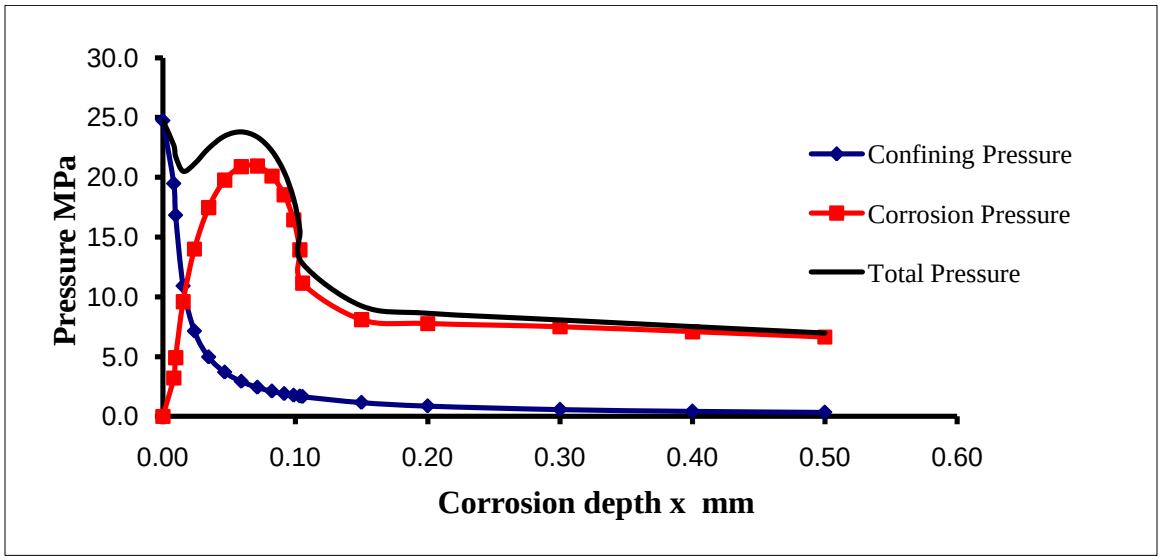

Figure 5.1 Variation of confining, corrosion, and total pressure with the corrosion depth x

Figure 5.2 shows the variation of ultimate bond strength, τ_{bu}, bond strength contribution of maximum confining pressure at anchorage bond failure, τ_{CP}, bond strength contribution due to adhesion, τ_{AD}, and bond strength contribution of corrosion pressure, τ_{COR}, versus corrosion depth, x. This figure (Fig. 5.2) demonstrates the ability of the proposed model to numerically predict the deterioration of bond between steel and concrete. One also can note the influence of the confining and corrosion pressures on the ultimate bond strength with the increase of corrosion depth. It is also observed from Fig. 5.2 that the ultimate bond strength curve is influenced first by the confining pressure with the onset of corrosion, however, with increase of the level of corrosion, the confining pressure becomes negligible and it will be highly influenced by corrosion pressure. Therefore, it can be concluded that the bond stress at the steel-concrete interface is a function of total contact pressure at the steel-concrete interface.

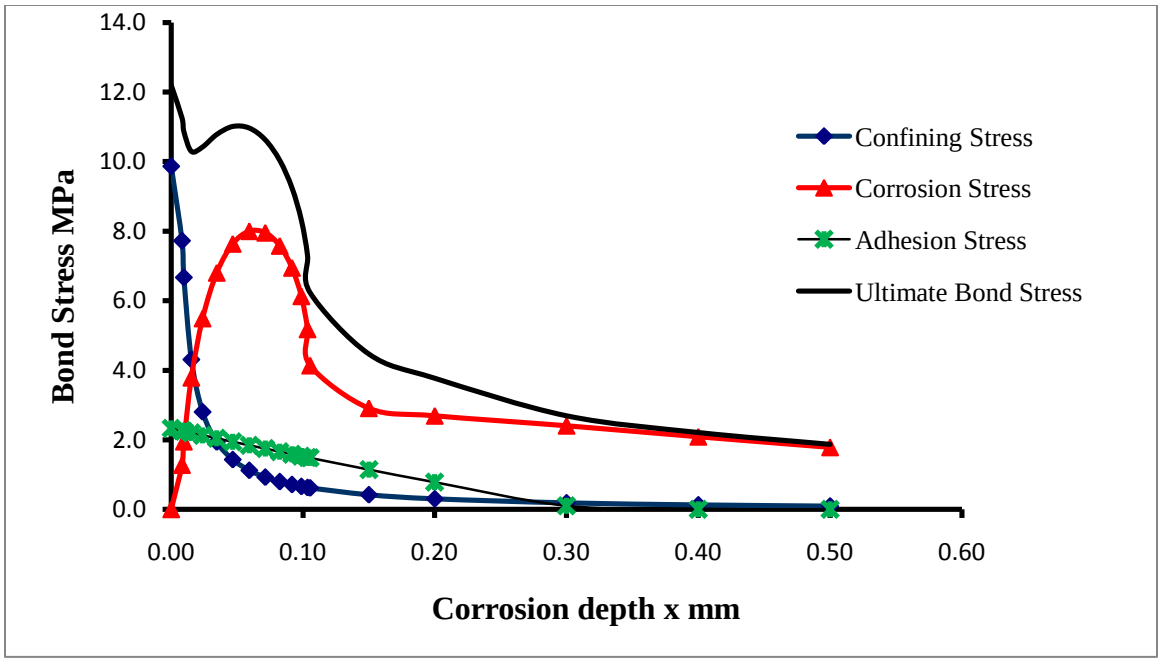

Figure 5.2 Variation of confining, corrosion and ultimate bond stresses with corrosion depth x

Table 5.1 Variation of corrosion pressure with crack front for partially cracked cylinder

Crack Front R_c mm	Crack Front Displacement u_c mm	Stiffness Reduction Factor α	Corrosion Pressure P_{cor} MPa	Effective Thickness Layer d_c mm	Corrosion Depth x mm	Crack Width w mm
			0.000		0.000	0.000
8	0.004	1.000	3.210	0.004	0.008	0.024
10	0.005	0.944	4.915	0.006	0.010	0.042
15	0.007	0.776	9.593	0.013	0.015	0.113
20	0.009	0.644	13.992	0.020	0.024	0.221
25	0.012	0.538	17.465	0.027	0.035	0.356
30	0.014	0.454	19.764	0.034	0.047	0.508
35	0.016	0.385	20.882	0.039	0.059	0.666
40	0.018	0.328	20.936	0.043	0.071	0.819
45	0.019	0.281	20.096	0.046	0.082	0.957
50	0.021	0.241	18.540	0.047	0.092	1.073
55	0.023	0.207	16.436	0.047	0.099	1.163
60	0.025	0.178	13.930	0.045	0.103	1.222
65	0.026	0.154	11.143	0.043	0.105	1.247

Table 5.2 Variation of bond stress with corrosion depth for partially cracked cylinder

Confining Pressure P_{conf} MPa	Total Pressure P_{total} MPa	Friction coef. u	Corrosion Stress τ_{cor} MPa	Confining Stress τ_{cp} MPa	Adhesion Stress τ_{AD} MPa	Ultimate Bond Stress τ_{bu} MPa
24.750	24.750	0.399	0.000	9.865	2.331	12.196
19.481	22.690	0.396	1.273	7.724	2.262	11.258
16.836	21.751	0.396	1.947	6.669	2.250	10.866
10.917	20.510	0.395	3.786	4.308	2.203	10.297
7.138	21.130	0.392	5.491	2.801	2.132	10.424
4.967	22.432	0.390	6.805	1.935	2.044	10.784
3.699	23.463	0.386	7.638	1.429	1.945	11.013
2.925	23.807	0.383	8.002	1.121	1.844	10.967
2.432	23.369	0.380	7.957	0.924	1.748	10.629
2.110	22.207	0.377	7.580	0.796	1.661	10.037
1.899	20.439	0.375	6.948	0.712	1.588	9.248
1.763	18.199	0.373	6.129	0.657	1.533	8.320
1.684	15.614	0.372	5.178	0.626	1.497	7.301
1.653	12.795	0.371	4.136	0.614	1.481	6.231

Table 5.3 Variation of corrosion pressure with corrosion depth for fully cracked cylinder

Corrosion Depth x mm	Effective Thickness Layer d_c mm	Stiffness Reduction Factor α	Corrosion Pressure P_{cor} MPa	Crack Width w mm	Confining Pressure P_{conf} MPa	Total Pressure P_{total} MPa
0.150	0.060	0.120	8.086	1.807	1.162	9.248
0.200	0.081	0.076	7.761	2.436	0.870	8.632
0.300	0.121	0.060	7.497	3.693	0.578	8.075
0.400	0.162	0.052	7.085	4.950	0.431	7.517
0.500	0.201	0.046	6.634	6.207	0.343	6.977

Table 5.4 Variation of bond stress with corrosion depth for fully cracked cylinder

Corrosion Depth x mm	Friction Coef. u	Corrosion Stress τ_{cor} MPa	Confining Stress τ_{cp} MPa	Adhesion Stress τ_{AD} MPa	Ultimate Bond Stress τ_{bu} MPa
0.150	0.418	2.908	0.418	1.145	4.471
0.200	0.302	2.690	0.302	0.783	3.774
0.300	0.185	2.404	0.185	0.107	2.695
0.400	0.127	2.087	0.127	0.000	2.214
0.500	0.092	1.782	0.092	0.000	1.874

5.2 Comparison of Results Using Different Analytical Bond Strength Models

In this section, a comparison of different parameters of the proposed analytical model with different models proposed by other researches is presented.

5.2.1 Comparison with Wang and Liu model (2004)

In this section, using the above mentioned example, a comparison between the proposed model, and Wang and Liu model is presented. Figure 5.3 shows the variation of corrosion pressure with the radius of the inner cylinder (using the idealization of the concrete cover thickness as thick walled cylinder) R_c for both the proposed model and the corrosion pressure calculated by Wang and Liu (2004). As seen in Fig. 5.3 the corrosion pressure in the proposed model is higher than the one calculated by Wang and Liu (2004). This can be attributed to the effect of anisotropy in the inner cylinder. The maximum corrosion pressure, $P_{crit} = 21.535 MPa$ at $R_c = 35 mm$ in the present model, while in Wang and Liu model, $P_{crit} = 13.784 MPa$ at $R_c = 40 mm$.

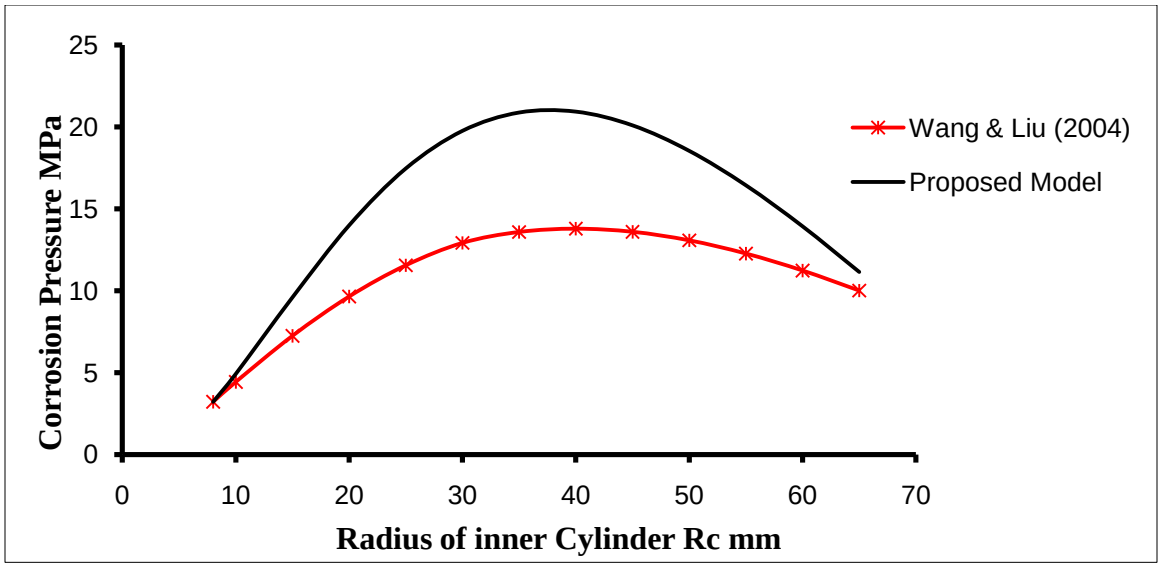

Figure 5.3 Variation of corrosion pressure with radius of inner cylinder Rc

Figure 5.4 shows the variation of the corrosion depth x with the front crack R_c. It can be noted from Fig. 5.4 that the variation of corrosion depth x in the present model is higher than the corrosion depth x calculated by Wang and Liu (2004) for the same front crack location R_c. Also, this can be attributed to anisotropy of the cracked cylinder in the present model while in Wang and Liu model the relationship was assumed to be linear with the same modulus of elasticity for radial and tangential directions. In the present model, when $R_c > 35mm$, the increase in the value of corrosion depth x to induce cracks is getting smaller, and when the cylinder almost fully cracked, the variation of the corrosion depth x almost zero, while in Wang and Liu model, the variation of the corrosion depth x is increasing linearly. The present model shows higher accuracy due to the fact that the cracks could only be stable when the internal pressure is lower than P_{crit} (Chernin et al. 2009), where P_{crit} is the maximum corrosion pressure which causes full cracking of the cylinder wall. According to Chenin et al. (2009), the cracks could only be stable at internal pressure less than P_{crit} .This means that at P_{crit}, the radial cracks should propagate through an uncracked outer part of the cylinder wall.

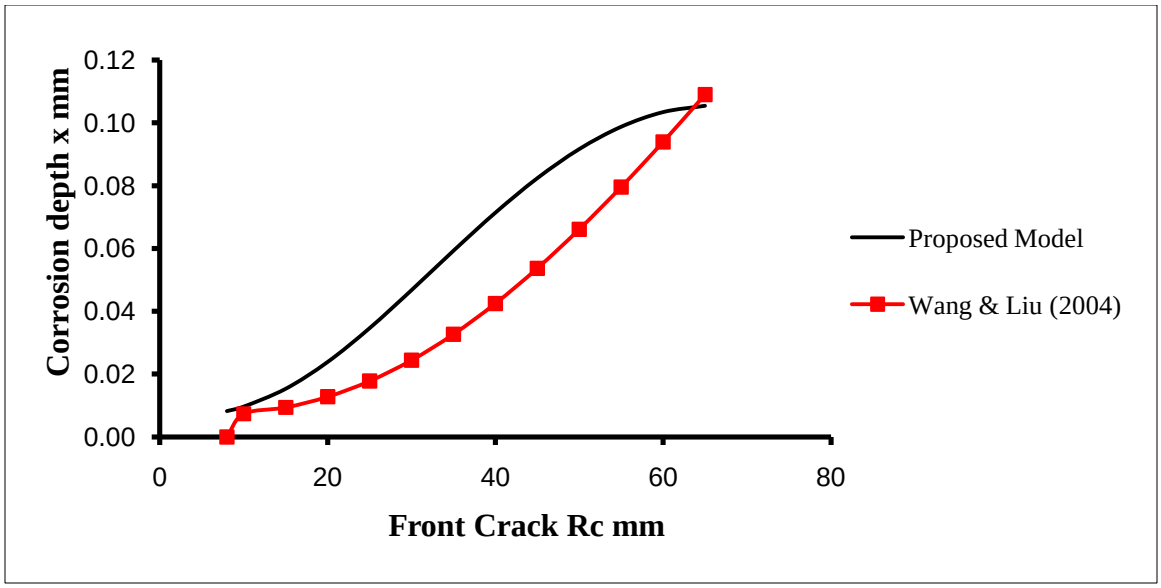

Figure 5.4 Variation of corrosion depth x with front crack Rc

5.2.2 Comparison with Bhargava et al. (2007)

The corrosion pressure versus corrosion depth for the proposed model is compared with the corrosion pressure calculated by Bhargava et al. (2007) as shown in Fig. 5.5. As seen in Fig. 5.5 with the increase of corrosion depth, the corrosion pressure in the proposed model is higher at first than the one calculated by Bhargava et al. (2007), however, with further increase of corrosion depth, the corrosion pressure of the proposed model is lower than that of Bhargava's. This is mainly attributed to the effect of anisotropy in the inner cylinder. Bhargava et al. assumed similar modulus of elasticity for the radial and tangential directions, while in the proposed model; a stiffness reduction factor was taken into account to calculate the modulus of elasticity in the tangential direction which is more accurate as shown in Fig. 4.7. It can be noted from Fig. 4.7 that the young modulus of elasticity for the radial and tangential directions are not equal in the cracked zone.

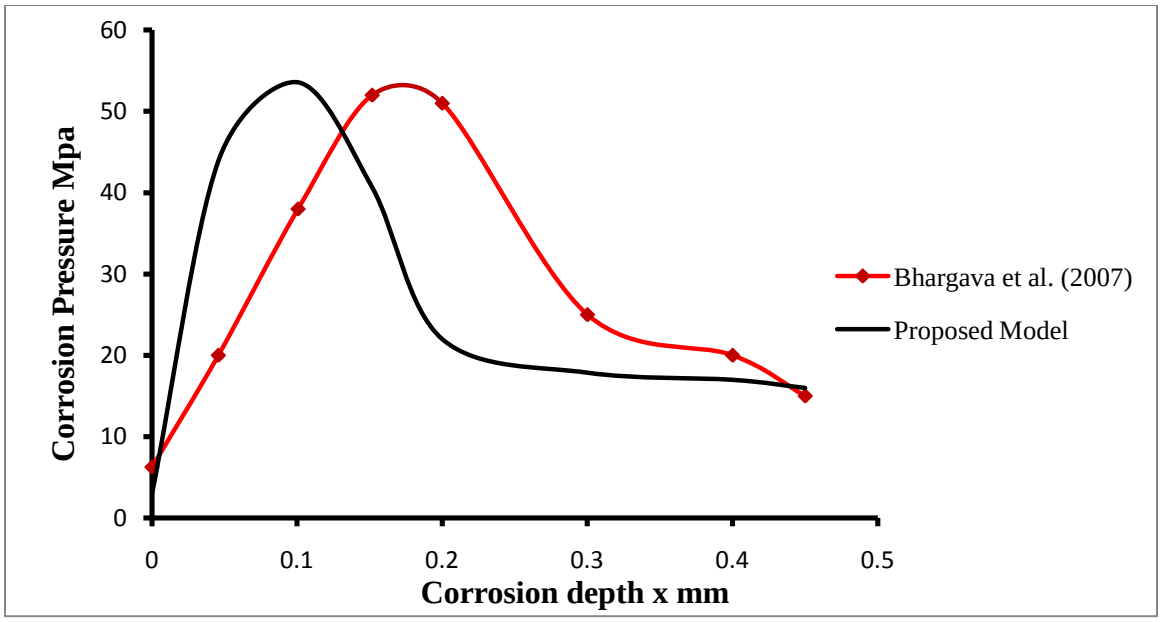

Figure 5.5 Variation of corrosion pressure with corrosion depth x

5.2.3 Comparison with Chernin et al. (2009)

The variation of the maximum corrosion pressure calculated by the proposed model P_{crit} with the ratio of concrete cover to the bar diameter compared with the finite element analysis by Chernin et al. (2009) is shown in Fig 5.6. It can be noted from Fig. 5.6 that good agreement has been observed at lower c/d up to 3.0, whereas for higher ratios, some deviation from finite element analysis is observed. This is mainly attributed to the calculation of the stiffness reduction factor which is assumed to vary exponentially with front crack ratio to concrete cover thickness in the proposed model.

The comparison between the corrosion pressure versus the radius of inner cylinder, R_c, for both the proposed model and the corrosion pressure calculated by Chernin et al. is shown in Fig. 5.7. It can be noted that the corrosion pressure by the proposed model, for lower values of R_c is slightly higher than that calculated by Chernin et al., whereas, for higher values of R_c, the calculated values is lower than that calculated by Chernin et al.. This is mainly attributed to the stiffness reduction factor calculated by Chernin et al., which is very high at higher values of R_c as shown in Fig. 4.9.

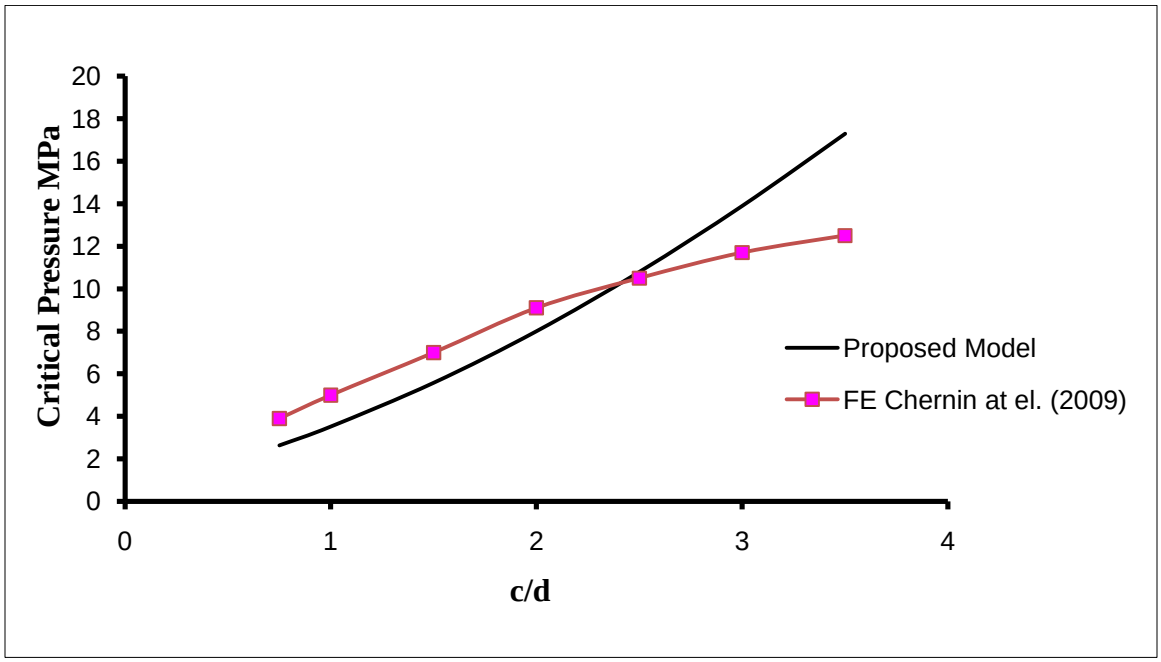

Figure 5.6 Variation of maximum corrosion pressure with c/d

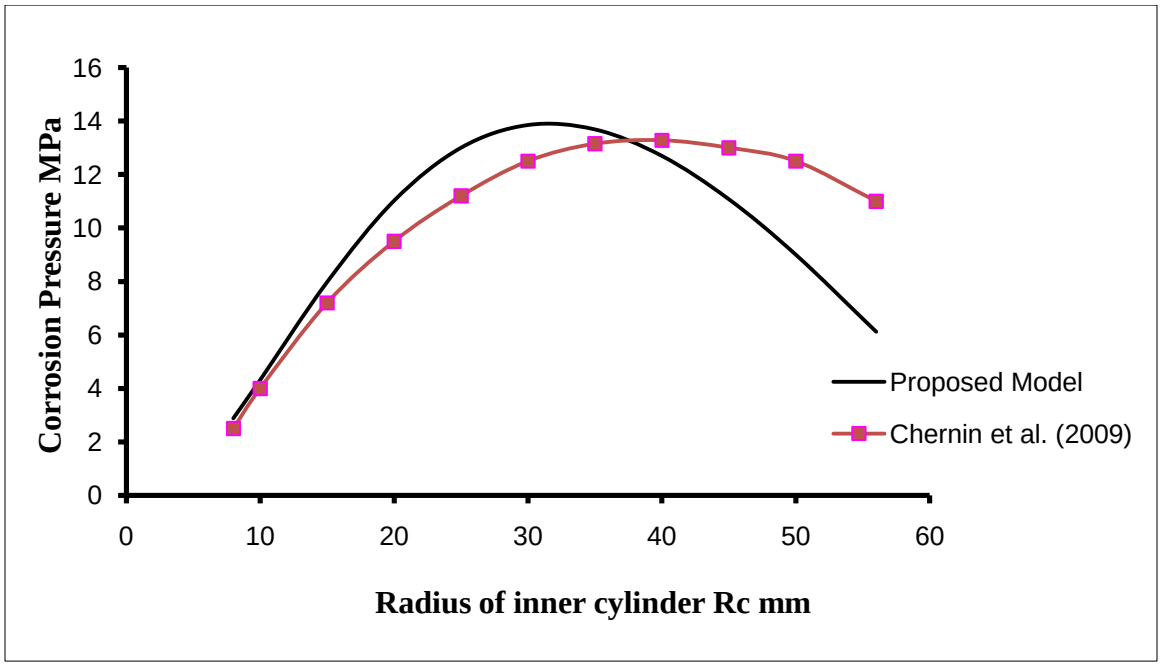

Figure 5.7 Variation of corrosion pressure with front crack Rc

5.3 Validation of the Model with Experimental Results by Other Researchers

To investigate and validate the performance of the proposed model, the effect of corrosion on bond strength between steel and concrete, numerical analysis are carried out for various experimental data performed by different researchers.

5.3.1 Validation of the model with the results of Almusallam et al. (1996)

The proposed model is used to analyse the results of cantilever bond tests conducted by Almusallam et al. (1996) to determine the effect of corrosion on the bond strength of the reinforced concrete and modes of failure of the specimens using three different stages: pre-cracking, cracking and post cracking, and the effect of corrosion on different crack widths and rib profile. The size of the cantilever specimens were 152 x 254 x 279 mm reinforced with 12 mm diameter reinforcing bars with 102mm embedment length. The concrete cover thickness was 63.75 mm, and the concrete compressive strength $f_c' = 30MPa$. The maximum size of the aggregate used was 19 mm. The ratio of the volume of corrosion products formed to the original volume of the reinforcing steel is assumed to be 2.5. The experimental results and the predicted values of the proposed model with the increase of corrosion depth are presented in Fig. 5.8. The variations of τ_{CP}, τ_{AD}, and τ_{COR}, with the increase of corrosion depth are also shown in the same figure for comparison reasons. The predicted values of the proposed model show very good agreement with the experimental results as shown in Fig. 5.8.

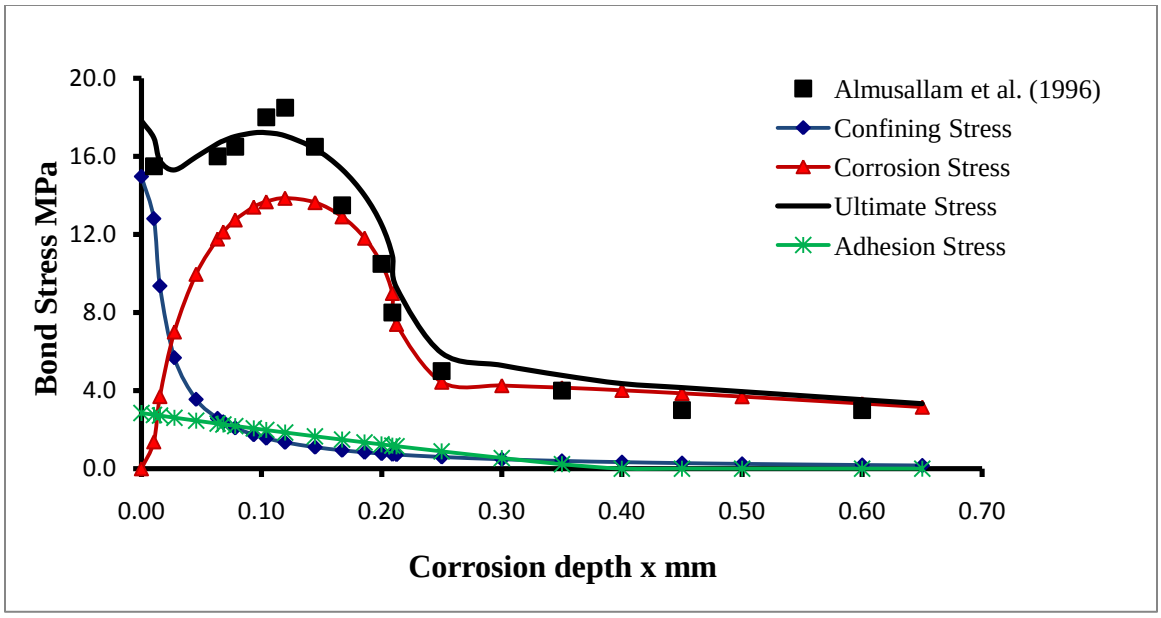

Figure 5.8 Comparison of Predicted Bond stress versus Corrosion Depth with Al-Musallam et al. (1996) Experimental Results

5.3.2 Validation of the model with the results of Al-Sulaimani et al. (1990)

Al-Sulaimani et al (1990) studied the effect of the corrosion on the behaviour of the steel-concrete bond, using 150 cubic specimens with centrally embedded 10 mm bars subjects to pullout test. Al-Sulaimani et al. found that the bond strength increased in the beginning up to a certain level of corrosion then decreased when corrosion was very high. They attributed the initial increase in bond to the increased roughness of the reinforcing bar surface with the growth of a firm layer of corrosion, whereas the loss in bond with further corrosion was due to the severe degradation of bar ribs, the lubricating effect of the flaky corroded metal on the bar surface, and the reduced concrete confinement of the bar due to the widening of the longitudinal corrosion crack. The concrete cover thickness was 70 mm, with a concrete compressive strength of $f_c' = 30MPa$. The ratio of the volume of corrosion products formed to the original volume of the reinforcing steel is assumed to be 4. The relationship between the corrosion mass loss percent $p_{mass}\%$ and the reduction in steel area percent $p_{area}\%$ was regressed as $p_{area} = 2.4622P_{mass}$. The experimental corrosion penetration depth was calculated as $x = 0.5D_i(1-\sqrt{1-0.01P_{area}})$ (Bhargava et al. 2007). Wang and Liu (2004) also adopted a similar approach to evaluate the

experimental corrosion penetration depth. The experimental results and the predicted values of the proposed model with the increase of corrosion depth are presented in Fig. 5.9. The variations of τ_{CP}, τ_{AD}, and τ_{COR}, with the increase of corrosion depth are also shown in the same figure for comparison reasons. The predicted values of the proposed model show very good agreement with the experimental results as shown in Fig. 5.9.

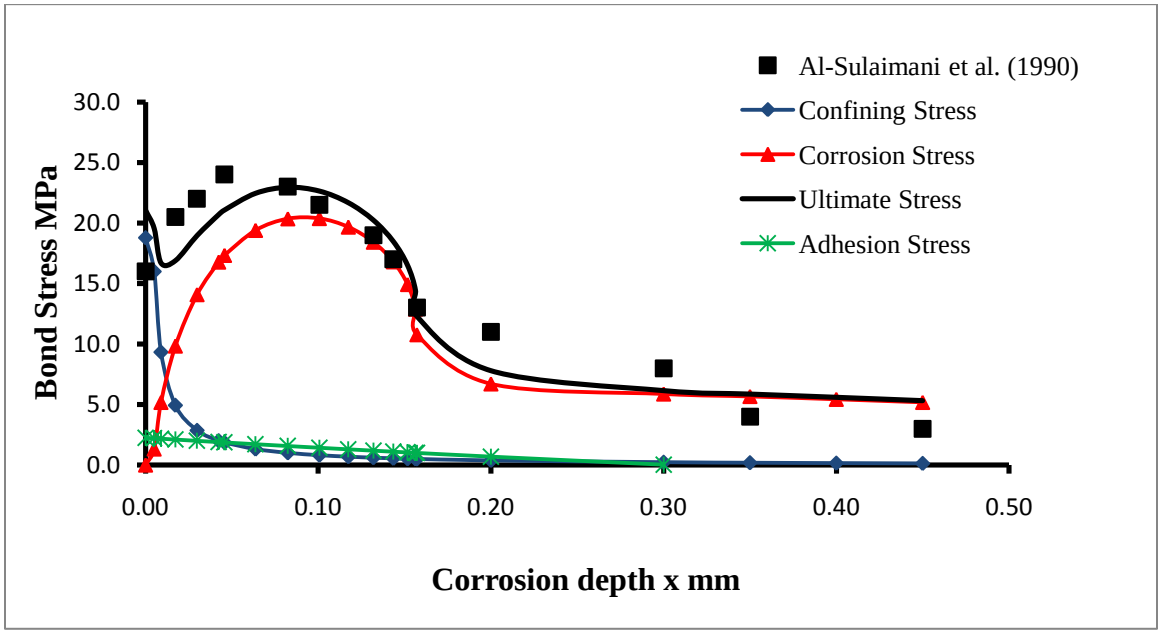

Figure 5.9 Comparison of Predicted Bond stress versus Corrosion Depth with Al-Sulaimani et al. (1990) Experimental Results

5.3.3 Validation of the model with the results of Cabrera and Ghiddoussi (1992)

The proposed bond model is also validated by using the results of Cabrera and Ghoddoussiss' (1992) pullout tests which were performed on 150 mm cubes with 12 mm diameter reinforcing bar centrally embedded in the cube to find the effect of corrosion on the bond strength at the steel-concrete interface. They used a concrete cover thickness of 69 mm, and a concrete compressive strength of $f_c' = 56MPa$. The corrosion penetration depth x is determined by $x = p_{mass}.d/400$ due to the relative agreement between measured reinforcement weight loss and calculated reinforcement weight loss by Faraday's law (Wang and Liu 2004). The ratio of the volume of corrosion products formed to the original volume of the reinforcing steel is assumed to be 3. The

experimental results and the variations of the predicted values of the proposed model with the increase of corrosion depth are presented in Fig. 5.10. The predicted values of the proposed model show very good agreement with the experimental results as shown in Fig. 5.10.

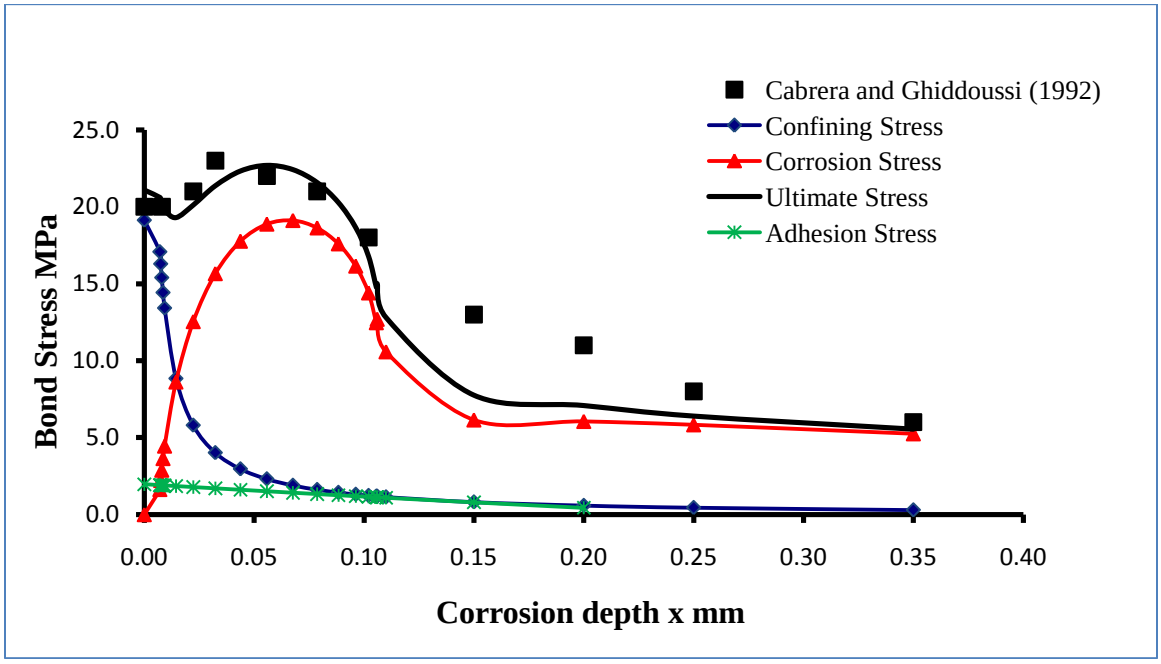

Figure 5.10 Comparison of Predicted Bond stress versus Corrosion Depth with Cabrera and Ghoddoussi (1992) Experimental Results

5.3.4 Validation of the model with the results of Lee et al. (2002)

The proposed bond model is also validated by using the results of Lee et al (2002) who studied the effect of reinforcement corrosion on the bond properties between concrete and reinforcement. The finite element analysis was also carried out on the basis of the results of the pullout tests. Lee et al carried out pullout tests on 65 mm concrete cubes with a 13 mm diameter reinforcing bar centrally embedded in the cube. The concrete compressive strength was $f_c' = 33MPa$. The ratio of the volume of corrosion products formed to the original volume of the reinforcing steel is assumed to be 2. The experimental results and

the variations of the predicted values of the proposed model with the increase of corrosion depth are presented in Fig. 5.11. The predicted values of the proposed model show very good agreement with the experimental results as shown in Fig. 5.11.

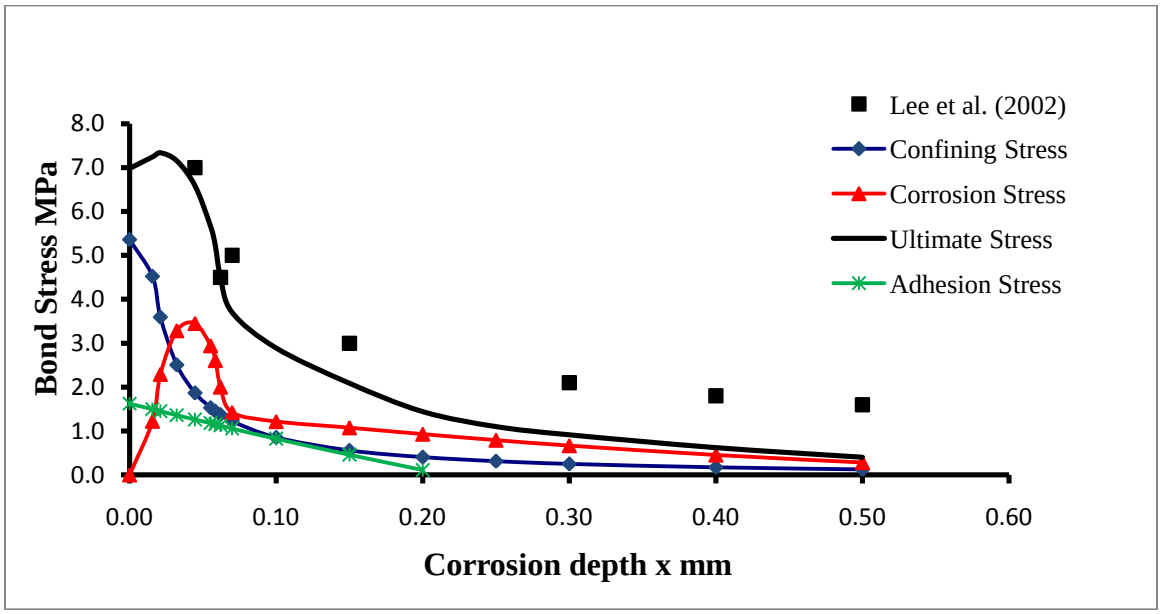

Figure 5.11 Comparison of Predicted Bond stress versus Corrosion Depth with Lee et al. (2002) Experimental Results

Chapter 6

CONCLUSIONS AND FUTURE RECMMENDATIONS

6.1. Summary and Conclusions

Bond between steel and concrete is an essential feature of reinforced concrete structures which enables the transfer of forces between steel and concrete. Therefore, the interaction between the steel bar and the surrounding concrete is fundamental because it influences many aspects of the behaviour of reinforced concrete such as cracking, deformability, and instability.

An analytical model that describes the bond stress at the steel-concrete interface in a reinforced concrete is developed where the contact pressure between steel and concrete is a key variable. Mechanical modeling the contact pressure and the friction develops the mechanical behaviour of contact interface between steel and concrete. In order to derive the mathematical expression for contact pressure at steel-concrete interface, concrete is assumed as a thick-walled cylinder subjected to internal pressure exerted from the growth of corrosion products on the concrete at the interface between the rust band (corrosion products) and concrete. The concrete in the inner cylinder is considered as an anisotropic material with stiffness degradation factor as an exponential function as shown in Equation 4.53 while at the outer cylinder, the concrete is treated as isotropic material.

The developed model (equation 4.45) shows that the contact pressure at the steel concrete interface depends on the bar diameter; tensile strength of concrete; crack width; maximum aggregate size; fracture energy coefficient; stiffness degradation factor; the volume of corrosion products formed compared to the volume of the original reinforcing steel that has corroded; modulus of elasticity; and poisons ratio of concrete.

The present study shows that the corrosion pressure increases in the beginning with the depth of corrosion attack and then later decreases. Hence, the confining pressure does not

play a significant role in ultimate bond strength as soon as the concrete cover cracks while the corrosion pressure plays a significant role in the ultimate bond strength. It is observed that the bond stress is influenced by the confining pressure at the onset of corrosion, however, with increase of the level of corrosion, the confining pressure becomes negligible and it will be highly influenced by corrosion pressure. Therefore, it can be concluded that the bond stress at the steel-concrete interface is a function of contact pressure at the steel-concrete interface.

The predicted values of the effected parameters have been verified with those of analytical, numerical and experimental observed data by other researchers. The corrosion pressure calculated in the present model shows more accurate results compared with other models due to the effect of anisotropy of cracked cylinder in the present model. Therefore, the stiffness degradation factor plays an important role in the determination of corrosion pressure, which in turn affects the bond stress at steel-concrete interface. In addition, the corrosion pressure in the present model is compared with the finite element analysis by Chernin et al. (2009). it was noted that there was good agreement has been observed at lower c/d ratio up to 3.0, whereas for higher ratios, some deviation from finite element analysis was observed. This is mainly attributed to the calculation of the stiffness reduction factor, which is assumed, exponentially varies with front crack ratio to concrete cover thickness.

The results of the proposed model were also validated with the experimental results obtained by Almusallam et al. (1996), Al-Sulaimani et al (1990), Lee et al. (2002), and Cabrera and Ghiddoussi (1992). A good agreement was noted between the results of the experiment and the proposed model; this shows a good validation of the model.

The current study is useful to determine the loss of flexural strength on reinforced concrete members such as beams and slabs due to loss of bond strength at steel-concrete interface. In addition, the proposed model would help to develop models for predicating the time for concrete cover cracking.

6.2. Future recommendations

This study considered the corrosion of regular reinforced concrete members with the effect of quite a few parameters, such as specimen bar diameter; tensile strength of concrete; crack width; maximum aggregate size; the volume of corrosion products formed compared to the volume of the original reinforcing steel that has corroded; modulus of elasticity; and poisons ratio of concrete. However, this was far from exhaustive and the following are a few recommendations for further analytical, numerical and experimental research:

1. The effect of transverse reinforcement on the contact pressure is not included; therefore, a future work is needed to include this effect on the bond stress.
2. Stiffness degradation factor plays an important role in the determination of the corrosion pressure; therefore, more experimental and theoretical studies are needed to understand the mechanical behavior of this factor on contact pressure, which in turn affects the bond stress at steel-concrete interface.
3. Develop the mathematical expression for contact pressure by considering the effect of rib profile at the steel-concrete interface.
4. Develop a bond stress model to take the affect of corrosion on flexural members.
5. Modeling the bond stress on corroded pre-stressing tendons in pre-stressed concrete structures

REFERENCES

ACI Committee 408 (1966), "Bond Stress - The State of the Art", Journal of the American Concrete Institute, Vol. 63, No. II, pp. 1161-1188.

ACI Committee 408 (1992), “Bond Under Cyclic Loads”, Journal of the American concrete Institute.

ACI Committee 408R (2003), "Bond and Development of Straight Reinforcing Bars in Tension", Journal of the American Concrete Institute.

Alavi-Fard, M., and Marzouk, H., (2002), “Bond Behavior of High Strength Concrete Under Reversed Pull-out Cyclic Loading”, Canadian Journal of Civil Engineering, Vol. 29, No. 2, pp.191-200.

Almusallam, A. A., Al-Gahtani, A. S., Aziz, A. R., and Rasheeduzzafar, (1996), “Effect of Reinforcement Corrosion on Bond Strength”, Construction and Building Materials, Vol. 10, No. 2, pp. 123-129.

Al-Sulaimani, G. J., Kaleemullah, M., Basunbul, I. A., and Rsheeduzzafar, (1990), “Influence of Corrosion Cracking on Bond Behavior and Strength of Reinforced Concrete Members”, ACI Structural Journal, Vol. 87, No. 2, pp. 220-231.

Amleh, L., and Ghosh, A., (2006), “Modeling the Effect of Corrosion on Bond Strength at the Steel Concrete Interface with Finite-Element Analysis”, Canadian Journal of Civil Engineering, Vol.33, No. 6, pp. 673-682.

Amleh, L., (2000),”Bond Deterioration of Reinforcing Steel in Concrete due to Corrosion”, PhD thesis, McGill University, Montreal, Canada.

Amleh, L., and Mirza, S., (1999), “Corrosion Influence on Bond between Steel and Concrete”, ACI Structural Journal, Vol. 96, No. 3, pp. 415–423.

Azher, S. A., (2005),”A Prediction Model for the Residual Flexural Strength of Corroded Reinforced Concrete Beams”, MASc Thesis, King Fahd University of Petroleum and Minerals, Saudi Arabia.

Bazant, Z., P., (1979), “Physical Model for Steel Corrosion in Concrete Sea Structures-Theory”, ASCE, Journal of Structural Division, Vol. 105, No. 6, pp. 1137-1153.

Bazant, Z., P., and Planas, J., (1998), “Fracture and Size Effect in Concrete and Other Quasibrittle Materials”, CRC Press, New York, USA.

Bhargava, K., Ghosh, A. K., Mori, Y., and Ramanujam, S., (2006), “Analytical Model for Time to Cover Cracking in RC Structures due to Rebar Corrosion”, Nuclear Engineering and Design Journal, Vol. 236, No. 11, pp. 1123-1139.

Bhargava, K., Ghosh, A. K., Mori, Y., & Ramanujam, S., (2007), “Models for Corrosion Induced Bond Strength Degradation in Reinforced Concrete”, ACI Materials Journal, Vol. 104, No. 6, pp. 594-603.

Cabrera, J. G., (1996), “Deterioration of Concrete Due to Reinforcement Corrosion”, Cement and Concrete Composites Journal, Vol. 18, No. 1, pp. 47-59.

Cabrera, J. G., and Ghoddoussi, P., (1992), “The Effect of Reinforcement Corrosion on the Strength of the Steel/Concrete Interface”, Proceedings, International Conference on Bond in Concrete, Riga, Latvia, pp. 11-24.

Cairns, J., and Abdullah, R., (1994), "Fundamental Tests on the Effect of an Epoxy Coating on Bond Strength", ACI Materials Journal, Vol. 91, No. 4, pp. 331-338.

Cairns, J., and Abdullah, R. B., (1996), “Bond Strength of Black and Epoxy-Coated Reinforcement- A Theoretical Approach”, ACI Materials Journal, Vol. 93, No. 4, pp.362-370.

Chernin, L., Val, D. V., and Volokh, K. Y., (2009),”Analytical Modelling of Concrete Cover Cracking Caused by Corrosion of Reinforcement”, Materials and Structures Journal, Vol. 43, No. 4, pp. 543-556.

Choi, O. C., and Lee, W. S., (2002), "Interfacial Bond Analysis of Deformed Bars to Concrete”, ACI Structural Journal, Vol. 99, No. 6, pp. 750-755.

Coronelli, D., and Gambarova, P.G., (2000), “A Mechanical Model for Bond Strength of Corroded Reinforcement in Concrete”, In Proceedings of EM2000, 14th ASCE Engineering Mechanics Conference, Austin, Tex. CD-ROM. American Society of Civil Engineers, Reston.

Coronelli, D., (2002), “Corrosion Cracking and Bond Strength Modeling for Corroded Bars in Reinforced Concrete”, ACI Structural Journal, Vol. 99, No. 3, pp. 267-276.

“Corrosion in Reinforced Concrete Structures”, (2005), in Bohni Hans (Ed.), Woodhead Publishing Limited, Cambridge, England.

Darwin, D., Tholen, M. L., Idun, E. K., and Zuo, J., (1996a), “Splice Strength of High Relative Rib Area Reinforcing Bars”, ACI Structural Journal, Vol. 93, No. 1, pp. 95-107.

Darwin. David, and Eheneze, K. Graham, (1993), "Effect of Deformation Height and Spacing on Bond Strength of Reinforcing Bars", ACI Structural Journal, Vol. 90, No. 6, pp. 646-657.

Eligehausen, R., (1979), “Bond in Tensile Lapped Splices of Ribbed Bars with Straight Anchorages”, Publication 301, German Institute for Reinforced Concrete, Berlin, 118 pp. (in German)

Ferguson, P. M., Breen, J. E., and Jirsa, J. O., (1988), “Reinforced Concrete Fundamentals”, 5th edition, John Wiley, New York, USA.

Gambarova, G.P., and Giuriani, E., (1985), “Discussion of `Study of the Transfer of Tensile Forces by Bond' by D. H. Jiang, S. P. Shah, and A. T. Andonian", ACI Journal, Proceedings Vol. 82, No. 3, pp 381-383.

Gambarova, P. G., Rossat, G. P., (1996), “Bond and Splitting in Reinforced Concrete: Test Results on Bar Pull-Out”, Materials and Structures Journal, Vol. 29, No. 5, pp. 267-276.

Giuriani, E., Pizzari, G., and Schumm, C., (1991), “Role of Stirrups and Residual Tensile Strength of Cracked Concrete on Bond”, ASCE, Journal of Structural Engineering, Vol. 117, No.1, pp. 1-18.

Girard, C., and Bastien, J., (2002), “Finite-Element Bond-Slip Model for Concrete Columns under Cyclic Loads”, ASCE, Journal of Structural Engineering, Vol. 128, No. 12, pp. 1502-1510.

Goto, Y., (1971), "Cracks Formed in Concrete around Deformed Tension Bars", ACI Structural Journal, Vol. 68, No. 4, pp 244-251.

Jeanty, P. R., Mitchell, D., and Mirza, M. S., (1988), “Investigation of ‘Top Bar’ Effects in Beams”, ACI Structural Journal, Vol. 85, No. 3, pp. 251-257.

Jin, W.L., and Zhao, Y. X., (2001), “Effect of Corrosion on Bond Behavior and Bending Strength of Reinforced Concrete Beams”, Journal of Zheijang University (SCIENCE), Vol. 2, No. 3, pp. 298-308.

Kemp, E. L., Brezny, F. S., and Unterspan, J. A., (1968), “Effect of Rust and Scale on the Bond Characteristics of Deformed Reinforcing Bars”, ACI Journal, Vol. 65, No. 9, pp 743-756.

Koch, G. H., Brongers, M. P. H., Thompson, N. G., Virmani, Y. P., and Payer, J. H., (2001), “Corrosion Costs and Preventive Strategies in the United States”, Federal Highway Administration (FHWA), Report FHWA-RD-01-156, 773 p.

Kyle, S., Hooton, R. D., and Pantazopoulou, S. J., (1999), “Corrosion Effects on Bond Strength in Reinforced Concrete”, ACI Structural Journal, Vol. 96, No. 6, pp. 915-922.

Lee, H. S., Noguchi, T., and Tomosawa, F., (2002), “Evaluation of the Bond Properties between Concrete and Reinforcement as a Function of the Degree of the Reinforcement Corrosion”, Cement and Concrete Research, Vol. 32, No. 8, pp. 1313-1318.

Li, C. Q., Melchers, R. E., and Zheng, J. J., (2006), “ Analytical Model for Corrosion-Induced Crack Width in Reinforced Concrete Structures”, ACI Structural Journal, Vol. 103, No. 4, pp. 479-487.

Liu, Y., and Weyers, R. E., (1998), “Modeling the time to Corrosion Cracking in Chloride Contaminated Reinforced Concrete Structures”, ACI Materials Journal, Vol. 95, No. 6, pp. 675-681.

Luke, J. J., Hamad, B. S., Jirsa, J. O., and Breen, J. E., (1981), “The Influence of Casting Position on Development and Splice Length of Reinforcing Bars”, Research Report No. 242-1, Center for Transportation Research, Bureau of Engineering Research, University of Texas at Austin, Tex., 153 pp.

Lundgren, K., and Gyltoft, K., (2000), “A Model for the Bond between Concrete and Reinforcement”, Magazine of Concrete Research, Vol. 52, No. 1, pp.53-63.

Lundgren, K., (2002), “Modelling the Effect of Corrosion on Bond in Reinforced Concrete”, Magazine of Concrete Research, Vol. 54, No. 3, pp.165-173.

Lundgren, K., (2005), “Bond Between Ribbed Bar and Concrete. Part 1: Modified Model”, Magazine of Concrete Research, Vol. 57, No. 7, pp.371-382.

Lundgren, K., (2005), “Bond Between Ribbed Bar and Concrete. Part 2: The Effect of Corrosion”, Magazine of Concrete Research, Vol. 57, No. 7, pp.383-395.

Lutz, L., A., and Gergely, P., (1967), “Mechanics of Bond and Slip of Deformed Bars in Concrete”, ACI Journal Proceedings, Vol. 64, No. 11, pp.711-721.

Lutz, L. A., Gergely, P., and Winter, G., (1966), "Mechanics of Bond and Slip of Deformed Reinforcing Bars in Concrete", Research Report No. 324, Department of Civil Engineering, Cornell University, New York, USA.

Martin, H., (1982), “Bond Performance of Ribbed Bars (Pull-Out-Tests) - Influence of Concrete Composition and Consistency “, International Conference – Bond in Concrete, Paisley, Scotland, pp. 289–299.

MacGregor, J.G., (1997), “Reinforced Concrete: Mechanics and Design”, Third Edition, Prentice Hall, Upper Saddle River, New Jersey, USA.

Mindess, S., (2003), “Concrete”, 2nd Edition, Prentice Hall, Upper Saddle River, New Jersey, USA.

Molina F., Alonso C., and Andrade C., (1993), “Cover Cracking as a Function of Bar Corrosion: Part 2 – Numerical Model”, Materials and Structures, Vol. 26, No. 9, pp.532-548.

Nawy, E. G., (1996), “Reinforced Concrete: A Fundamental Approach”, 3rd Edition, Prentice Hall Canada Inc., Toronto, Canada, pg. 415.

Nielsen, A., (1985), "Durability" Beton Bogen (The Concrete Book), Edited by Aa. D. Herholdt, Cbr. F.P. Justesen, P. Nepper-Christensen, and A. Nilesen, Aalborg, Portland, pp. 200-43.

Nielson, C. V., and Bicanic, N., (2002), “Radial Fictitious Cracking of Thick-Walled Cylinder due to Bar Pull-Out”, Magazine Concrete Research, Vol. 54, No. 3, pp. 215-221.

Orangun, C. O., Jirsa, J. O., and Breen, J. E., (1977), “Reevaluation of Test Data on Development Length and Splices”, ACI Journal, Proceedings Vol. 74, No. 3, pp. 114-122.

Pantazopoulou, J., and Papoulia, K. D., (2001), “Modeling Cover-Cracking due to Reinforcement Corrosion in RC Structures”, ASCE, Journal of Engineering Mechanics, Vol. 127, No. 4, pp.342-351.

Pantazopoulou, J., and Tastani, S. P., (2002), “Experimental Evaluation of the Direct Tension Pullout Tests”, Bond in Concrete – from research to standards, Budapest.

Park, R., and Paulay, T., (1975), "Reinforced Concrete Structures," John Wiley & Sons, Inc. New York, USA.

Raymond, E.U., and Henry, R. L., (1965), “Influence of normal pressure on bond strength”, Journal of American Concrete Institute, Vol. 62, No.5, pp. 577-586.

Rehm, G., (1961), "Uber die Grunlagen des Verbundes Zwischen Stahl und Beton" Deutscher Ausschuss fijr Stahlbeton, Heft 138, Wilhelm Emest und Sohn, Berlin, Germany.

Rehm, G., (1968), “The Basic Principles of the Bond between Steel and Concrete”, Translation No. 134, Cement and Concrete association, London, UK, pp. 66.

Richardson, M. G., (2002), “Fundamentals of Durable Reinforced Concrete”, Modern Concrete Technology Series, Taylor and Francis Group, Edition 1, New York, USA, pp. 51-75.

Rodriguez, J., Ortega, L.M., and Casal, J., (1997), “Load Carrying Capacity of Concrete Structures with Corroded Reinforcement”, Construction and Building Materials, Vol. 11, No. 4, 1997, pp. 239-248.

Task Group Bond Models, (2000), "Bond of Reinforcement in Concrete", State of the art report, Federal Institute of Technology Lausanne, Swiss.

Tepfers, R. A., (1973), “A Theory of Bond Applied to Overlapping Tensile Reinforcement Splices for Deformed Bars”, Publication 73:2, Division of Concrete Structures, Chalmers University of Technology, Goteborg, Sweden, 328 pp.

Tepfers, R. A., (1979), “Cracking of Concrete Cover along Anchored Deformed Reinforcing Bars”, Magazine of Concrete Research, Vol. 31, No. 106, pp. 3-12

Timoshenko, S. P., (1956), “Strength of Materials Part 11: Advanced Theory and Problems”, Princeton, New Jersey, USA, D. Van Nostrand Company Inc., pp. 205-210.

Timoshenko, S. P., and Goodier, J. N., (1970), “Theory of Elasticity”, McGraw Hill Book Co., New York, USA.

Treece, R. A., and Jirsa, J. O., (1989), "Bond Strength of Epoxy-Coated Reinforcing Bars", ACI Materials Journal, Vol. 86, No. 2, pp. 167-174.

Wang X., and Liu X., (2004), "Modelling Effects of corrosion on Cover Cracking and Bond in Reinforced Concrete", Magazine of Concrete Research, Vol. 56, No. 4, pp. 191-199.

Wang X., and Liu X., (2004), "Modeling Bond Strength of Corroded Reinforcement without Stirrups", Cement and Concrete research, Vol. 34, No. 4, pp 1331-1339.

Yoon, S., Wang, K., Weiss, W. J., and Shah, P. S., (2000), "Interaction between Loading Corrosion and Serviceability of Reinforced Concrete", ACI Materials Journal, Vol. 97, No. 6, pp.637-644.

Zhong, J., Gardoni, P., and Rosowsky, D., (2010), "Stiffness Degradation and Time to Cracking of Cover in Reinforced Concrete Structures Subject to Corrosion", Journal of Engineering Mechanics, Vol. 136, No. 2, pp. 209-219.

Zhou, K., Martin-Pérez, B., and Lounis, Z, (2005), "Finite Element Analysis of Corrosion Induced Cracking, Spalling and Delimitation of RC Bridge Decks", 1st Canadian Conference on Effective Design of Structures, Hamilton, Canada, pp. 187-196

Zuo, J., and Darwin, D., (1998), "Bond Strength of High Relative Rib Area Reinforcing Bars", SM Report No. 46, University of Kansas Center for Research, Lawrence, Kansas, USA, 350 pp.

Zuo, J., and Darwin, D., (2000), "Splice Strength of Conventional and High Relative Rib Area Bars in Normal and High-Strength Concrete", ACI Structural Journal, Vol. 97, No. 4, pp. 630-641.